Characterization of Soil Particle Size Distributions by Water Pressure During Sedimentation

by

Lei Zhang

A dissertation submitted in partial fulfillment
of the requirements for the degree of
Doctor of Philosophy
(Civil Engineering)
in the University of Michigan
2026

Doctoral Committee:

Professor Roman D. Hryciw, Chair
Assistant Professor F. Estéfan T. Garcia
Professor Radoslaw L. Michalowski
Professor Nathan D. Sheldon

Lei Zhang

leileizh@umich.edu

ORCID iD: 0000-0003-1595-9399

© Lei Zhang 2026

Dedication

To my family, with love and gratitude!

Acknowledgements

First and foremost, I would like to express my deepest gratitude to my advisor, Professor Roman D. Hryciw, for his dedicated guidance, patient support, unwavering trust, and genuine care throughout my Ph.D. studies. He provided clear direction for my research while giving me the freedom to explore my own ideas, encouraging me to think independently and take initiative. No matter how busy he was, he always made time to listen to my questions, discuss possible solutions, and offer thoughtful advice whenever I faced important decisions or research setbacks. During a particularly challenging period when I repeatedly encountered setbacks in my experiments, he reassured me with the words, "We are engineers; we can solve everything." Those words gave me the confidence to persevere and have remained a lasting source of inspiration whenever I encounter an impasse in my research. From him, I learned not only how to conduct rigorous scientific research, but also the importance of perseverance, responsibility, and resilience in the face of difficulties. I will carry these invaluable lessons and qualities with me throughout my future career and strive to pass them on to my own students.

I would also like to thank the members of my dissertation committee: Professor F. Estéfan T. Garcia, Professor Radoslaw L. Michalowski, and Professor Nathan D. Sheldon. I am deeply grateful for the time they devoted to reviewing my dissertation and for the valuable suggestions, thoughtful insights, and constructive feedback they provided. Their guidance and support throughout my doctoral studies have also meant a great deal to me.

Professor Garcia was particularly supportive during periods when I felt uncertain about my circumstances and future career. He always took the time to understand my concerns, discuss possible paths forward, and offer thoughtful advice and encouragement. His genuine care helped me navigate the uncertainties of both doctoral study and professional development with greater confidence. Professor Michalowski's continued guidance and encouragement during the Advanced Soil Mechanics course helped me rebuild my confidence. Later, while I served as a Graduate Student Instructor, his advice on teaching helped me improve my approach, fulfill my responsibilities more effectively, and grow into a more confident and capable instructor. Professor

Sheldon brought a valuable sedimentological perspective to my dissertation. His insights and suggestions helped me examine my research within a broader scientific context and beyond a purely geotechnical engineering perspective, greatly expanding my understanding of the work and its broader significance.

I am also deeply grateful to my former advisors, Professor Ping Yang, Professor Wuwei Mao, and Professor Keping Chen. Throughout my Ph.D. studies, they continued to care about my progress and well-being and offered me constant support and encouragement. Their thoughtfulness and kindness have meant a great deal to me.

I owe special thanks to Steve Donajkowski. His exceptional technical expertise and dedication were essential to the experimental systems at the center of this dissertation. He was always willing to help and approached every project with remarkable commitment. Through his expert advice and outstanding machining and fabrication skills, he transformed my ideas and designs into reliable experimental systems. His generosity toward students and willingness to devote his time and expertise to their research were truly invaluable. Without his assistance, the development of the *u*-Sed, m-Sed, and Delta-Sed systems would not have been possible.

I am also sincerely grateful to Tobias Pace for his technical assistance throughout my research. Whenever problems arose with my equipment, he readily helped me troubleshoot and modify the system until it functioned properly. I would also like to express my sincere gratitude to Andrea Ventola for her guidance and encouragement when I first arrived at the University of Michigan. Her kindness and support helped me adjust quickly to the academic and research environment and made my transition into the program much smoother. I also thank the faculty and staff in the Department of Civil and Environmental Engineering for their kindness and support, which made me feel respected, valued, and welcomed throughout my time at the University of Michigan.

I would also like to acknowledge the assistance of ChatGPT, developed by OpenAI, during the preparation of this dissertation. It provided support in improving English expression, refining sentence structure, suggesting alternative wording, and enhancing the clarity and logical flow of the manuscript.

I gratefully acknowledge the Michigan Department of Transportation for providing the soil specimens used in this research and Validyne Engineering for calibrating the pressure transducers. I also acknowledge the financial support provided by the Department of Civil and Environmental

Engineering and the Graham Sustainability Institute at the University of Michigan, as well as by the National Science Foundation under Award No. 1825189.

My doctoral journey was also enriched by the care, companionship, and support of many wonderful friends. My heartfelt thanks go to Sam, Songjie, Deba, Weibing, Fan, Yumeng, Hui, Tianming, Minghui, Wen, Liuyun, Zhichen, Jason, Haiqiang, and Langhao. Your encouragement and the many ways in which you stood by me sustained me through difficult moments, while your companionship filled this journey with many meaningful and cherished memories.

Finally, I owe my deepest gratitude to my family for their unwavering love, support, and encouragement throughout this journey. Their constant belief in me gave me strength during the most challenging moments and made every accomplishment more meaningful. I would also like to express my heartfelt appreciation to my beloved Zekun. You have been a constant source of strength and the person I could rely on without hesitation. Your love, patience, understanding, and constant encouragement carried me through the many challenges of this journey. I am profoundly grateful to have you by my side.

Table of Contents

Dedication ii

Acknowledgements iii

List of Tables ix

List of Figures x

List of Appendices xiii

Abstract xiv

Chapter 1 Introduction 1

1.1 Determination of Particle Size Distribution of Sands 3

1.2 Determination of Particle Size Distribution of Fines 9

1.3 Research Objectives and Dissertation Organization 15

1.3.1 Research Objectives for Sands 15

1.3.2 Research Objectives for Fine-Grained Soils 16

1.3.3 Dissertation Organization 18

Chapter 2 Particle-Size Determination Using Settling Velocity Models 20

2.1 Development of Particle Settling-Velocity Models 21

2.2 Ahrens (2000) Model 25

2.3 Jiménez and Madsen (2003) Model 27

2.4 Application of Settling-Velocity Models to Particle-Size Determination 29

2.5 Chapter Summary 30

Chapter 3 The *u*-Sed Test 32

3.1 The *u*-Sed System Hardware 32

3.2 Pressure Time Histories 34
3.3 The *u*-Sed Test Procedure 37
3.4 Tested Materials and Results 38
3.5 Repeatability and Sensitivity Analysis 46
3.6 Comparison with the Other Methods for PSD Analysis 50
3.7 Chapter Summary 51
Chapter 4 The m-Sed Test 53
4.1 The m-Sed System Hardware 54
4.2 Pressure Stages during an m-Sed Test 57
4.3 Manometer Material and Diameter Selection 61
4.4 The m-Sed Test Procedure 63
4.5 Tested Materials and Test Results 64
4.6 Repeatability and Comparison with the *u*-Sed Test 69
4.7 Factors Affecting PSD Determination in the *u*-Sed and m-Sed Tests 71
4.8 Chapter Summary 75
Chapter 5 The Δ-Sed Test 77
5.1 Sedimentation Theory for Fines 78
5.2 Soil Concentration Determination during Sedimentation 80
5.3 Numerical Simulation 84
5.4 Influence of Port Configuration 85
5.4.1 Influence of Vertical Spacing between Ports 85
5.4.2 Influence of Upper Port Depth 87
5.5 Influence of Soil Specimen and Suspension Temperature 88
5.6 The Δ-Sed System Hardware 91
5.7 Tested Materials and Results 92

5.8 Repeatability and Sensitivity Analysis 94
5.9 Δ-Sed Particle Size Testing Range 98
5.10 Chapter Summary 98
Chapter 6 Summary and Future Recommendations 101
6.1 Summary 101
6.1.1 The *u*-Sed test 101
6.1.2 The m-Sed test 103
6.1.3 The Δ-Sed test 104
6.2 Future Recommendations 105
6.2.1 Scaling of the *u*-Sed and m-Sed Systems for Larger Specimens 106
6.2.2 Reduction of the Δ-Sed Test Duration 107
6.2.3 Integration of Image Analysis for Particle-Shape Characterization 108
6.2.4 Development of a Unified Sedimentation Test for Sands and Fines 109
Appendices 111
Bibliography 117

List of Tables

Table 1.1: Standard Sieve Designations and Sand-Size Subdivisions. 4

Table 3.1: Tested soil specimens, size composition and sedimentation duration. 39

Table 3.2: Comparison of particle size distribution metrics between sieve and *u*-Sed. 45

Table 3.3: Comparison of specific gravity and specimen mass. 46

Table 4.1: Tested Soil Specimens and Size Composition 65

Table 4.2: Comparison of Particle Size Distribution Metrics between Sieve and m-Sed. 68

Table 4.3: Comparison of Specific Gravity and Specimen Mass 69

Table 5.1: Tested Soil Specimens 93

Table B.1: Density and Viscosity of Water as a Function of Temperature 114

List of Figures

Figure 1.1: Sieve stack mounted in a shaker for sieve analysis. 6

Figure 1.2: ASTM 152H hydrometer used for fine-grained soil sedimentation analysis. 10

Figure 1.3: Hydrometer analysis of a dispersed fine-grained soil suspension. 11

Figure 2.1: Turbulent and laminar flow coefficients for Ahrens' model. 26

Figure 2.2: Coefficients A_{JM} and B_{JM}. 28

Figure 3.1: The *u*-Sed system: (a) Sedimentation column and pressure transducer during a test; (b) close-up view of the pressure port and the push-to-connect fitting; and (c) close-up view of the base and pedestal. 33

Figure 3.2: Pressure stages during a *u*-Sed test 35

Figure 3.3: Typical pressure time histories for fine, medium, coarse, and gap-graded sands. 37

Figure 3.4: Images of the 16 soil specimens with their percentages of coarse, medium, and fine sand. 40

Figure 3.5: Particle size distributions for mixtures of coarse, medium, and fine sand. 43

Figure 3.6: Particle size distributions for uniform coarse, uniform medium, and uniform fine sands. 44

Figure 3.7: Repeatability analysis of *u*-Sed test: (a) using Ahrens' model; and (b) using Jiménez and Madsen's model. 47

Figure 3.8: Effect of specific gravity (G_s) deviations on *u*-Sed results: (a) using Ahrens' model; and (b) using Jiménez and Madsen's model. 48

Figure 3.9: Effect of kinematic viscosity deviations on *u*-Sed results: (a) using Ahrens' model; and (b) using Jiménez and Madsen's model. 48

Figure 3.10: Effect of Soil specimen weight on *u*-Sed test results: (a) using Ahrens' model; and (b) using Jiménez and Madsen's model. 49

Figure 4.1: The m-Sed system hardware: (*A*) the bottom section of sedimentation column, (*B*) the top section of sedimentation column, (*C*) close-up view of the base and pedestal. 55

Figure 4.2: Schematic Diagram of the m-Sed System. 56

Figure 4.3: Four stages during an m-Sed test. 58

Figure 4.4: Typical manometer water height time histories for fine, medium, coarse and gap-graded sands. 61

Figure 4.5: The eight tested soil specimens with their percentages of coarse, medium and fine sand. 66

Figure 4.6: Comparison of PSDs from the m-Sed and sieve tests. 67

Figure 4.7: Repeatability Assessment of the m-Sed test 70

Figure 4.8: Comparison of PSD results from the m-Sed, *u*-Sed, and sieve tests. 71

Figure 4.9: Effect of CSF values on particle settling velocity. 73

Figure 4.10: The effect of CSF values on PSDs from the m-Sed test. 74

Figure 5.1: Schematic illustration of sampling zones for sedimentation-based particle size analysis methods: pipette, hydrometer, ISP, and Δ-Sed. 81

Figure 5.2: Effect of vertical spacing between pressure ports on numerical Δ-Sed test results: (a) Δz = 2 cm; (b) Δz = 6 cm; (c) Δz = 10 cm; (d) Δz = 14 cm. 86

Figure 5.3: Effect of upper pressure port depth on numerical Δ-Sed test results: (a) h_A = 0 cm; (b) h_A = 10 cm; (c) h_A = 20 cm; (d) h_A = 25 cm. 88

Figure 5.4: Performance of the numerical Δ-Sed test for different soil specific gravities: (a) G_s = 2.5; (b) G_s = 2.7; (c) G_s = 2.9; (d) G_s = 3.1. 89

Figure 5.5: Performance of the numerical Δ-Sed test under different suspension temperatures: (a) T = 5 °C; (b) T = 15 °C; (c) T = 25 °C; (d) T = 35 °C 90

Figure 5.6: Performance of the numerical Δ-Sed test for different soil gradations: (a) well-graded distribution; (b) gap-graded distribution; (c) random distribution 1; (d) random distribution 2. 90

Figure 5.7: The Δ-Sed system: (a) sedimentation cylinder and differential pressure transducer; (b) close-up view of the pressure port and push-to-connect fitting; and (c) hand agitator. 92

Figure 5.8: Comparison of PSDs from Δ-Sed and hydrometer tests for four fine-grained soils: (a) Silica powder; (b) Goldart clay; (c) Mills Creek silt; (d) Black River clay. 94

Figure 5.9: Repeatability analysis of the Δ-Sed test. 95

Figure 5.10: Effect of assumed soil specific gravity deviations on the Δ-Sed test results. 96

Figure 5.11: Effect of assumed suspension temperature deviations on the Δ-Sed test results. 96

Figure 5.12: Effect of evaporation on the Δ-Sed test results. 97

List of Appendices

Appendix A: Derivation of *u*-Sed Test Equations 111

Appendix B: Temperature-Dependent Density and Viscosity of Water 114

Abstract

Particle size distribution (PSD) is a fundamental soil index that provides initial indications of engineering properties including strength, stiffness, compressibility, and hydraulic conductivity. Yet PSD determination still relies heavily on century-old techniques with significant limitations. Sieve analysis of sands is inherently noisy, laborious, energy-intensive, and time-consuming, while yielding only a limited number of discrete data points. Hydrometer analysis of fine-grained soils requires repeated manual readings, making it labor-intensive and operator-dependent; it also yields only sparse data and is susceptible to surface foam that obscures the meniscus and to suspension disturbance caused by repeated hydrometer insertion and removal. This dissertation develops a family of sedimentation-based systems that determine high-resolution PSDs from water-pressure responses during particle settling: the *u*-Sed and m-Sed tests for sands and the Delta-Sed test for fine-grained soils. Across all three systems, particle size is inferred from settling velocity, while the corresponding percent finer is determined from the measured pressure response in the soil-water mixture during sedimentation.

The *u*-Sed test uses a pressure transducer connected to a fixed sidewall port in a water-filled sedimentation column. As a sand specimen settles and sorts by size, the pressure decrease is used to determine the fraction of specimen mass remaining above the port. Settling time and distance are combined with established settling-velocity models to obtain sieve-equivalent particle sizes. Tests on 16 sands spanning the ASTM sand-size range of 0.075 to 4.75 mm yielded PSDs that agreed closely with sieve results and the tests were highly repeatable.

The m-Sed test extends the same principle by replacing the electronic pressure transducer and data acquisition system with a simple manometer. Tests on eight engineered sands showed excellent agreement with both sieve and *u*-Sed results, demonstrating that comparable accuracy can be achieved without electronic pressure sensing. Requiring no electrical power and designed for easy transport, the highly portable m-Sed system is well suited to field testing, remote locations, and other environments where electronic instrumentation is impractical.

The Delta-Sed test applies a different measurement framework to an initially uniform suspension of fines. The differential pressure between two vertically separated fixed ports determines the average soil concentration within the intervening interval, which is taken to represent the local concentration at its midpoint. Each differential-pressure measurement independently yields a percent-finer value, while the corresponding Stokes-equivalent diameter is inferred from settling velocity, consistent with conventional hydrometer analysis. Numerical simulations were used to evaluate the spatial-averaging approximation and to optimize the port configuration. Experimental validation using four fine-grained materials with contrasting mineralogical and plasticity characteristics showed close agreement with hydrometer results and excellent repeatability. The recommended particle-size range for the Delta-Sed test is 0.002 to 0.075 mm.

Together, the three tests establish a comprehensive sedimentation-based framework for determining high-resolution PSDs across the sand and fine-grained particle-size ranges while overcoming many of the operational and measurement limitations of conventional sieve and hydrometer analyses.

Chapter 1 Introduction

Particle size distribution (PSD) is one of the most fundamental index properties of soils in geotechnical engineering. It describes the relative proportions of particles within a soil specimen over a range of sizes and provides a first-order description of the material from which many engineering interpretations begin. Although soil behavior is also affected by particle shape, mineralogy, relative density, fabric, stress history, pore fluid chemistry, and drainage condition, PSD remains one of the most widely used descriptors because it directly dictates soil classification and provides an initial indication of key engineering properties, including shear strength, stiffness, compressibility, and hydraulic conductivity.

In routine geotechnical practice, PSD provides the primary basis for classifying coarse-grained soils and, together with plasticity characteristics, contributes to the classification and interpretation of fine-grained soils. This classification is not merely descriptive. It provides an initial framework for anticipating how a soil may behave in engineering applications, including foundations, embankments, pavement subgrades, slopes, tunnels, filters, drainage layers, and earth-retaining structures. The distinction among gravel, sand, silt, and clay size fractions is therefore one of the earliest and most consequential steps in soil characterization.

For coarse-grained soils, PSD is especially important because gradation influences packing, void structure, and interparticle contact. Uniformly graded sands contain a relatively narrow range of particle sizes and may form more open pore structures, whereas well-graded sands achieve denser packing as smaller particles occupy the voids between larger particles. Gap-graded soils exhibit complex behavior because the absence of intermediate particle sizes affects both mechanical response and hydraulic stability. PSD-derived parameters such as D_{10}, D_{30}, D_{50}, D_{60}, the coefficient of uniformity C_u, and the coefficient of curvature C_c are routinely used to describe gradation, control soil classification, imply permeability, evaluate filter compatibility, and guide engineering judgment in design and quality control.

The fine fraction of a soil is important. The amount of material passing the No. 200 sieve can substantially alter the engineering behavior of an otherwise sand-sized material. Small

amounts of silt or clay occupy pore spaces between larger grains, reduce hydraulic conductivity, affect compaction behavior, and influence the rate at which excess pore pressures dissipate under loading. As fines content increases, the mechanical response may transition from being governed primarily by grain-to-grain friction between sand particles to being controlled by the fine-grained matrix. Accurate determination of the fine fraction is therefore critical for evaluating drainage, settlement, liquefaction susceptibility, frost susceptibility, internal erosion potential, and the suitability of soils for engineered fills and foundation support.

For fine-grained soils, PSD provides essential information on the relative proportions of silt- and clay-sized particles. Although Atterberg limits, mineralogy, and particle surface chemistry play dominant roles in interpreting the behavior of clays and plastic silts, particle size is an important factor in understanding sedimentation behavior, hydraulic conductivity, compressibility, consolidation rate, and erosion or transport potential.

In sedimentation-based PSD analysis, the reported particle size is an equivalent diameter inferred from settling behavior rather than a direct measurement of the true geometric dimensions of each particle. Nevertheless, the resulting distribution remains an important descriptor for comparing fine-grained soils and interpreting differences in their particle-size-dependent behavior.

The importance of PSD extends well beyond conventional soil classification. In construction materials engineering, aggregate gradation affects the performance of concrete, asphalt, base courses, filters, and drainage materials. In geoenvironmental engineering, PSD influences contaminant transport, sediment mobility, particle retention, and the migration of fines. In hydraulic and coastal engineering, sediment size strongly influences erosion, deposition, dredging behavior, beach nourishment performance, and sediment transport. In earthwork construction, PSD controls whether a borrow material satisfies project specifications and whether it can be compacted efficiently to achieve target density and performance. Thus, reliable PSD measurement is needed across geotechnical, geoenvironmental, transportation, coastal, mining, and materials engineering.

Because PSD enters so many engineering decisions, the accuracy and resolution of PSD measurements are consequential. A PSD curve is often interpreted through characteristic particle sizes and gradation coefficients, but those values depend on how well the complete distribution is measured. Sparse or inaccurate PSD data may lead to misleading interpolation between measured points, erroneous classification, inaccurate estimates of permeability or gradation coefficients, and

poor assessment of fines content. This is especially important for soils with broadly graded, gap-graded, or otherwise irregular distributions. PSD determination should therefore not be regarded as a simple routine measurement of secondary importance. Rather, it is a foundational soil characterization task whose accuracy directly affects the reliability of subsequent geotechnical interpretation, design, and construction decisions.

1.1 Determination of Particle Size Distribution of Sands

In geotechnical engineering, sand-sized particles are defined as particles ranging from 0.075 mm to 4.75 mm according to the Unified Soil Classification System ASTM D2487-17 (ASTM 2017). Because particles within this size range are sufficiently large to be mechanically separated by woven-wire openings, the particle size distribution of sands is determined by mechanical sieve analysis. Sieve analysis remains the most established reference method for sand PSD determination because it is standardized, conceptually simple, and mass-based.

Mechanical sieve analysis is standardized for sand and has long served as a conventional reference procedure for sand-sized granular materials in geotechnical engineering. The method is based on a simple physical separation principle: a dry specimen of known mass is passed through a series of sieves with progressively smaller openings, and the mass retained within each size interval is used to determine the PSD. For sands, the relevant size interval is bounded by the No. 4 sieve opening of 4.75 mm and the No. 200 sieve opening of 0.075 mm, corresponding to the full ASTM sand-size range. The standard sieve numbers, standard sieve sizes specified in ASTM E11-24 (ASTM 2024), and corresponding sand-type subdivisions within the ASTM sand-size range (ASTM 2017) are summarized in Table 1.1.

Table 1.1: Standard Sieve Designations and Sand-Size Subdivisions.

Standard Sieve Number	Standard Size (mm)	Sand-Size Subdivision
No. 4	4.75	Coarse Sand
No. 5	4.00	
No. 6	3.35	
No. 7	2.80	
No. 8	2.36	
No. 10	2.00	
No. 12	1.70	Medium Sand
No. 14	1.40	
No. 16	1.18	
No. 18	1.00	
No. 20	0.850	
No. 25	0.710	
No. 30	0.600	
No. 35	0.500	
No. 40	0.425	
No. 45	0.355	Fine Sand
No. 50	0.300	
No. 60	0.250	
No. 70	0.212	
No. 80	0.180	
No. 100	0.150	
No. 120	0.125	
No. 140	0.106	
No. 170	0.090	
No. 200	0.075	

In a conventional sieve analysis, according to ASTM C136/C136M-19 (ASTM 2019), a representative specimen is first obtained and reduced to an appropriate testing mass. The specimen is then dried to constant mass, in an oven maintained at 110 ± 5°C, so that the resulting PSD is calculated on a dry-mass basis. A set of sieves is selected according to the particle-size range of interest and the level of gradation detail required. The sieves are nested in descending order of

opening size, with the largest opening at the top, progressively smaller openings below, and a pan at the bottom to collect particles passing the smallest sieve.

The dried specimen is placed on the top sieve, and the sieve stack is shaken using a mechanical sieve shaker, as shown in Fig. 1.1. During agitation, particles repeatedly encounter the sieve openings while bouncing, tumbling, and rotating into different orientations. Particles pass through openings larger than their effective sieve-equivalent dimensions and are retained on the first sieve whose opening is too small for them to pass. In this way, the specimen is separated into discrete size fractions ranges. To obtain reliable separation, the mass retained on any individual sieve must be limited so that particles have sufficient opportunity to reach the mesh openings during the sieving process. Otherwise, sieve overloading can prevent smaller particles from passing through the mesh and bias the resulting PSD. When necessary, overloading may be reduced by adding intermediate sieves, splitting the specimen into multiple portions, or using sieves with larger frame dimensions.

After sieving, the mass retained on each sieve and in the pan is measured. The total recovered mass is checked against the original dry specimen mass to ensure that material loss during testing is acceptably small. The cumulative percentage retained and cumulative percentage passing each sieve are then calculated relative to the original dry mass. The PSD is plotted as percent finer by mass versus sieve opening size on a semilogarithmic scale. Characteristic particle sizes such as D_{10}, D_{30}, D_{50}, D_{60}, together with gradation indices such as the coefficient of uniformity C_u and coefficient of curvature C_c, can then be obtained from the plotted distribution and used for soil classification and engineering interpretation.

Although sieve analysis is the standard method for sand PSD determination, it has several known limitations. The procedure is labor-intensive and time-consuming because the sieve stack must be assembled and mechanically shaken, retained material must be weighed on each sieve, and the sieves must be cleaned after each test. The method also requires laboratory equipment such as an oven, sieve stack, pan, balance, and mechanical sieve shaker. The sieve shaker generates noise and vibration, and fine particles can become airborne during handling and shaking. In addition, the woven-wire mesh of the sieves is susceptible to clogging, deformation, and tearing, particularly when many tests are performed or when sieves are overloaded such as by very mono-sized sand specimens. These limitations become especially important when a large number of

PSDs are required for construction quality control, borrow-material evaluation, sediment mapping, or large-scale site characterization.

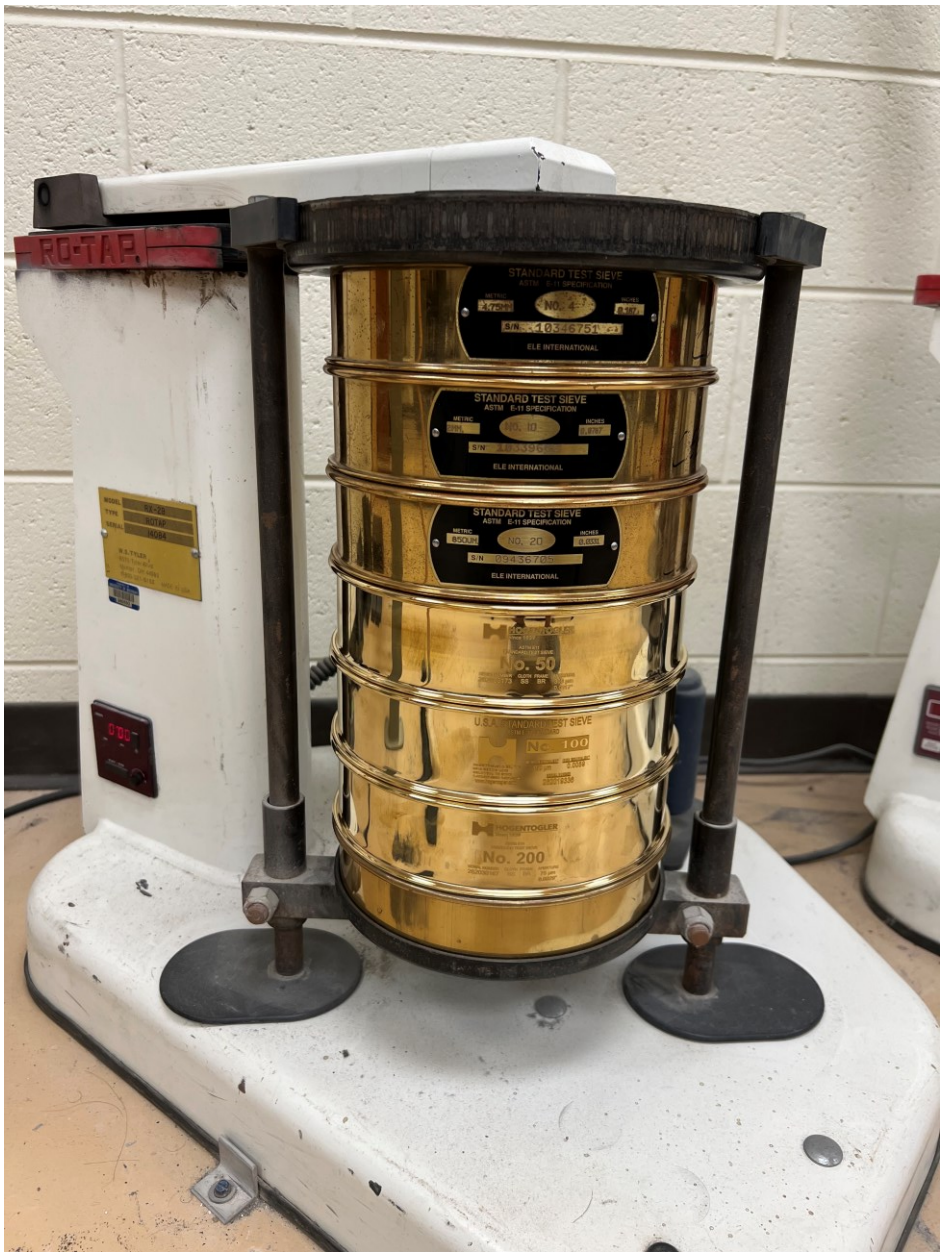


Figure 1.1: Sieve stack mounted in a shaker for sieve analysis.

Another limitation of sieve analysis is that it yields relatively sparse data. A sieve test gives the mass fraction passing or retained at selected sieve openings, but it does not measure the distribution between successive sieve sizes. A smooth PSD curve drawn through sieve data points

is therefore an interpolation rather than a continuous measurement. This limitation is particularly important for broadly graded, gap-graded, or irregularly graded sands, for which the true distribution between two neighboring sieve openings may deviate from an assumed smooth curve. Finally, because sieve analysis relies on repeated mechanical shaking, weak, friable, porous, or highly angular particles may undergo abrasion or degradation during the test, especially if prolonged shaking is required. Such particle breakdown can generate additional finer fragments and shift the measured PSD toward apparently finer sizes. These multiple issues and limitations have motivated the development of alternative PSD methods that do not rely on mechanical separation by shaking.

To overcome the limitations of mechanical sieving, Ohm and Hryciw (2013) developed the translucent segregation table (TST) test, in which coarse sand and gravel particles are segregated by size on an inclined, back-lit translucent table instead of being mechanically separated by shaking through a stack of sieves. The particles are then photographed from above and digitally separated using watershed segmentation; their image-based dimensions are then interpreted using an ellipsoidal particle idealization to compute sieve-equivalent opening sizes. The resulting PSDs showed generally good agreement with conventional sieve results.

This progression from mechanical sieving to image-based analysis was further extended in the SedImaging test developed by Ohm and Hryciw (2014). Unlike the TST test, in which particles are segregated on an inclined translucent table before image acquisition, SedImaging uses sedimentation itself as the size-sorting mechanism. A soil–water mixture is released into a water-filled column, where particles settle at different velocities and become spatially sorted by size before accumulating in a glass-windowed sediment accumulator. The resulting soil assembly is then photographed and analyzed incrementally with height using a wavelet transformation approach. Because the wavelet-based image analysis requires particles within each local image region to have a very narrow size range, the prior segregation by sedimentation is essential. The wavelet index obtained from each local image region is converted to pixels per particle diameter using a calibration developed from images of pre-sieved sands. SedImaging was developed for particles between 0.075 and 2.0 mm, could also estimate the percentage of fines, and produced PSDs that agreed reasonably well with sieve results while yielding far more data points than conventional sieve analysis.

Following the original SedImaging system, subsequent work focused on making sedimentation-based image analysis more practical, more field-deployable, and applicable to a broader range of sand sizes. Ventola and Hryciw (2019) developed FieldSed as a field-portable version of the SedImaging hardware. FieldSed retained the same fundamental principle: particles are sorted by sedimentation through a water-filled column, the deposited soil assembly is photographed, and Haar wavelet transform (HWT) analysis is used to convert image texture into sieve-equivalent particle sizes. However, the system replaced the large laboratory apparatus with a lightweight transparent acrylic column, allowed four-sided imaging of the deposited specimen, required smaller specimen masses, and enabled parallel testing of multiple specimens. Its field applicability was demonstrated using Kalamazoo River sediments, where more than 100 PSDs were generated in a riverside field laboratory and quality-control tests showed repeatable results comparable to conventional sieve analyses (Ventola and Hryciw 2019; Ventola et al. 2020b).

This development was further advanced by the Sed360 system (Ventola and Hryciw 2023a), which improved image acquisition and automation while retaining sedimentation as the size-sorting mechanism. Sed360 uses a cylindrical sedimentation column mounted on a precision rotating stage; as the column rotates, images are captured at fixed angular increments and narrow vertical strips are stitched into an unwrapped 360° image of the sedimented soil surface. This design increased the surface area available for image analysis, reduced manual intervention, and enabled better characterization of larger sand particles than was possible with the earlier square-column systems. Because the expanded Sed360 image geometry made it possible to analyze a much wider particle-size range, the fixed-size HWT analysis windows used in earlier SedImaging methods became insufficient. Ventola and Hryciw (2023b) therefore developed an autoadaptive HWT procedure in which larger analysis windows are selected for coarser particles near the base of the sedimented column and progressively smaller windows are selected for finer particles toward the top. With an updated calibration between wavelet index and particle size, the autoadaptive method produced PSDs across the full sand-size range of 0.075–4.75 mm with strong agreement to sieve results.

Taken together, these studies show a clear progression from mechanical size sorting to sedimentation-assisted optical granulometry. In sieve analysis, particle separation is achieved mechanically by shaking particles through a stack of sieves. In the TST test, particles are segregated on an inclined translucent table before image analysis. In SedImaging, FieldSed, and

Sed360, sedimentation itself becomes the sorting mechanism, after which the resulting soil assembly is interpreted optically. However, despite these advances, the SedImaging family of methods remains fundamentally dependent on optical image acquisition and image-based particle-size interpretation. Particle sizes are not measured directly, but are inferred from image texture through wavelet-based indices that must be calibrated to sieve-equivalent particle sizes. Because these calibrations were developed from pre-sieved soils, the resulting particle sizes are ultimately tied to sieve-defined size scales, and site-specific calibration may be needed when close agreement with sieve results is required for repeated quality-control testing. In addition, soils with unusual particle textures, intraparticle color variations, rough surfaces, or nonstandard material origins may cause image-based methods to deviate from sieve results because optical texture can be interpreted as smaller particle-scale features (Ohm and Hryciw 2014). The reliance on camera-based measurement also introduces practical requirements related to image resolution, magnification, lighting, focus, cropping, and image stitching. These issues became more evident as Sed360 expanded the analyzed size range: the original calibration had to be updated, fixed HWT analysis windows became inadequate, and autoadaptive window sizing was required to handle the full sand-size range (Ventola and Hryciw 2023b).

Thus, although sedimentation-assisted image analysis represents a substantial advance over mechanical sieving, its practical implementation still depends on specialized optical measurement conditions, image-processing decisions, and calibration relationships that connect image texture to sieve-equivalent particle size. A simpler sedimentation-based approach is therefore desirable—one that retains the key advantage of sedimentation-induced size sorting, but determines the PSD from direct, and easily measurable physical quantities. Ideally, such a method would require minimal equipment, avoid sensitivity to lighting, focus, magnification, cropping, and image-stitching, and reduce dependence on extensive empirical calibration for different soils or testing environments. This need motivates the pressure-monitored sedimentation methods developed in this dissertation, particularly the *u*-Sed and m-Sed tests presented in Chapters 3 and 4, in which the distribution of particle mass during settling is detected through water-pressure measurements and used to develop nearly continuous PSDs.

1.2 Determination of Particle Size Distribution of Fines

For fine-grained soils (silts and clays), the particle size distribution is commonly determined by sedimentation analysis rather than mechanical sieving. Because particles smaller

than the No. 200 sieve opening are too fine to be separated efficiently by conventional woven-wire sieves, their sizes are inferred from their settling velocities in a fluid. The hydrometer analysis has long served as the standard sedimentation-based method for determining the gradation of the fine-grained fraction of soils. In ASTM D7928 (ASTM 2021), the hydrometer method is specified for determining the particle-size distribution of material finer than the No. 200 sieve opening (0.075 mm), and its results may be combined with sieve analysis to obtain a complete gradation curve when both coarse and fine fractions are present.

ASTM D7928 permits either a 151H or 152H hydrometer. The 151H hydrometer measures the specific gravity of the suspension relative to distilled water, whereas the 152H hydrometer, as shown in Fig. 1.2, is commonly used because its scale is related to the mass concentration of soil particles remaining in suspension. A conventional hydrometer test setup is shown in Fig. 1.3. The test is performed in a 1000-mL sedimentation cylinder containing a dispersed soil-water suspension. The hydrometer is inserted into the suspension at prescribed elapsed times, and its reading is used to estimate the concentration of particles still remaining in suspension at the hydrometer's effective depth.

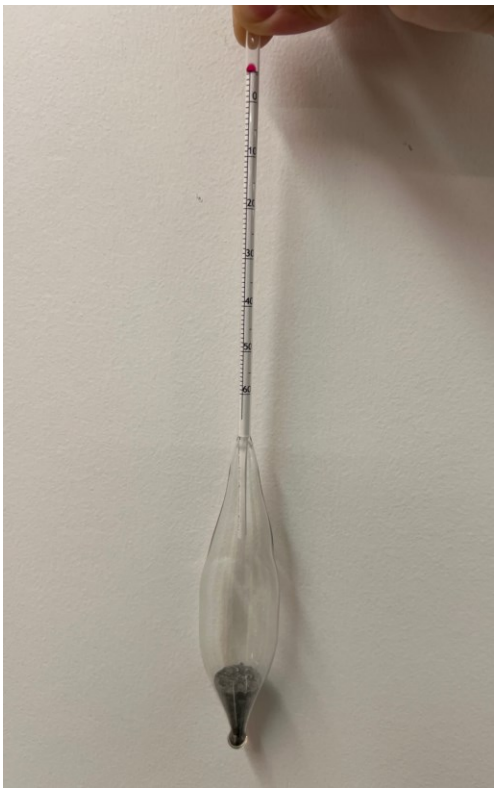


Figure 1.2: ASTM 152H hydrometer used for fine-grained soil sedimentation analysis.



Figure 1.3: Hydrometer analysis of a dispersed fine-grained soil suspension.

The theoretical basis of hydrometer analysis is Stokes' law (Stokes 1851). Larger particles settle faster than smaller particles; therefore, after a soil suspension is homogenized and then allowed to stand, particles become sorted by size. At a given elapsed time, particles larger than a certain size are assumed to have settled below the effective measurement depth of the hydrometer, while smaller particles remain in suspension above that depth. The hydrometer reading at that time

provides an estimate of the concentration of suspended particles, and Stokes' law is used to compute the corresponding particle diameter from the elapsed time and effective fall distance.

It is important to emphasize that the particle diameter obtained in hydrometer analysis is not the true geometric diameter of a silt or clay particle. Rather, it is an equivalent spherical diameter: the diameter of a smooth sphere, with the assumed particle density, that would settle at the same terminal velocity as the soil particle under the same fluid conditions. This interpretation is fundamentally different from sieve analysis. In sieve analysis, particle size is defined by physical passage through a square mesh opening. In hydrometer analysis, particle size is defined indirectly from settling velocity. Thus, the reported "silt-size" or "clay-size" diameter is a sedimentation-equivalent size, not a direct measurement of the actual length, width, thickness, or projected area of an individual particle. This distinction is especially important for clay particles, which are platy rather than spherical, and for fine particles whose mineral density, shape, surface chemistry, and degree of flocculation can influence settling behavior.

Hydrometer analysis begins with preparation of a representative specimen. The specimen is mixed with distilled or demineralized water and a dispersing agent, commonly sodium hexametaphosphate, to prevent fine particles from coalescing or flocculating. The slurry is dispersed, transferred to a sedimentation cylinder, and diluted to a prescribed total volume, typically 1000 mL. Before sedimentation begins, the suspension is thoroughly agitated to create a uniform initial concentration throughout the cylinder. Once mixing stops, the timer is started and particles begin settling under gravity. Hydrometer readings are then taken at prescribed elapsed times, commonly from 1 min to 1440 min, with additional readings possible when greater resolution is desired. Temperature measurements are also required because fluid density and viscosity affect both hydrometer readings and calculated settling velocities.

Each hydrometer reading must be corrected before it can be used to calculate the PSD. The measured reading is affected by the temperature of the suspension, the presence of dispersant, the hydrometer meniscus, and the effective depth associated with the hydrometer bulb. The effective depth is the fall distance used in the Stokes' law calculation. It depends on the position of the hydrometer's center of buoyancy relative to the suspension surface. After these corrections are applied, the hydrometer reading gives the percentage of the sedimentation specimen still in suspension at that elapsed time. The corresponding particle diameter is computed from Stokes'

law using the effective depth and elapsed time. Repeating this process for all hydrometer readings produces a set of discrete points on the fine-grained portion of the PSD curve.

Although hydrometer analysis is the standard method for fine-grained soil PSD determination, its implementation has several practical and interpretive limitations. First, the test is inherently manual and operator-dependent. Hydrometer readings must be taken at selected elapsed times, and each reading requires the operator to insert the hydrometer, wait for it to stabilize, read the stem at the meniscus, and remove and clean the hydrometer. Consequently, the accuracy of the test depends strongly on the operator's timing, handling technique, and ability to read the hydrometer consistently. Because readings are taken only at prescribed times, the resulting PSD is represented by a limited number of discrete data points rather than by a continuous record of the sedimentation process. ASTM D7928, for example, specifies readings at selected times such as 1, 2, 4, 8, 15, 30, 60, 240, and 1440 min.

A second limitation is that the hydrometer itself physically enters the suspension. Repeated insertion and removal can disturb the settling particles and the developing concentration profile, particularly during the early portion of the test when concentration gradients change rapidly. ASTM D7928 therefore specifies careful insertion and removal procedures, but the need to repeatedly place a floating instrument into the suspension remains an inherent feature of the method. In addition, hydrometer readings can be difficult because the stem must be clean and dry, the hydrometer should not bob or rotate, and the reading is taken at the top of the meniscus. Foam at the suspension surface can further obscure the meniscus and hinder reliable readings. These issues make the test susceptible to reading errors by inexperienced laboratory personnel.

These limitations have motivated the development of automated alternatives to conventional hydrometer analysis. An improved method should preserve the well-established sedimentation basis of fines PSD determination, but reduce manual operation, avoid repeated intrusion into the suspension, minimize meniscus- and foam-related reading errors, and generate a higher-resolution record of the sedimentation process.

One early attempt to automate sedimentation-based PSD determination was the C-GRAINS method developed by Zhang and Tumay (1995) for silts. They utilized a differential pressure transducer to measure the difference in pressure between two elevations in a sedimentation column. From this difference, the average soil concentration in the zone between the two elevations could be computed. They assumed that this was the concentration at the

elevation of the lower-pressure measurement port (i.e., the upper port). By making the separation distance between the two elevations as small as possible (while still being able to accurately detect a pressure difference), there would be less inherent error in the approximation. However, the reported PSDs did not show satisfactory agreement with those obtained from hydrometer analysis.

More recently, Durner et al. (2017) proposed the Integral Suspension Pressure (ISP) method, which deduces the PSD of fines by measuring a single-point pressure at a fixed depth within a soil suspension. It then applies an integral evaluation approach that reconstructs the continuous PSD curve by matching simulated and observed pressure data. While conceptually advanced, its inverse-model formulation is complex: an assumed PSD must be used to forward-calculate the pressure response, and multiple fitting parameters are iteratively adjusted until the simulated and measured pressure histories converge. Because the PSD is inferred through inverse fitting of multiple coupled parameters rather than calculated directly from pressure readings, the data reduction procedure can be opaque for many users.

In addition, because the ISP method relies on a single pressure measurement, its results are vulnerable to fluid-level-induced zero-offset errors, including apparent baseline shifts caused by evaporation or by the delayed return of water droplets retained on the cylinder wall after mixing. For example, a mere 1 mm decrease in the suspension surface level due to evaporation translates to a decrease in absolute pressure of approximately 9.8 Pa. In the ISP framework, this reduction is erroneously interpreted as the settling of approximately 4 g of soil particles past the measurement depth. This results in a substantial error of up to 17.5% in the computed percent finer by weight. Durner and Iden (2021) recognized the post-mixing drainage of thin water droplets from the cylinder walls as a source of bias in the early pressure record. The user manual (METER Group 2026) for this system confirms that this is a source of error, and an attempt is made to compensate for it by subtracting an empirical drainage function from the pressure recording. However, the amount, distribution, and return timing of retained water droplets will vary from one test to the next; therefore, the same fixed empirical correction cannot accurately eliminate this baseline error in every test. More critically, the integral evaluation approach inherent to the ISP method causes discrete measurement errors to accumulate, which progressively skews the derived PSD curve. Finally, the ISP protocol requires the pressure sensor to be inserted into the suspension after it has been homogenized, which disrupts the free settlement of soil particles.

Other automated or quasi-continuous sedimentation methods have also been explored (Nemes et al. 2002; Kovács et al. 2004; Kaszubkiewicz and Papuga 2023), but they generally do not cancel baseline disturbances associated with evaporation or post-mixing wall drainage; moreover, their data reduction requires graphical, derivative-based, or fitting-based interpretation rather than direct conversion of fixed-port measurements into independent PSD data points.

These limitations motivate the Delta-Sed test, hereafter denoted as the Δ-Sed test for brevity, developed in this dissertation, which retains the sedimentation framework of hydrometer analysis, but determines suspension concentration from differential pressure between two fixed sidewall ports, allowing each pressure reading to be converted directly into an independent PSD data point for fine-grained soils.

1.3 Research Objectives and Dissertation Organization

The overarching objective of this dissertation is to develop and validate a family of complementary sedimentation-based testing systems for determining particle size distributions of sands and fine-grained soils from water-pressure response during particle settling. Across all three systems, the two components of a PSD data point are determined independently: particle size is inferred from settling velocity, whereas the corresponding percent finer is determined from the measured hydraulic pressures. Although the systems share this general framework, sands and fine-grained soils require different initial conditions and different relationships between the measured response and percent finer. The research objectives are therefore presented separately for sands and fine-grained soils in Sections 1.3.1 and 1.3.2, respectively, followed by an overview of the dissertation structure in Section 1.3.3.

1.3.1 Research Objectives for Sands

The primary research objective for sand-sized soils is to develop and validate sedimentation-based alternatives to conventional sieve analysis that can generate high-resolution PSDs without mechanically separating a specimen through a stack of sieves or optically sizing individual particles. The two systems developed for this purpose—the *u*-Sed and m-Sed tests—share the same fundamental measurement framework. A dry sand specimen is introduced near the top of a water-filled sedimentation column, where differential settling causes coarser particles to reach a fixed measurement elevation before finer particles. The change in water pressure at the port elevation reflects the mass of particles remaining above it. Normalizing the instantaneous

response between the initial and final measurement stages provides the fraction of specimen mass remaining above the measurement elevation and, consequently, the percent finer by mass at each elapsed time. Independently, the settling time and travel distance determine the corresponding particle settling velocity, which is converted to a sieve-equivalent particle size using an appropriate settling-velocity model.

Within this framework, the objective of the *u*-Sed research is to establish the theoretical and experimental basis for determining sand PSDs from electronically recorded water-pressure measurements. Specific objectives are to derive the governing relationships among water pressure, particle mass, percent finer, soil specific gravity, and specimen mass; implement suitable settling-velocity models for particle-size determination; and evaluate the accuracy, repeatability, and practical limitations of the resulting PSDs through comparisons with conventional sieve analyses for sands spanning the ASTM sand-size range.

Building on the *u*-Sed framework, the objective of the m-Sed research is to develop a field-portable alternative that replaces the electronic pressure transducer and data acquisition system with a simple manometer. This requires establishing the relationships between changes in manometer water level, particle mass remaining above the measurement port, percent finer, and soil specific gravity while accounting for fluid exchange between the sedimentation column and the manometer. Additional objectives are to identify a manometer configuration with sufficient response and measurement stability, validate the resulting PSDs against both sieve and *u*-Sed results, and assess the repeatability and practical applicability of the system. The m-Sed test is thereby intended to retain the accuracy and high resolution of the *u*-Sed concept while eliminating the need for electronic pressure sensing and external electrical power for water pressure measurement.

1.3.2 Research Objectives for Fine-Grained Soils

The research objective for fine-grained soils is to develop and validate an automated alternative to conventional hydrometer analysis using a measurement framework appropriate for the sedimentation of silts and clays. The sand-based framework cannot be applied directly to fines because it requires particles to be released near the top of the column and to settle individually. Fine particles cannot be introduced in this manner: dry fines are difficult to disperse, whereas a concentrated slurry tends to descend in unstable plumes rather than settle as individual particles. Consequently, sedimentation analysis of fines must begin with a fully dispersed and spatially

uniform suspension, as is done in conventional hydrometer analysis. Under this condition, percent finer is determined from the time-dependent soil concentration at a specified settling depth, while the corresponding particle size is inferred from settling velocity using Stokes' law.

Within this framework, the objective of the Δ-Sed research is to establish the theoretical and experimental basis for determining fine-grained soil PSDs from differential-pressure measurements between two fixed sidewall ports. Specific objectives are to derive the relationship between differential pressure and the average soil concentration within the measurement interval; evaluate the use of this interval-averaged concentration to approximate the local concentration at the midpoint; relate the resulting concentration to percent finer and the corresponding Stokes-equivalent particle diameter; and optimize the measurement depths and port spacing through numerical simulation. Further objectives are to use the differential-pressure configuration to reject common-mode pressure changes caused by variations in suspension-surface elevation, validate the accuracy and repeatability of the resulting PSDs through comparisons with conventional hydrometer analyses, and establish the recommended particle-size range and practical limitations of the test. Because each differential-pressure measurement is interpreted independently, the Δ-Sed test is also intended to generate high-resolution PSDs without global inverse fitting of the complete pressure record.

Taken together, the *u*-Sed and m-Sed tests address sand-sized particles, whereas the Δ-Sed test addresses the fine-particle range. The *u*-Sed and m-Sed systems are interchangeable while the Δ-Sed is complementary to them. Collectively, they establish a unified sedimentation-based framework for determining high-resolution PSDs over the particle-size range investigated in this dissertation while addressing many of the operational and measurement limitations of conventional sieve and hydrometer analyses.

1.3.3 Dissertation Organization

This dissertation is organized into six chapters.

Chapter 1: establishes the engineering significance of soil particle size distribution, reviews conventional and alternative methods for determining the PSDs of sands and fines, and identifies the methodological limitations and research objectives addressed in this dissertation.

Chapter 2: provides the theoretical basis for determining particle size from settling velocity in this dissertation. It reviews the development of particle settling-velocity models applicable across different settling regimes, with particular emphasis on the models adopted in this dissertation: Stokes' law (Stokes 1851) for fine-grained soils and the models proposed by Ahrens (2000) and Jiménez and Madsen (2003) for sands.

Chapter 3: presents the development and validation of the *u*-Sed test for determining high-resolution sand PSDs from electronically recorded water-pressure measurements during sedimentation. It describes the system hardware, pressure-time response, governing equations, and testing procedure, including the determination of percent finer, particle size, soil specific gravity, and specimen mass. The method is evaluated using sands spanning the ASTM sand-size range, followed by analyses of repeatability, measurement sensitivity, and comparisons with conventional and alternative PSD methods.

Chapter 4: presents the m-Sed test, which extends the *u*-Sed measurement framework by replacing the electronic pressure transducer and data acquisition system with a simple manometer. The chapter describes the system hardware and pressure stages, derives the governing equations while accounting for fluid exchange between the sedimentation column and manometer, and evaluates the effects of manometer material and tube diameter. The resulting PSDs are validated against both sieve and *u*-Sed results, and the repeatability of the method, the influence of particle shape, and other factors affecting measurement accuracy are examined.

Chapter 5: develops the Δ-Sed test for determining the PSDs of fine-grained soils from differential-pressure measurements between two fixed sidewall ports. The chapter first establishes the sedimentation theory for an initially uniform suspension and derives the relationships among differential pressure, suspension concentration, percent finer, and particle size. Numerical simulations are then used to evaluate the spatial-averaging approximation and optimize the measurement depths and port spacing. The effects of specimen characteristics and suspension temperature are examined, after which the system hardware and experimental results are presented. The method is evaluated through comparisons with conventional hydrometer analyses, repeatability and sensitivity analyses, and an assessment of the recommended particle-size range.

Chapter 6: summarizes the principal findings from the development and validation of the *u*-Sed, m-Sed, and Δ-Sed tests. It then identifies directions for future research, including scaling of the *u*-Sed and m-Sed systems for larger specimens, reduction of the Δ-Sed test duration, integration of image analysis for particle-shape characterization, and development of a unified sedimentation test for sands and fines.

Chapter 2 Particle-Size Determination Using Settling Velocity Models

The sedimentation-assisted image-analysis methods reviewed in Chapter 1 use differential settling primarily to sort particles before their dimensions are determined optically. In the *u*-Sed, m-Sed, and Δ-Sed tests developed in this dissertation, settling behavior instead provides the basis for particle-size determination itself. The measured pressure response is used to determine the percent finer, while the elapsed settling time and corresponding travel distance provide the particle settling velocity. A suitable settling-velocity relationship is then used to determine the particle size associated with each percent-finer measurement, thereby generating the PSD.

Settling-velocity models are conventionally applied as forward relationships: particle size, particle density, fluid properties, and, when required, particle-shape characteristics are specified to predict terminal settling velocity. Their application in the systems developed in this dissertation requires the inverse operation. Settling velocity is determined experimentally, and the governing relationship is solved for the corresponding particle size. The selection of an appropriate model is therefore central to the accuracy and interpretation of the resulting PSD. Fine particles generally settle within the viscous regime represented by Stokes' law, whereas sand-sized particles extend into transitional and turbulent regimes in which fluid inertia and particle morphology become increasingly important.

This chapter establishes the settling-velocity framework used for particle-size determination throughout the dissertation. It first presents the theoretical basis, assumptions, and applicability of Stokes' law and explains its use in determining the equivalent spherical diameters reported by conventional hydrometer analysis and the Δ-Sed test. The subsequent development of settling-velocity relationships beyond the Stokes regime is then reviewed, including the extension from ideal spheres to natural, non-spherical sediment particles. Particular attention is given to the models proposed by Ahrens (2000) and Jiménez and Madsen (2003), which are adopted for determining sieve-equivalent particle sizes in the *u*-Sed and m-Sed tests. Finally, the chapter explains how the selected relationships are applied to convert measured settling velocities into particle sizes consistent with the corresponding conventional reference methods.

***

Portions of this chapter are adapted from Zhang and Hryciw (2025), which described the application of particle settling-velocity models to particle-size determination in a sedimentation-based testing system.

2.1 Development of Particle Settling-Velocity Models

The development of particle settling-velocity models can be traced at least to Stokes's law (Stokes 1851). Stokes derived the drag force acting on a sphere settling slowly through a viscous fluid. When combined with the force equilibrium of a freely settling sphere, this result yields the classical Stokes settling-velocity relationship. Although limited to spherical particles settling within the creeping-flow regime, Stokes' law established the fundamental relationship among settling velocity, particle size, particle–fluid density difference, and fluid viscosity. It therefore provided the theoretical foundation from which subsequent settling-velocity models were developed.

Consider an isolated, rigid sphere of diameter *D* settling through an initially stationary fluid. The particle is subjected to its downward gravitational force, an upward buoyant force, and a drag force opposing its motion. Immediately after release, the particle accelerates under the net effect of its weight and buoyancy. As the particle accelerates, the drag force increases until it balances the particle's submerged weight—the difference between its weight and the buoyant force. At this condition, the net force on the particle becomes zero and the particle settles at a constant terminal velocity.

Within the low-Reynolds-number limit considered by Stokes, the viscous drag force acting on the sphere is:

$$F_D = 3\pi\mu D v \tag{2.1}$$

where F_D is the drag force, μ is the dynamic viscosity of the fluid, and v is the terminal settling velocity. The net downward force resulting from the difference between the gravitational and buoyant forces is:

$$F_G - F_B = \frac{\pi D^3}{6} \times \left(\rho_S - \rho_f\right) g \tag{2.2}$$

where ρ_s and ρ_f are the densities of the particle and fluid, respectively, and g is the acceleration due to gravity. At terminal velocity, the drag force is equal to this net downward force:

$$3\pi\mu D v = \frac{\pi D^3}{6}(\rho_s - \rho_f) g \tag{2.3}$$

Solving Equation (2.3) for the settling velocity gives:

$$v = \frac{(\rho_s - \rho_f) g D^2}{18\mu} \tag{2.4}$$

Equation (2.4) shows that, under Stokes settling conditions, terminal settling velocity is proportional to the square of particle diameter and to the density difference between the particle and the surrounding fluid. The strong dependence of settling velocity on particle diameter produces the size-dependent sorting that forms the basis of sedimentation analysis.

The applicability of Stokes' law is governed primarily by the particle Reynolds number:

$$Re_p = \frac{\rho_f v D}{\mu} \tag{2.5}$$

which represents the ratio of inertial to viscous forces in the flow surrounding the particle. Stokes' law corresponds to the creeping-flow regime, in which $Re_p \ll 1$, viscous forces dominate, and fluid-inertia effects are negligible. Under these conditions, the drag force varies linearly with settling velocity. More specifically, ISO 13317-1 (ISO 2024) recommends that the particle Reynolds number not exceed 0.25 if the error in the calculated Stokes diameter is to remain within approximately 3%.

The derivation of Stokes' law and its application to sedimentation analysis require idealizations at both the single-particle and suspension scales. At the single-particle scale, the particle is represented as a rigid, smooth sphere settling at terminal velocity through a quiescent, incompressible Newtonian fluid having constant density and viscosity. The dimensions of the sedimentation vessel must be sufficiently large relative to the particle diameter for wall and end effects to be negligible. Although a particle undergoes a brief period of acceleration after release, its terminal velocity is assumed to be attained over a time and distance that are negligible relative to those involved in the sedimentation measurement.

Additional assumptions are required when the single-particle relationship is applied to a soil suspension. The suspension must be sufficiently dilute and fully dispersed for the particles to settle independently, without significant collisions, flocculation, interparticle interference, or hindered-settling effects. The particles are also assumed not to undergo physical or chemical changes in the suspending fluid. When a single particle-density value is used to interpret the entire sedimentation record, the effective particle density is further assumed to be uniform and independent of particle size.

Because natural silt and clay particles are generally non-spherical, the diameter determined from Stokes' law does not represent a direct measurement of particle geometry. Instead, it is an equivalent spherical diameter: the diameter of a sphere having the same density and terminal settling velocity as the actual particle in the same fluid under creeping-flow conditions. The particle size obtained from Stokes' law is therefore a sedimentation-equivalent size rather than a geometric dimension of the particle.

In civil engineering, conventional hydrometer analysis provides a direct application of Stokes' law to particle-size determination. For a particle settling through an effective distance L over an elapsed time t, its settling velocity is expressed as $v = L/t$. Substitution of this relationship into Equation (2.4) gives:

$$D = \sqrt{\frac{18\mu L}{(\rho_s - \rho_f)gt}} \tag{2.6}$$

During a hydrometer test, the hydrometer reading is used to determine the concentration, and consequently the mass percentage, of particles remaining in suspension at a specified elapsed time and effective measurement depth. Equation (2.6) then provides the corresponding equivalent spherical diameter. Thus, the hydrometer measurement determines the percent finer, whereas Stokes' law establishes the particle size associated with that measurement.

The applicability of Stokes' law is not governed by particle diameter alone, but by the particle Reynolds number, which also depends on settling velocity and the properties of the particle and fluid. As particle diameter and settling velocity increase, fluid-inertia effects become progressively more important and the creeping-flow assumption underlying Stokes' law is no longer satisfied. For quartz particles with a specific gravity of approximately 2.65 settling in water at 20°C, the criterion $Re_p = 0.25$ corresponds to a particle diameter of approximately 0.07 mm. Stokes' law therefore becomes progressively less accurate as particle size approaches and enters the sand-size range.

To extend the practical prediction of sphere settling velocity beyond the creeping-flow regime, Gibbs et al. (1971) conducted a systematic experimental investigation of the relationship between sphere size and terminal settling velocity. They measured the settling velocities in water of 216 glass spheres ranging from 50 to 5,000 μm in diameter. Because the size, density, and spherical geometry of the particles were accurately known, these measurements provided a

controlled data set covering the transition from viscous-dominated to inertia-influenced settling. Based on the experimental results, Gibbs et al. proposed the following empirical relationship:

$$v = \frac{-3\eta + \sqrt{9\eta^2 + gr^2\rho_f(\rho_s - \rho_f)(0.015476 + 0.19841r)}}{\rho_f(0.011607 + 0.14881r)} \tag{2.7}$$

where v is the terminal settling velocity; η is the dynamic viscosity of the fluid; g is the acceleration of gravity; ρ_f is the density of the fluid; ρ_s is the density of the sphere; and r is the sphere radius.

Within the experimentally investigated diameter range of 50–5,000 μm, the calculated settling velocities using Eq. (2.7) generally differed from the measured values by less than 2.5%. For spheres smaller than approximately 50 μm, Equation (2.7) produces results essentially identical to those obtained from Stokes' law. The Gibbs et al. relationship therefore extended sphere settling-velocity prediction well beyond the creeping-flow range. Nevertheless, because it was developed from smooth glass spheres, it did not explicitly account for the irregular shapes of natural sediment particles.

Subsequent researchers proposed numerous settling-velocity models applicable to natural, non-spherical sediments, including Hallermeier (1981), Dietrich (1982), van Rijn (1984), Cheng (1997), Ahrens (2000), Guo (2002), Jiménez and Madsen (2003), Camenen (2007), Bagheri and Bonadonna (2016), Song et al. (2017), and Waldschläger and Schüttrumpf (2019). These models account for the non-spherical characteristics of natural particles to varying degrees: some explicitly incorporate particle shape and roundness, whereas others represent typical natural-grain behavior implicitly through empirical calibration. Collectively, these progressively refined formulations have demonstrated good performance in predicting the settling velocities of sand and other natural sediments over broad ranges of particle size and flow regime.

Most settling-velocity relationships were developed as forward models in which particle size, particle density, fluid properties, and, where required, particle-shape characteristics are specified as inputs and terminal settling velocity is predicted as the output. They have been applied extensively in sedimentology and hydraulic and coastal engineering, where settling velocity is commonly required to describe sediment transport and deposition. In geotechnical engineering, however, these models have received comparatively limited attention and have been less commonly applied in reverse to determine sand particle size from a measured settling velocity.

For application to sand particle-size determination in this dissertation, the models proposed by Ahrens (2000) and Jiménez and Madsen (2003) were selected because they provide a favorable balance between computational simplicity and predictive accuracy. The Ahrens model provides a continuous relationship across laminar, transitional, and turbulent settling regimes without requiring an explicit particle-shape parameter. The Jiménez and Madsen model similarly applies across the sand-size range while also allowing particle shape and roundness to be considered. These two models are described in the following sections.

2.2 Ahrens (2000) Model

Ahrens (2000) reevaluated previously published experimental data for the settling of natural sediment particles and developed a single continuous relationship for predicting sediment fall velocity across laminar, transitional, and turbulent settling regimes. Using traditional geotechnical notation, the Ahrens equation is:

$$v = C_l \left(G_s \frac{\gamma_w}{\gamma_f} - 1 \right) g \frac{d^2}{\vartheta} + C_t \sqrt{\left(G_s \frac{\gamma_w}{\gamma_f} - 1 \right) g d} \tag{2.8}$$

where v is the particle fall velocity; d is the characteristic (sieve) diameter of the particle; ϑ is the kinematic viscosity of the fluid; g is the acceleration due to gravity; γ_w is the unit weight of pure water at 4°C; γ_f is the unit weight of fluid; C_l and C_t are the coefficients for the laminar and turbulent flow regimes, respectively.

As shown in Fig. 2.1, C_l dominates in the laminar regime (very fine sand and silt), C_t dominates in the turbulent regime (medium and coarse sand) and both contribute in larger fine sands. The coefficients shown in Fig. 2.1 are calculated as:

$$C_l = 0.055 \tanh[12A^{-0.59} \exp(-0.0004A)] \tag{2.9}$$

$$C_t = 1.06 \tanh[0.016A^{0.50} \exp(-120/A)] \tag{2.10}$$

in which A is the *Archimedes buoyancy index*:

$$A = \frac{\left(G_s \frac{\gamma_w}{\gamma_f} - 1 \right) g d^3}{\vartheta^2} \tag{2.11}$$

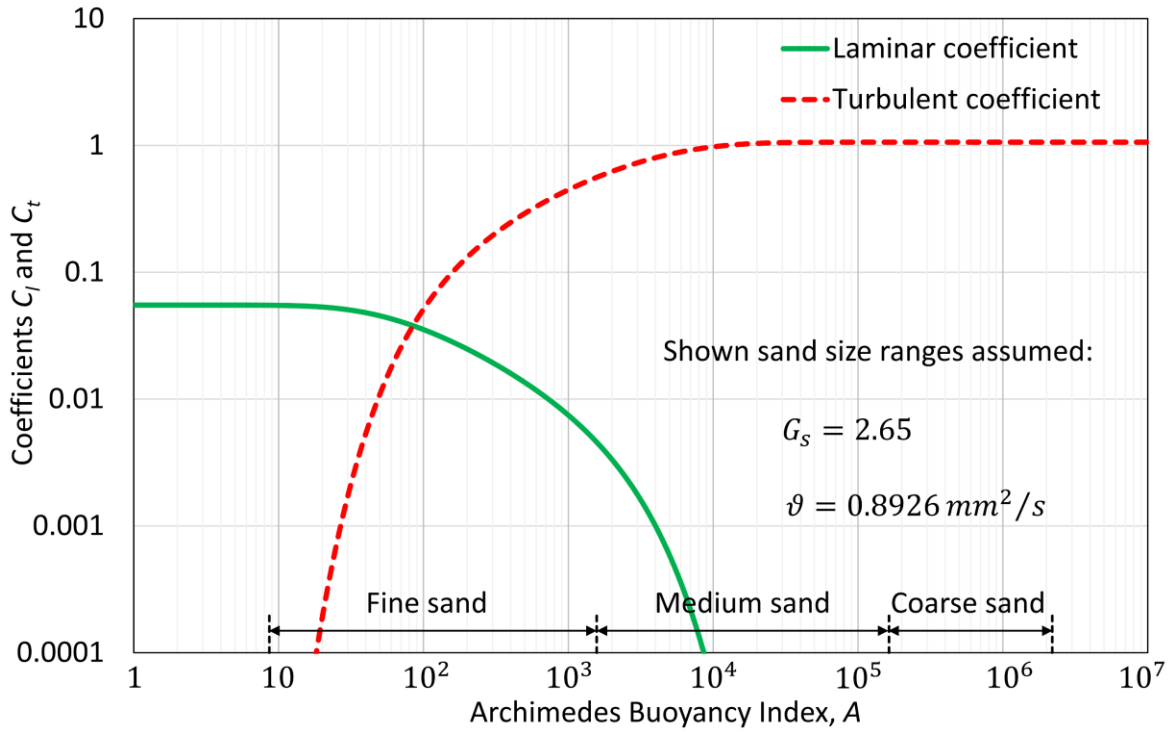


Figure 2.1: Turbulent and laminar flow coefficients for Ahrens' model.

An important advantage of the Ahrens model for particle-size determination is that its characteristic particle-size variable, *d*, is defined on a sieve-diameter basis. The particle size obtained by applying the model can therefore be compared directly with the particle sizes reported by conventional sieve analysis. The model also requires only particle specific gravity and fluid properties in addition to settling velocity, making it relatively simple to implement.

The principal limitation of the Ahrens model is that it does not explicitly account for particle shape or roundness. Particles having the same sieve diameter and specific gravity are assigned the same settling velocity regardless of differences in morphology. Ahrens developed the model for typical natural sands, which were characterized as somewhat angular rather than perfectly spherical. The model is therefore well suited to many natural sands but may be less representative of particles having strongly platy, elongated, or otherwise atypical shapes. The Jiménez and Madsen (2003) model described in the following section provides an alternative formulation in which particle shape and roundness are explicitly considered.

2.3 Jiménez and Madsen (2003) Model

Jiménez and Madsen (2003) developed a settling-velocity model applicable across the sand-size range while explicitly accounting for the effects of particle shape and roundness. Similar to the Ahrens (2000) model, the Jiménez and Madsen model provides a continuous relationship across different settling regimes. However, rather than representing all natural sands using a single empirical relationship, it incorporates particle morphology through two dimensionless coefficients. The model is expressed as:

$$v = \frac{(G_s-1)gd_N^2}{A_{JM}d_N^{3/2}\sqrt{(G_s-1)g}+4B_{JM}\vartheta} \tag{2.12}$$

The parameters A_{JM} and B_{JM} are Jiménez & Madsen's dimensionless coefficients which are found from Fig. 2.2. These two coefficients depend on particle roundness which is described only qualitatively as "well-rounded", "natural sand" or "crushed". The two parameters also depend on overall particle shape, which was quantified by a *Corey Shape Factor*, CSF = $c/(ab)^{0.5}$ in which a, b, and c are the longest, intermediate, and shortest axes of the particle respectively.

Jiménez and Madsen point out that in many practical situations the sand will be a "naturally worn quartz" with CSF ≈ 0.7 for which A_{JM} = 0.954 and B_{JM} = 5.121. As shown in Fig. 2.2, as CSF increases, both A_{JM} and B_{JM} decrease. Similarly, as particle roundness increases from "crushed" to "natural sand" to "well rounded", the parameters A_{JM} and B_{JM} also decrease. Consequently, according to Eq. (2.12), as roundness and sphericity increase, particle settling velocity increases.

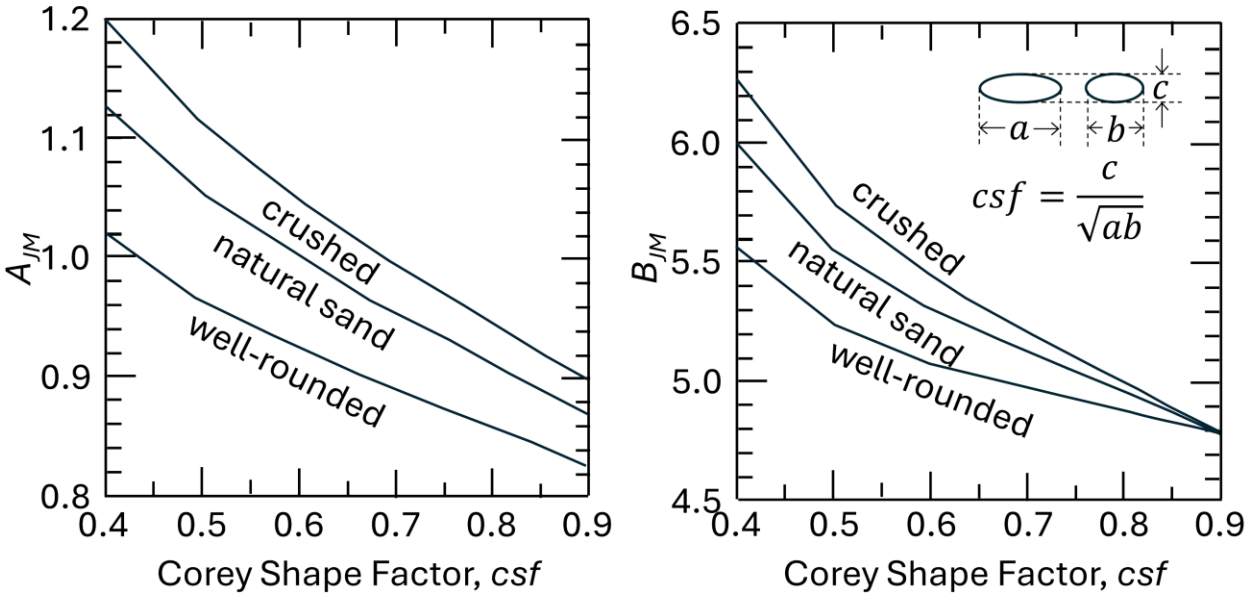


Figure 2.2: Coefficients A_{JM} and B_{JM}.

Unlike the Ahrens model, which is expressed directly in terms of characteristic sieve diameter, the Jiménez and Madsen model uses the nominal diameter, d_N. The nominal diameter is defined as the diameter of a sphere having the same volume as the actual particle. Jiménez and Madsen used Raudkivi's (1990) approximation of the nominal diameter being $d_s/0.9$ where d_s is the sieve diameter. This empirical conversion is adopted in this dissertation so that particle sizes determined using the Jiménez and Madsen model can be reported on the same sieve-diameter basis as conventional sieve-analysis results.

The principal advantage of the Jiménez and Madsen model is its explicit representation of particle morphology. It can therefore distinguish among particles having the same nominal diameter and specific gravity but different shapes or degrees of roundness. This capability makes the model particularly useful for sands having strongly platy, elongated, angular, or well-rounded particles that may not conform to the typical natural-sand behavior represented by the Ahrens model. Its application, however, requires information regarding particle shape and roundness, and its resulting nominal diameter must be converted empirically to a sieve-equivalent diameter. Thus, the model provides greater flexibility in representing particle morphology at the cost of additional characterization and data interpretation.

2.4 Application of Settling-Velocity Models to Particle-Size Determination

All three testing systems developed in this dissertation determine a PSD by independently obtaining the two quantities that define each point on the distribution: percent finer and particle size. The measured pressure response is used to determine the percent finer, whereas the elapsed settling time and corresponding travel distance are used to determine settling velocity. The pressure measurement and particle-size calculation are therefore independent but are associated through their common elapsed time. Pairing the percent finer obtained at each measurement time with the corresponding particle size produces the PSD.

For a particle settling through a known distance L during an elapsed time t, the settling velocity is calculated $v = L/t$. The relevant settling distance depends on the configuration of the testing system. In the u-Sed and m-Sed tests, it is the vertical distance traveled by a sand particle from its release elevation to the pressure port elevation. In the Δ-Sed test, it is the effective settling depth from the suspension surface to the midpoint of the differential-pressure measurement interval. The measured settling velocity is then converted to particle size using the model appropriate for the particle-size range and the desired particle-size interpretation.

Most settling-velocity models are formulated as forward relationships in which particle size and the relevant particle and fluid properties are specified to predict terminal settling velocity. In the systems developed in this dissertation, settling velocity is known from the measured settling time and distance, while particle size is unknown. The model must therefore be applied in reverse. For a given settling velocity, particle specific gravity, and fluid condition, the particle diameter is determined such that the settling velocity predicted by the model matches the measured value.

For fine-grained soils, Stokes' law provides an explicit relationship between settling velocity and particle diameter. Substitution of $v = L/t$ into Stokes' law gives Equation (2.6), from which the particle diameter can be calculated directly. The resulting diameter is an equivalent spherical diameter: the diameter of a sphere having the same density and terminal settling velocity as the actual soil particle under the same fluid conditions. This is the same particle-size definition used in conventional hydrometer analysis. Stokes' law is therefore adopted in the Δ-Sed test so that the particle sizes obtained from the two methods have a consistent sedimentation-based interpretation.

For sand-sized particles, the Ahrens (2000) and Jiménez and Madsen (2003) models are applied beyond the Stokes range. Because the particle-size variables also appear within the

coefficients or nonlinear terms of these models, the corresponding particle diameter is determined numerically. For each measured settling velocity, a trial particle diameter is introduced into the selected model, the predicted settling velocity is calculated, and the particle diameter is iteratively adjusted until the predicted and measured settling velocities agree. Because settling velocity increases monotonically with particle size for fixed particle and fluid properties, this procedure yields a unique positive particle-size solution within the applicable range of the model.

The particle-size definitions used by the two sand models differ. In the Ahrens model, the particle-size variable, d, is defined as the characteristic sieve diameter and can therefore be reported directly on the same basis as conventional sieve-analysis results. The model provides a relatively simple relationship for typical natural sands but does not explicitly distinguish among particles having different shapes or degrees of roundness.

In contrast, the Jiménez and Madsen model initially yields the nominal diameter d_N, defined as the diameter of a sphere having the same volume as the actual particle. The coefficients A_{JM} and B_{JM} are selected according to the Corey Shape Factor and particle-roundness category before the model is inverted. Once d_N has been determined, it is converted to the corresponding sieve diameter using the approximation $d_s = 0.9d_N$ proposed by Raudkivi (1990). The resulting particle sizes can therefore be compared directly with those obtained from conventional sieve analysis while retaining the ability to account explicitly for particle morphology.

Accordingly, two different particle-size interpretations are used in this dissertation. Particle sizes of fine-grained soils determined using Stokes' law are reported as equivalent spherical diameters consistent with hydrometer analysis. Particle sizes of sands determined using the Ahrens or Jiménez and Madsen model are reported on a sieve-diameter basis consistent with sieve analysis. These definitions recognize that particle size in sedimentation analysis is inferred from settling behavior rather than measured directly from particle geometry, while ensuring that the resulting PSDs remain comparable with those obtained from the corresponding conventional reference methods.

2.5 Chapter Summary

This chapter established the settling-velocity framework used to determine particle size in the sedimentation-based testing systems developed in this dissertation. The development of particle settling-velocity models was traced from Stokes' law, which describes the settling of spherical particles within the creeping-flow regime, to relationships applicable to larger and non-

spherical particles. The model proposed by Gibbs et al. (1971) extended settling-velocity prediction beyond the Stokes regime for spherical particles, while subsequent models were developed to represent the settling behavior of natural sediments across broader ranges of particle size, shape, and settling regime.

For fine-grained soils, Stokes' law is adopted in the Δ-Sed test to determine equivalent spherical diameters consistent with conventional hydrometer analysis. For sands, the models proposed by Ahrens (2000) and Jiménez and Madsen (2003) are adopted to determine particle sizes on a sieve-diameter basis. The Ahrens model provides a relatively simple relationship for typical natural sands, whereas the Jiménez and Madsen model explicitly incorporates particle shape and roundness. In each testing system, settling velocity is obtained from the measured settling time and travel distance, and the appropriate relationship is applied in reverse to determine the corresponding particle size. These models provide the particle-size component of the PSD determination framework applied in the following chapters, while the measured pressure response provides the corresponding percent finer.

Chapter 3 The *u*-Sed Test

Chapter 2 established the settling-velocity relationships used in this dissertation to convert particle settling velocity into the corresponding particle size. Building on this framework and the initial uSed proof-of-concept study reported by Zhang et al. (2024), this chapter presents the *u*-Sed test, a sedimentation-based method for determining the particle size distributions (PSDs) of sands from water-pressure measurements. In the *u*-Sed test, elapsed settling time and known travel distance are used with the selected settling-velocity models to determine particle size, while the pressure time history is used to determine the corresponding percent finer. Pairing each particle size with its corresponding percent finer produces a nearly continuous PSD.

The chapter begins by describing the *u*-Sed hardware, including the sedimentation column, pressure port, pressure transducer, and data acquisition system. The pressure stages during a *u*-Sed test are then introduced and used to develop the pressure-based relationships for determining the fluid unit weight, soil specific gravity, specimen mass, and percentage of particles finer than a given particle size. The practical testing procedure is subsequently described. Test results are then presented for 16 sand specimens covering a wide range of gradations, particle shapes, angularities, specific gravities, and geologic origins. The resulting *u*-Sed PSDs are compared with sieve-based PSDs, and the repeatability and sensitivity of the method are evaluated. Finally, the *u*-Sed test is compared with sieve analysis and digital image analysis, and its principal advantages and limitations are discussed.

***

Portions of this chapter are adapted from Zhang and Hryciw (2025), which introduced the *u*-Sed test for determining sand particle size distributions by water pressure measurements during sedimentation.

3.1 The *u*-Sed System Hardware

The *u*-Sed system consists of a sedimentation column and a pressure transducer, as shown in Fig. 3.1. The clear acrylic column measures 1.8 m (6 ft) in height, with an opening diameter of

25.4 mm (1 inch) and a wall thickness of 3.2 mm (1/8 inch). The base of the column sits on a detachable acrylic base and pedestal with two O-rings to ensure water tightness.

Located 16 cm above the pedestal is a port that connects to the pressure transducer. The pressure port inlet is angled at 30° from vertical to prevent the falling particles from entering a tube that connects to the pressure transducer. The elevation of the pressure port ensures that it remains above the top of the fully settled soil specimen. Typically, a 50 g soil specimen would settle to approximately an 8 cm height, but to provide extra collection space for larger specimens or to perform two individual tests without removing the soil, the port is located 16 cm above the top of the pedestal.

The pressure transducer is a model UYY-30 kPa made by the Chaoyuan Instrument Factory in China. It has a measurement range of 0 to 30 kPa with an accuracy of ±0.005 kPa. The transducer is integrated with a YBY-801 data acquisition system by the Liyang Jincheng Testing Instrument Factory in China, which records at a sampling frequency of up to 10 readings per second. The transducer housing has a small vent hole to expel trapped air from the tubing and transducer chamber. Connection to the pressure port is via a 9.5 mm (3/8 inch) diameter plastic tube and a push-to-connect fitting affixed to the pressure port.

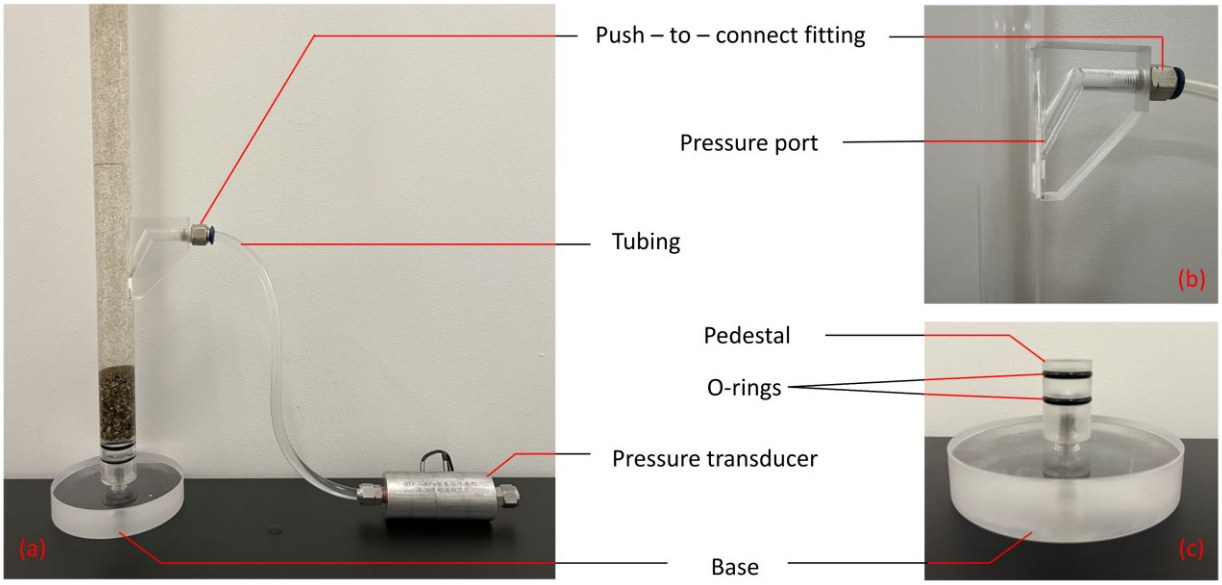


Figure 3.1: The *u*-Sed system: (a) Sedimentation column and pressure transducer during a test; (b) close-up view of the pressure port and the push-to-connect fitting; and (c) close-up view of the base and pedestal.

3.2 Pressure Time Histories

The top of Fig. 3.2 illustrates ten moments in time before, during and after sedimentation of the soil particles through the water column. The bottom of Fig. 3.2 shows a pressure time history schematic corresponding to the time sequence above. During Stage A water is being introduced into the column and the pressure rises accordingly. The water level is brought to Level #1 at a height h_1 above the pressure port. It is held there for a few seconds in Stage B to record the pressure, u^B. During Stage C water is raised to Level #2 at a height of h_2 above the port and held there during Stage D for a second pressure reading, u^D. The unit weight of the fluid in the sedimentation column, γ_f is then computed by:

$$\gamma_f = \frac{u^D - u^B}{h_2 - h_1} \tag{3.1}$$

In Stage E the soil particles are introduced into the column as quickly as possible so that they all have about the same starting sedimentation time. The rapid introduction of the soil into the column causes a steep rise in pressure to the level shown by Stage F. During Stage F the particles are sorting while settling through the column, but none have yet arrived at the pressure port elevation, so the pressure remains constant at u^F. In Stage G the particles are passing the port, so the pressure diminishes with time. Finally, at Stage H, all the particles have travelled past the pressure port and settled at the bottom of the column, thus the pressure is once again constant, this time at u^H. The final pressure during Stage H is slightly higher than during Stage D because the water level has risen due to upward displacement of the fluid by the solid particles. This affords the opportunity to compute the specific gravity of the solids, G_s by:

$$G_s = \left(\frac{u^F - u^H}{u^H - u^D} + 1\right)\frac{\gamma_f}{\gamma_w} \tag{3.2}$$

where $\gamma_w = 9.807\ \mathrm{kN/m^3}$, the unit weight of water at 4°C. The derivation of Eq. (3.2) is in Appendix A.

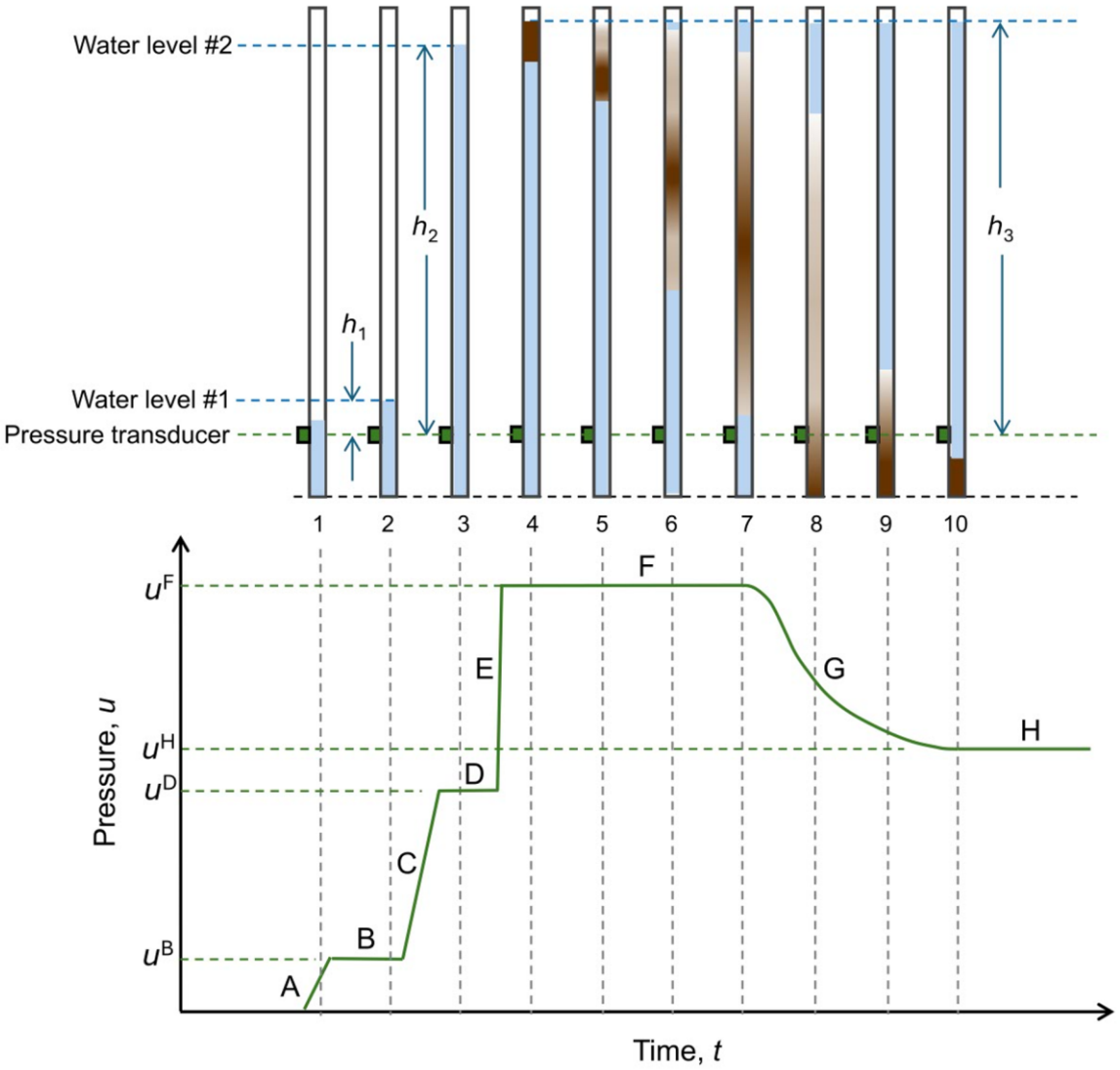


Figure 3.2: Pressure stages during a *u*-Sed test.

The difference in pressure between Stages F and H reflects the total weight of solids which is computed by:

$$W_S = \frac{(u^F - u^H) A_c G_s \gamma_w}{G_s \gamma_w - \gamma_f} \tag{3.3}$$

where A_c is the inside cross-sectional area of the sedimentation column. The derivation of Eq. (3.3) is also in Appendix A. It follows from Eq. (3.3) that the weight of solids still above the pressure port at any time during Stage G is:

$$W_S^G = \frac{(u^G - u^H) A_c G_s \gamma_w}{G_s \gamma_w - \gamma_f} \tag{3.4}$$

The ratio of Eq. (3.4) to Eq. (3.3) is the fraction of specimen solids by weight still above the pressure port at any time during Stage G:

$$\frac{W_S^G}{W_S} = \frac{(u^G - u^H)}{(u^F - u^H)} \tag{3.5}$$

Because of particle sorting over the settling distance, at any pressure u^G the percent by weight of particles that are finer than the particle at the port elevation at that moment is given by Eq. (3.5) × 100%. Equation (3.5) reveals that W_s is not needed to develop the PSD. However, if the specimen weight is obtained using a laboratory scale prior to sedimentation, a comparison to the computed value of W_s by Eq. (3.3) serves as a check on the test quality. While knowledge of W_s is optional, the values of γ_f and G_s as computed by Eqs. (3.1) and (3.2) respectively will be needed by the particle settling velocity models.

As shown in Fig. 3.1, the pressure transducer sits at a lower elevation than the pressure port. Therefore, it will record a pressure higher than at the port. However, Eqs. (3.1) to (3.5) utilize only differences in pressures during the various test stages. Therefore, the difference in elevations between the pressure transducer and the port is arbitrary and has no effect on the results, but the elevation must remain fixed during the period of any single test.

Figure 3.3 contains actual example recorded pressure time histories for fine, medium, coarse and gap-graded sands. Only Stages F, G and H are shown in Fig. 3.3. It is no coincidence that the pressure time histories resemble traditional particle size distribution curves. The remaining task is to convert the time axis to particle sizes. For this, we turn to earlier research by sedimentologists as detailed in Chapter 2.

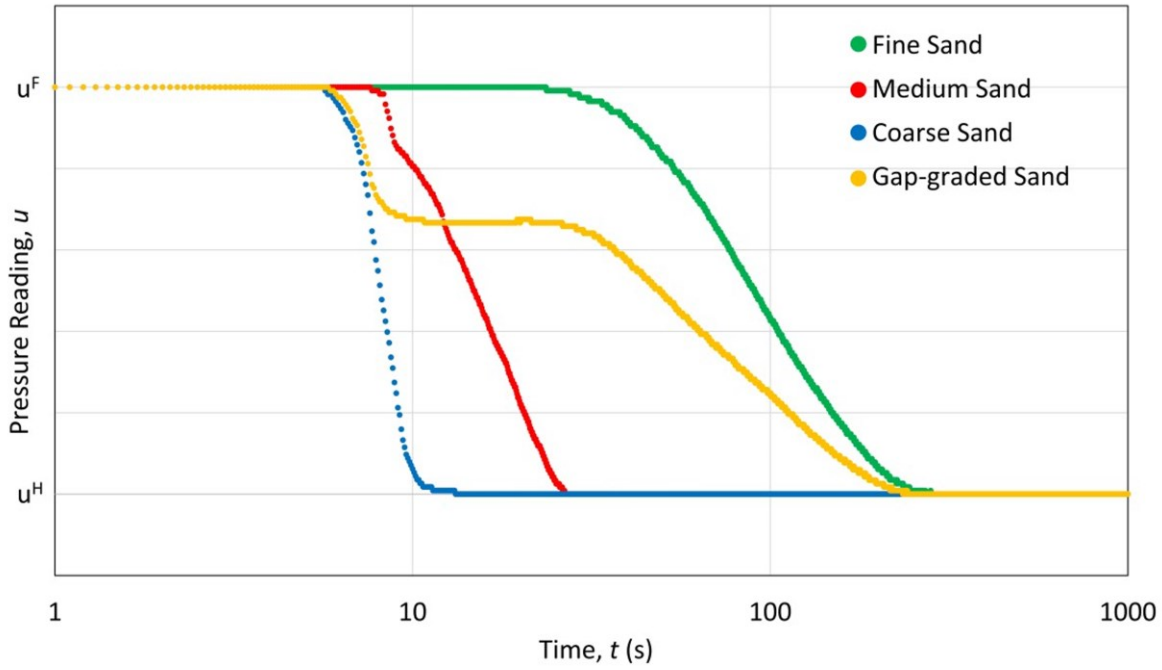


Figure 3.3: Typical pressure time histories for fine, medium, coarse, and gap-graded sands.

3.3 The *u*-Sed Test Procedure

A *u*-Sed test begins by measuring the water temperature and determining the corresponding kinematic viscosity from the temperature–viscosity chart provided in Appendix B, which was developed using data from Anton Paar (2026). The sedimentation column is then filled with water to approximately mid-height. Opening the vent valve on the pressure transducer allows water to drain from the column until the level drops slightly below water level #1 in Fig. 3.2. This drainage purges air bubbles from the lines and the pressure transducer chamber. Using a squeeze bottle, water is then gently added to the column until the meniscus rises back to water level #1. The corresponding pressure reading, u^B is recorded. Water is then added to the column until the meniscus reaches water level #2 at which the new pressure, u^D is obtained. The unit weight of the column fluid is then computed by Eq. (3.1). In the current *u*-Sed system h_2-h_1 is fixed at 1.40 m. Note that the water does not need to be fully de-aired. For that matter, the fluid need not even be water, but for convenience, the use of tap water equilibrated to room temperature is recommended. It was also observed that there is virtually no change in γ_f during a day of *u*-Sed testing. Therefore, if the same source of room-temperature water is used, pressures u^B and u^D do not need to be recorded in every *u*-Sed test.

Continuous pressure recording begins just before the soil is introduced into the column and continues at 0.1 s intervals until test completion. Nominally, a 50 g specimen of dry soil is used. It is introduced as instantaneously as possible into the column using a wide-mouth funnel so that all particles begin settling at about the same time. The soil particles settle through the column and sort themselves by size as they advance towards the pressure transducer port. As described earlier, the passage of particles past the port causes a drop-off in pressure. The readings stabilize once all particles have passed the port. The time required for settlement depends on the smallest particle size in the specimen. This is typically under 15 s for coarse sand, less than 30 s for medium sand, and less than 5 min for fine sand. Once all the particles pass the pressure port, the recording ends and the pressure time history is converted to a PSD as described in the following section.

3.4 Tested Materials and Results

The pressure time histories provide the percentage of soil particles by weight that have (and have not) yet passed the pressure port as a function of time. In other words, the percent by weight of particles in a specimen that are larger (and smaller) than the particles at the pressure port elevation at any instant in time. In sieving language, this is equivalent to the "percent coarser" (and "percent finer") by weight than a given sieve opening size. The settling velocity of a particle at the port elevation at any time is obtained using an average travel distance of $(h_2 + h_3)/2$ (Fig. 3.2). Equation (2.8) by Ahrens or Equation (2.12) by Jiménez & Madsen is then solved for the particle size passing the pressure port at any given time.

To evaluate the accuracy and precision of the *u*-Sed test and to compare results with sieve-based PSDs, ten soils were pre-sieved for one hour and reconstituted in specific fine, medium and coarse fractions for testing. Two of the sands, Michigan 2NS and Griffin, IN are natural glacial quarry materials exhibiting a wide range of particle sizes. Each of these two sands was used to produce four different gradations as listed in Table 3.1.

Table 3.1: Tested soil specimens, size composition and sedimentation duration.

No.	Name	Grain Size			Particle Size		Sedimentation
		Coarse (%)	Medium (%)	Fine (%)	Maximum (mm)	Minimum (mm)	Duration (s)
1	Michigan 2NS	51	32	17	4.75	0.106	120.8
2	Griffin, IN	23	29	48	4.75	0.106	143.6
3	Big Island, HI	23	77	0	4.75	0.425	26.0
4	Griffin, IN	41	59	0	4.75	0.425	25.9
5	Michigan 2NS	33	0	67	4.75	0.075	235.0
6	Michigan 2NS	60	0	40	4.75	0.075	237.3
7	Griffin, IN	0	60	40	2.00	0.106	118.3
8	Michigan 2NS	0	78	22	2.00	0.106	131.9
9	Stoney River®	100	0	0	4.75	2.00	14.0
10	Petco sand®	100	0	0	4.75	2.36	13.2
11	GloFish sand®	100	0	0	4.75	2.36	10.1
12	BFAO	0	100	0	2.00	1.00	11.3
13	Griffin, IN	0	100	0	2.00	0.425	28.6
14	New Madrid, MO	0	0	100	0.425	0.075	262.2
15	Costa Rica	0	0	100	0.212	0.075	191.9
16	Treasure Island, CA	0	0	100	0.425	0.106	148.4

Three sands, Petco®, Stoney® and GloFish® are commercially available aquarium sands. They were specifically obtained to evaluate the *u*-Sed test using the most challenging materials: uniform coarse sands. One material is an artificial Brown Fused Aluminum Oxide (BFAO) which is crushed and used commercially as an abrasive. It was selected for the study because of its extreme angularity and relatively high specific gravity compared to the other sands. A sand from Treasure Island in San Francisco Bay and a sand from New Madrid, MO were chosen for their historical significance in geotechnical earthquake engineering. A very dark, basalt-rich beach sand from Costa Rica was chosen because of its high specific gravity and fine size uniformity. Finally, a partly volcanic/partly calcareous sand from the Big Island in Hawaii was included for its unusual constituent blend. Images of all 16 specimens are shown in Fig. 3.4 and the sieve-based size compositions of each specimen are listed in Table 3.1. The images in Fig. 3.4 were collected using the vision cone penetrometer described by Ventola et al. (2020a). The image resolution is 246.6 pixels per mm and the images in Fig. 3.4 all display the same 8.5 mm × 8.5 mm fields of view.

The three numbers in parentheses correspond to the percentages of coarse, medium, and fine sand, respectively.



Figure 3.4: Images of the 16 soil specimens with their percentages of coarse, medium, and fine sand.

The first half of the 16 specimens in Table 3.1 (and Fig. 3.4) were various mixtures of coarse (c), medium (m) and fine (f) sand. The ASTM (2017) definitions of particle size were used. Two of the specimens were only c & m, two were only m & f, two were only c & f (i.e., gap-graded), and two contained all three sizes, c, m, and f. The second half of the specimens in Table

3.1 were entirely either c, m or f. The maximum and minimum particle sizes, along with the sedimentation durations are also included in Table 3.1. The sizes reported in Table 3.1 were based on sieve opening sizes and therefore do not necessarily represent the actual maximum or minimum particle sizes present in the specimens. In all 16 tests, the *u*-Sed pressure time histories were converted to PSDs using both the Ahrens (2000) and Jiménez & Madsen (2003) settling velocity models and Eq. (3.5).

The Ahrens model does not consider particle shape or angularity, therefore its implementation was simple and straightforward for all 16 specimens. For the Jiménez and Madsen model, CSF = 0.7 as recommended for "natural sands" was used for all specimens except No. 9 Stoney River, No. 10 Petco and No. 11 GloFish. As observed in Fig. 3.4, these three sands are plate-like. Therefore, 25 randomly selected particles of each sand were measured by a caliper to obtain their three orthogonal dimensions, *a*, *b* and *c*. The average computed CSF values were found to be approximately 0.5 for all three materials. This value was therefore used to produce these coarse sands' PSDs by the Jiménez and Madsen model.

For the Jiménez and Madsen model, the "natural sand" curve in Fig. 2.2 was used for all specimens except No. 10 Petco, No. 11 GloFish and No. 12 BFAO. Once again referring to the images in Fig. 3.4 we see that these three sands are very angular. Therefore, the "crushed sand" curve in Fig. 2.2 was used for these three materials.

Figure 3.5 compares the PSD curves obtained from the *u*-Sed test and those determined by sieving for the mixed size specimens (No. 1 to No. 8). The PSD curves generated by both the Ahrens and Jiménez & Madsen models showed almost perfect agreement with the PSD points obtained by sieving. Figure 3.6 compares the *u*-Sed PSD curves to sieving results for the uniform-sized specimens (No. 9 to No. 16). For Specimens No. 13 to No. 16 (all "natural sands") both the Ahrens and Jiménez & Madsen models are once again almost perfectly aligned with the sieve data. For the crushed No. 12 BFAO, the Jiménez and Madsen model is slightly better than Ahrens in terms of agreement with the sieving results. The anticipated big difference between the two models occurs for the three commercial plate-like aquarium sands, the Jiménez & Madsen (2003) model fits the sieve data better than Ahrens' model does. The explanation is obvious, - there was no provision in the earlier Ahrens (2000) model for the plate-like shape of these coarse sands.

Note that in Figures 3.5 and 3.6 what may appear as curves being "fitted" to sieve data are not curve fits at all. They are actually hundreds of *u*-Sed data points. Also, given the strong

agreement between the sieve and u-Sed test results, curve fits to the sieve data were omitted to maintain visual clarity of the u-Sed data points.

A comparison of particle size distribution metrics (D_{60}, D_{30}, and D_{10}) between the sieve and u-Sed tests is presented in Table 3.2. The Jiménez and Madsen curves were used for the plate-like or angular Specimens (No. 9 to No. 12). For all others, the Ahrens curves were used. However, there was very little difference between the two. The D_{60}, D_{30}, and D_{10} values were used to calculate the mean absolute error (MAE) to quantify the agreement between sieving and the u-Sed test. From the D_{60}, D_{30}, and D_{10} values, the coefficients of uniformity, C_u and curvature, C_c were also computed and are compared in Table 3.2. Collectively, the close agreement across all evaluated PSD metrics confirms that the u-Sed test reliably reproduces the gradation characteristics obtained from sieve analysis. The remaining differences are considered negligible relative to the natural spatial variability of soil PSDs within a deposit and the variability associated with sampling, specimen preparation, and routine laboratory testing.

Table 3.3 compares G_s values obtained by the u-Sed test (Eq. 3.2) and those from conventional ASTM specific gravity tests (ASTM 2023). The table also compares the soil specimen mass determined by the u-Sed test (Eq. 3.3) to values measured by a laboratory weight scale. The results show that the u-Sed test determines both the specific gravity and the mass of the soil specimens very well.

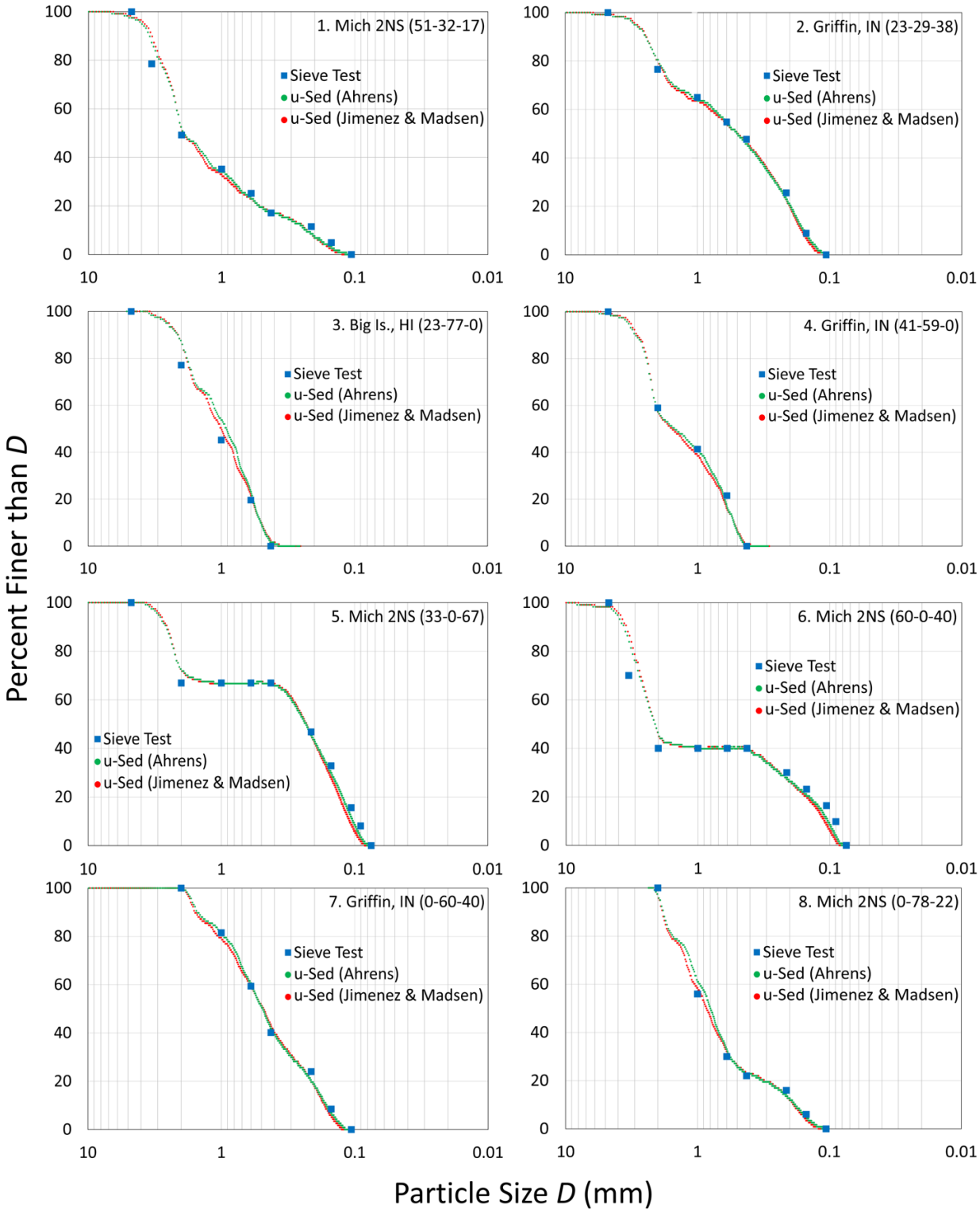


Figure 3.5: Particle size distributions for mixtures of coarse, medium, and fine sand.

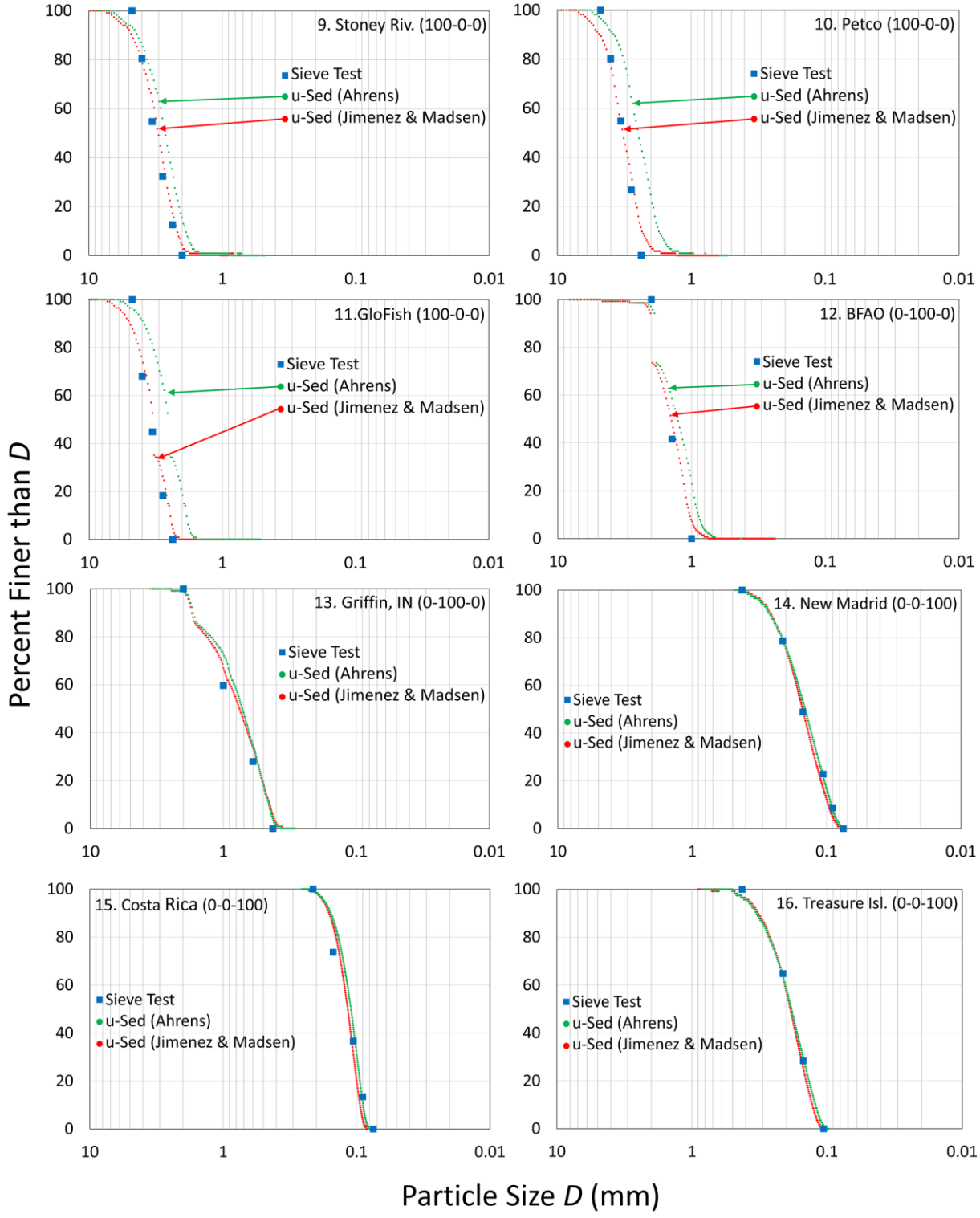


Figure 3.6: Particle size distributions for uniform coarse, uniform medium, and uniform fine sands.

Table 3.2: Comparison of particle size distribution metrics between sieve and *u*-Sed.

No.	Name	Sieve			*u*-Sed			MAE (mm)	C_u		C_c	
		D_{60} (mm)	D_{30} (mm)	D_{10} (mm)	D_{60} (mm)	D_{30} (mm)	D_{10} (mm)		Sieve	*u*-Sed	Sieve	*u*-Sed
1	Michigan 2NS	2.3	0.80	0.21	2.2	0.81	0.23	0.04	10.95	9.57	1.33	1.30
2	Griffin, IN	0.75	0.25	0.16	0.75	0.26	0.16	0	4.69	4.69	0.52	0.56
3	Big Island, HI	1.2	0.71	0.51	1.1	0.68	0.51	0.04	2.35	2.16	0.82	0.82
4	Griffin, IN	2.1	0.76	0.52	2.1	0.75	0.53	0.01	4.04	3.96	0.53	0.51
5	Michigan 2NS	0.29	0.14	0.090	0.30	0.15	0.10	0.01	3.22	3.00	0.75	0.75
6	Michigan 2NS	2.8	0.23	0.090	2.5	0.24	0.10	0.11	31.11	25.00	0.21	0.23
7	Griffin, IN	0.60	0.30	0.15	0.60	0.30	0.16	0	4.00	3.75	1.00	0.94
8	Michigan 2NS	1.0	0.60	0.18	0.96	0.57	0.18	0.02	5.56	5.33	2.00	1.88
9	Stoney River®	3.2	2.7	2.2	3.2	2.6	2.2	0.03	1.45	1.45	1.04	0.96
10	Petco sand®	3.5	2.8	2.5	3.5	2.8	2.4	0.03	1.40	1.46	0.90	0.93
11	GloFish sand®	3.5	2.8	2.5	3.3	2.8	2.4	0.10	1.40	1.38	0.90	0.99
12	BFAO	1.6	1.3	1.1	1.6	1.2	1.0	0.07	1.45	1.60	0.96	0.90
13	Griffin, IN	1.0	0.61	0.46	0.83	0.57	0.45	0.07	2.17	1.84	0.81	0.87
14	New Madrid, MO	0.16	0.12	0.092	0.16	0.12	0.092	0	1.74	1.74	0.98	0.98
15	Costa Rica	0.13	0.10	0.088	0.12	0.10	0.09	0	1.48	1.33	0.87	0.93
16	Treasure Island, CA	0.20	0.15	0.12	0.20	0.15	0.12	0	1.67	1.67	0.94	0.94

Table 3.3: Comparison of specific gravity and specimen mass.

No.	Name	Specific Gravity			Specimen Mass		
		u-Sed	ASTM	Difference	*u*-Sed (g)	Weight Scale (g)	Difference (%)
1	Michigan 2NS	2.70	2.66	0.04	50.16	49.72	0.9
2	Griffin, IN	2.66	2.68	0.02	49.94	49.66	0.6
3	Big Island, HI	2.86	2.89	0.03	49.10	49.57	1.0
4	Griffin, IN	2.66	2.68	0.02	49.52	49.67	0.3
5	Michigan 2NS	2.71	2.66	0.05	49.74	49.62	0.2
6	Michigan 2NS	2.72	2.66	0.06	50.16	49.73	0.9
7	Griffin, IN	2.66	2.68	0.02	49.52	49.73	0.4
8	Michigan 2NS	2.70	2.66	0.04	50.16	49.61	1.1
9	Stoney River®	2.62	2.62	0	49.77	49.64	0.3
10	Petco sand®	2.51	2.52	0.01	49.69	49.78	0.2
11	GloFish sand®	2.53	2.60	0.07	49.14	49.61	1.0
12	BFAO	3.94	3.94	0	49.84	49.85	0
13	Griffin, IN	2.70	2.68	0.02	49.94	49.62	0.6
14	New Madrid, MO	2.63	2.65	0.02	49.00	49.26	0.5
15	Costa Rica	3.00	3.04	0.04	48.65	49.10	0.9
16	Treasure Island, CA	2.64	2.65	0.01	49.42	49.85	0.9

3.5 Repeatability and Sensitivity Analysis

To evaluate *u*-Sed test repeatability, a 50 g specimen from Griffin, IN, composed of 34% coarse sand, 33% medium sand, and 33% fine sand was tested three times. As shown in Fig. 3.7, the results are virtually indistinguishable using either the Ahrens or the Jiménez & Madsen models, thus confirming test repeatability.

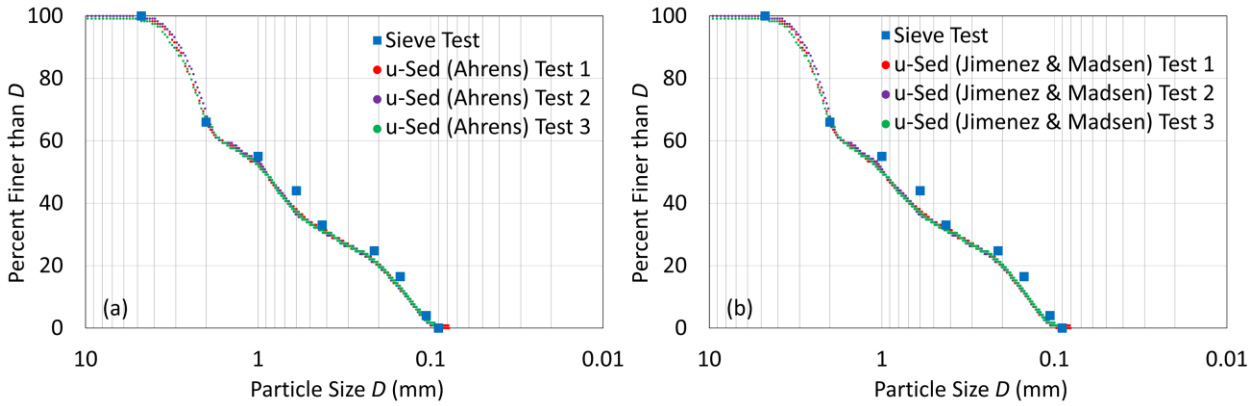


Figure 3.7: Repeatability analysis of *u*-Sed test: (a) using Ahrens' model; and (b) using Jiménez and Madsen's model.

Next, a sensitivity analysis was conducted to evaluate the resilience of *u*-Sed PSDs to deviations in specific gravity and kinematic viscosity as input parameters to the Ahrens and Jiménez & Madsen models. This parametric analysis was applied to the pressure-time history from the test on Specimen #2 - Griffin, IN. Specifically, assumed values of 2.63, 2.68, and 2.73 for G_s were used. Similarly, assumed values of water kinematic viscosity, ϑ of $0.9344\ mm^2/s$, $0.8926\ mm^2/s$, and $\vartheta = 0.8539\ mm^2/s$ (corresponding to water temperatures of 23 °C, 25 °C and 27 °C respectively) were investigated. The results are shown in Figures 3.8 and 3.9. It is noted that a kinematic viscosity of $0.8926\ mm^2/s$ (corresponding to the actual laboratory temperature of 25 °C) was used in the analysis of G_s variations (Fig. 3.8) while the actual (ASTM test-based) G_s of 2.68 was used when evaluating the effect of ϑ variations (Fig. 3.9). The two figures illustrate that small variations in G_s and ϑ have negligible effects on *u*-Sed PSDs. As for the influence of unit weight of water, as previously noted, the assumption that $\gamma_f = \gamma_w$ is very acceptable as it has almost no effect on PSDs.

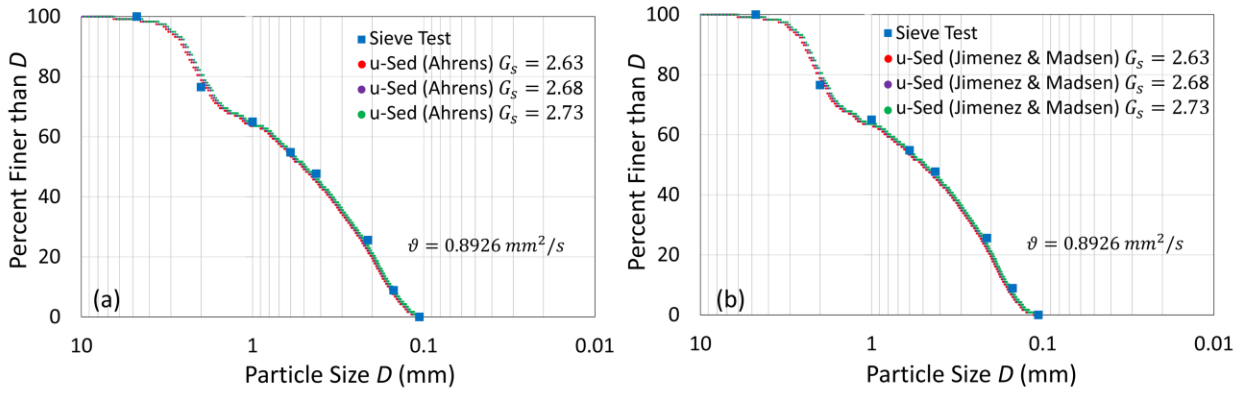


Figure 3.8: Effect of specific gravity (G_s) deviations on *u*-Sed results: (a) using Ahrens' model; and (b) using Jiménez and Madsen's model.

To examine the influence of specimen weight on *u*-Sed test results, three Griffin, IN specimens, each comprised of a mixture of coarse, medium, and fine sand with identical particle size distributions (determined through sieve analysis) were prepared with weights of 40.00 g, 50.00 g, and 60.00 g. As shown in Figure 3.10, the *u*-Sed results for the three soil specimen weights align perfectly with the sieve data points thus confirming that for the 40 g to 60 g range the specimen weight does not affect the PSD.

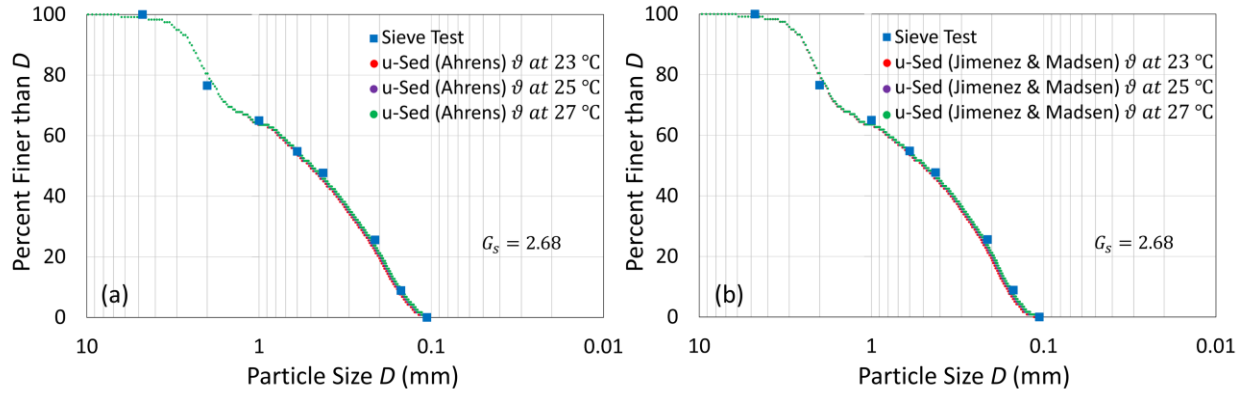


Figure 3.9: Effect of kinematic viscosity deviations on *u*-Sed results: (a) using Ahrens' model; and (b) using Jiménez and Madsen's model.

It is very noteworthy that there are discrepancies between the three *u*-Sed based PSDs at locations between the sieve data points in Figure 3.10. These are not errors but rather, a reflection of the fact that the three specimens were constituted from pre-sieved sands in specific size ranges. There is no control over the actual particle sizes between the discrete sieve opening sizes and

therefore, the PSDs are truly different there. While a sieve test provides "correct" information at (and only at) the precise sieve data point locations, smooth connecting curves between discrete sieve points are always at the "artistic license" of the interpreter. By contrast, the *u*-Sed test provides tens to hundreds of actual data points between the sparse sieve points. The practical implication is that the *u*-Sed test provides more accurate values of D_{60}, D_{30}, D_{10} for soil classification than sieving can.

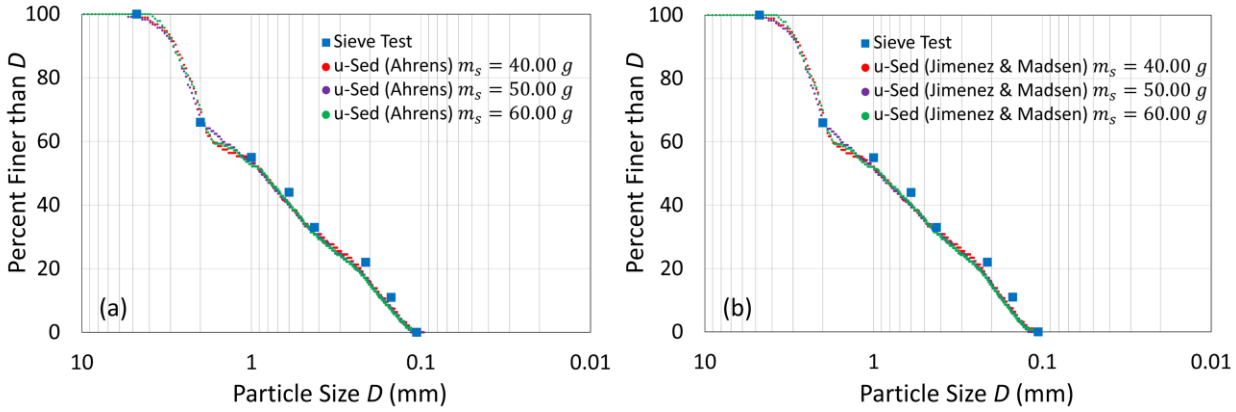


Figure 3.10: Effect of Soil specimen weight on *u*-Sed test results: (a) using Ahrens' model; and (b) using Jiménez and Madsen's model.

In the current version of the *u*-Sed system, which features a sedimentation column inner diameter of 1 inch, the accuracy of the pressure transducer (±5 Pa) establishes the smallest reliably measurable soil mass. This 5 Pa corresponds to a soil mass of approximately 0.41 g for soil with G_s = 2.65. When the soil specimen mass is less than 40 g, the precision of the PSD results, expressed as "Percent Finer than *D*" is up to +/-1%. At the other end, specimens weighing more than 60 g could cause errors associated with the relatively small inside cross-sectional area of the column. As specimen size increases, the time it takes for all particles to enter the water at the start of the test increases. Thus, the assumption that sedimentation of all particles begins at the same time becomes less valid. Based on these considerations, a specimen mass of 50 g (with an acceptable range of 40 g to 60 g) is recommended for the current *u*-Sed system dimensions.

Another important design parameter is the height of the sedimentation column, and more specifically, the distance between the column water surface and the pressure port elevation. If this distance is too short, the peak pressure (u^F) may not stabilize at a constant value before the first

particle reaches the pressure port. The absence of a reliable value of u^F would make PSD determination impossible. An adequate water surface to pressure port distance allows for the formation of a stable u^F and also enhances particle sorting by size during sedimentation. However, an excessively long distance would extend the test duration, and very tall columns would be impractical for a laboratory. Through extensive *u*-Sed testing, a distance of 1.5 m has been determined to be optimal for the entire sand particle size range (0.075 – 4.75 mm). This distance ensures a stable u^F reading and effective particle sorting by size while maintaining a reasonable test duration and a practical column height.

Finally, the specifications for data acquisition rate and the pressure transducer resolution are important for obtaining smooth and accurate PSDs. A sampling frequency of 10 readings per second is recommended to ensure good data fidelity. A transducer accuracy no greater than ±6 Pa is essential for reliably detecting pressure variations.

3.6 Comparison with the Other Methods for PSD Analysis

The *u*-Sed test offers significant advantages over sieving and advanced techniques such as digital image analysis (DIA) for PSD determination of sands. It is very efficient, requiring significantly less testing time than sieving. The *u*-Sed hardware is compact, having a much smaller laboratory footprint than a sieve shaker. As mentioned earlier, unlike sieve tests which provide only 6 to 8 discrete PSD data points, the *u*-Sed generates nearly continuous PSD curves. It is portable, quiet, dust-free, has no moving parts, requires minimal cleaning and maintenance, and it consumes considerably less energy. Another major advantage of the *u*-Sed test is that the hardware does not require a calibration; it relies only on pressure differences between different testing stages. Lastly, it provides a reasonably accurate value for soil specific gravity with no additional effort, time, or equipment.

The shortcomings of sieve analysis are well known to the geotechnical engineering community and require no elaboration here. Digital image analysis (DIA), which includes dynamic image analysis, for PSD determination solves some of the problems inherent with sieve analysis but it has its own unique limitations. The three main issues are 1) development of appropriate hardware for specimen preparation and image acquisition, 2) a limited range of identifiable particle sizes at a fixed camera magnification and, 3) to be accepted by the civil/geotechnical engineering community, - essential calibration or correction of results to standard sieve-based definitions of particle size. The University of Michigan research group has spent over three decades addressing

these issues with some limited successes. Nevertheless, there is an important role that DIA can play in conjunction with the *u*-Sed test. Neither sieving nor the *u*-Sed provide information on particle shape or angularity, while DIA does. Moreover, for very coarse sands, as this study has shown, the angularity (or roundness) and the shape (i.e. the CSF) are desired for use in the Jiménez and Madsen model. DIA can provide such information by photographing the coarse fractions of sedimented sands through the *u*-Sed column and employing the image analysis techniques developed by Zheng and Hryciw (2017, 2018), Ventola and Hryciw (2023a), and others for roundness and shape analysis.

There are two rare but notable limitations of the *u*-Sed test that must be mentioned. If the specific gravities of sand particles in a specimen vary much from one size range to another, the PSDs will naturally be skewed. There is no easy solution for such a situation. It would require sorting a specimen by particle size using sieves and performing separate *u*-Sed tests on each particle size range. The second limitation occurs if particles are porous. In this case, trapped air bubbles can alter the effective densities and settling velocities of particles, leading to errors in PSDs.

3.7 Chapter Summary

This chapter introduced the *u*-Sed test, a sedimentation-based method for determining the particle size distributions of sands. The method uses the natural sorting of particles as they settle through a water column. A pressure transducer connected to a fixed port records the decrease in water pressure as particles pass the port elevation. This pressure-time history provides the percentage of specimen solids remaining above the port at each instant, while established settling-velocity models are used to convert settling time into the size of the particle at pressure port. In this way, the *u*-Sed test produces a nearly continuous PSD without mechanically separating the specimen into discrete size fractions.

The governing pressure relationships were developed from the pressure stages observed during a *u*-Sed test. These relationships show that the PSD can be determined from pressure differences alone, independent of the absolute elevation of the pressure transducer. The pressure measurements also provide estimates of the specimen mass and the specific gravity of the soil solids, giving the method an internal check on test quality. The practical testing procedure was then described, including water introduction, removal of trapped air from the pressure line, rapid introduction of the soil specimen, and continuous pressure recording during sedimentation.

The performance of the *u*-Sed test was evaluated using 16 sand specimens with different gradations, particle shapes, angularities, specific gravities, and geologic origins. The resulting PSDs showed strong agreement with sieve-based PSDs across the full sand-size range. For most natural sands, the Ahrens and Jiménez and Madsen settling-velocity models produced similar results. For plate-like or highly angular coarse particles, the Jiménez and Madsen model provided better agreement because it explicitly accounts for particle shape and roundness. The *u*-Sed-derived values of specific gravity and specimen mass also agreed well with values obtained from conventional ASTM testing and laboratory weighing.

The repeatability and sensitivity analyses confirmed the robustness of the method. Repeated tests on the same specimen produced nearly indistinguishable PSDs, and small deviations in assumed specific gravity and water kinematic viscosity had negligible effects on the computed results. Specimen masses between 40 g and 60 g also produced consistent PSDs, supporting the use of a nominal 50 g specimen for the current 1-inch-diameter sedimentation column.

Compared with the conventional sieve test, the *u*-Sed test offers several important advantages. It is faster, quieter, dust-free, compact, low-energy, and requires minimal cleaning and maintenance. More importantly, whereas a sieve test provides only a small number of discrete PSD points and requires inferred curves between sieve openings, the *u*-Sed test generates tens to hundreds of actual data points from a single continuous pressure record. Compared with digital image analysis, the *u*-Sed test avoids challenges associated with particle segmentation, camera magnification, specimen preparation, and calibration to sieve-equivalent particle sizes. Its hardware also requires no empirical calibration because the analysis relies on pressure differences between well-defined testing stages.

The *u*-Sed test does have limitations. It does not directly measure particle shape or angularity, so supplemental image analysis may be useful when testing highly angular or plate-like coarse sands. The method may also be affected by unusual materials, such as porous particles with trapped air or specimens in which specific gravity varies substantially among particle-size fractions. Overall, however, the *u*-Sed test provides a simple, accurate, and practical pressure-based alternative to sieving for determining nearly continuous PSDs of sand-sized soils.

Chapter 4 The m-Sed Test

Chapter 3 introduced the *u*-Sed test, which demonstrated that nearly continuous particle size distributions (PSDs) of sands can be obtained from water pressure measurements during sedimentation. Although the *u*-Sed test offers major advantages over conventional sieve analysis, it relies on an electronic pressure transducer and data acquisition system. This dependence has several practical limitations, including the need for electrical power, possible sensor failure, voltage fluctuations, short circuits in wet environments, and the need for periodic calibration or replacement of electronic components. These requirements may limit the use of the test in remote field locations, resource-limited settings, disaster-affected regions, and other environments where electrical equipment is inconvenient or unreliable.

This chapter presents the manometer sedimentation (m-Sed) test as a field-portable and electricity-free version of the pressure-based sedimentation concept. In the m-Sed test, the pressure transducer from the *u*-Sed system is replaced by a simple polyurethane rubber manometer tube connected to the sedimentation column. This substitution eliminates the need for electrical power and electronic pressure sensing while retaining the same fundamental principle: particles sort by size during sedimentation, and the pressure response at a fixed port provides the basis for determining the PSD. Chapter 3 showed that the Ahrens (2000) and Jiménez and Madsen (2003) models produced similar results for typical natural sands, while the Jiménez and Madsen model additionally accommodates variations in particle shape and roundness. Accordingly, the Jiménez and Madsen model is adopted for particle-size determination in the m-Sed test.

This chapter first describes the m-Sed system hardware, including the two-part sedimentation column, manometer port, manometer tube, and water-level scale. The pressure stages during an m-Sed test are then introduced, and the governing relationships are derived with consideration of the bidirectional fluid flow between the sedimentation column and the manometer. The effects of manometer material and diameter are subsequently evaluated because these properties influence capillarity, inertial response, and measurement accuracy. The practical testing procedure is then described, followed by validation using eight engineered sand specimens

spanning the ASTM sand-size range. The resulting PSDs are compared with those obtained from sieve analysis and the *u*-Sed test. Finally, the repeatability of the method, the influence of particle shape, and other factors affecting m-Sed results are examined.

***

Portions of this chapter are adapted from Zhang and Hryciw (2026), which introduced the manometer sedimentation system for determining sand particle size distributions.

4.1 The m-Sed System Hardware

The m-Sed test system hardware consists of a sedimentation column and a manometer as shown in Figure 4.1 and schematically in Figure 4.2. The *sedimentation column* is in two parts for ease of packing and transport. The *top section* is 80 cm (31.5 in.) long, the *bottom section* is 100 cm (39.4 in.) in length. The column has an inside diameter of 25.4 mm (1.0 in.) and an outside diameter of 31.8 mm (1.25 in.). The top section is seated and glued into an *upper coupler*. The inside of the bottom of the upper coupler is fitted with two O-rings to prevent leakage when it attaches to the *bottom section* of the sedimentation column. The *bottom section* of the sedimentation column is also seated and permanently glued into a *lower coupler* as shown in Figures 4.1 and 4.2. The lower portion of the lower coupler is fitted onto a *pedestal* which is fitted with another set of two O-rings to prevent leakage. The pedestal is permanently centered atop a 117.0 mm (4.6 in.) diameter, 25.4 mm (1.0 in.) thick *base*. As shown in Figure 4.1, almost all the m-Sed hardware is made of clear acrylic.

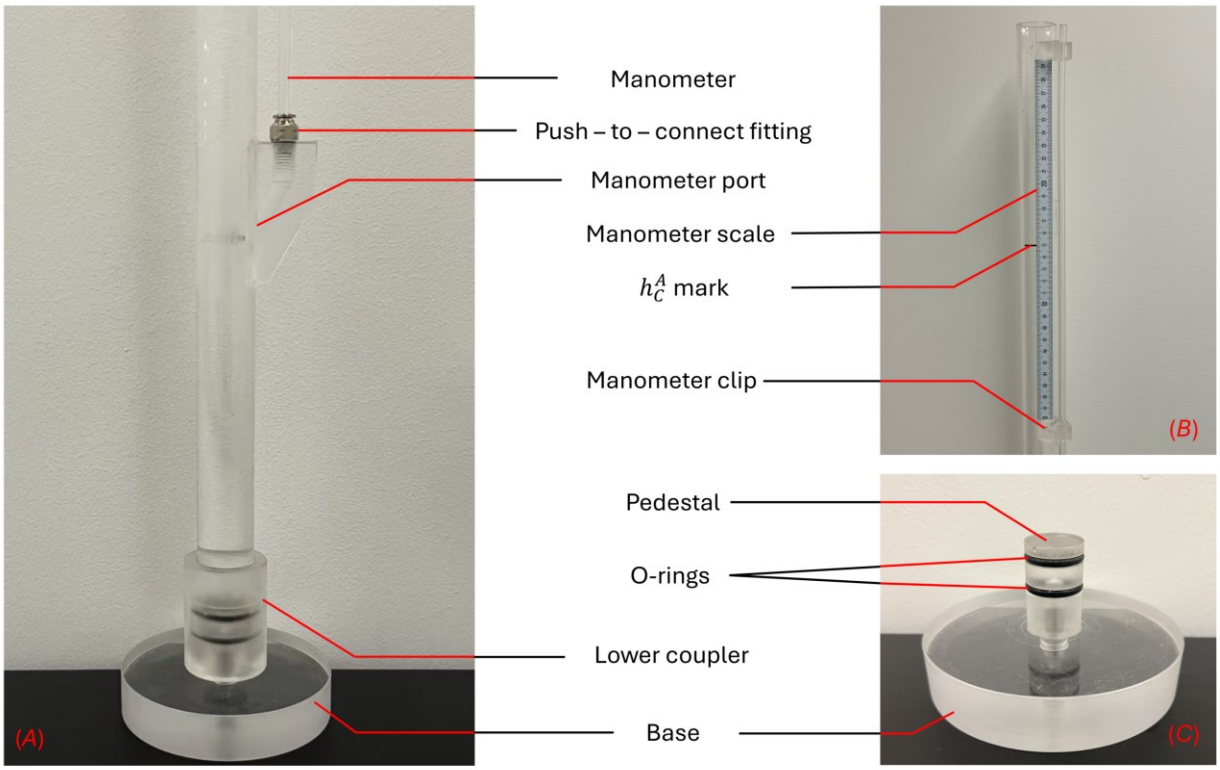


Figure 4.1: The m-Sed system hardware: (*A*) the bottom section of sedimentation column, (*B*) the top section of sedimentation column, (*C*) close-up view of the base and pedestal.

When assembled, the *manometer port* (the column-to-manometer connector) is located 160.0 mm (6.3 in.) above the pedestal. This provides ample volume for all specimen particles to accumulate below the port. It should also be noted that the connecting bore in the manometer port assembly is angled 30 degrees from vertical. This is to prevent soil particles from entering and settling in the connector. The *manometer* itself is a flexible polyurethane rubber tube of 3.2 mm (1/8 in.) inside diameter and 6.4 mm (1/4 in.) outside diameter. The selections of the manometer material and diameter were intrinsically linked to the dynamic pressure responses during testing and will therefore be discussed later in the dissertation. Because it can be loosely coiled for transport, the manometer tube can be continuous over its entire 1550 mm (61 in.) length. It attaches to the port assembly using a simple *push-to-connect* fitting. To keep it securely in place, the manometer tube is attached to the sedimentation column using five *clips*. These clips are permanently glued to the sedimentation column. Lastly, a *scale* with a precision of 1 mm is attached to the upper section of the sedimentation column for reading water levels in the manometer.

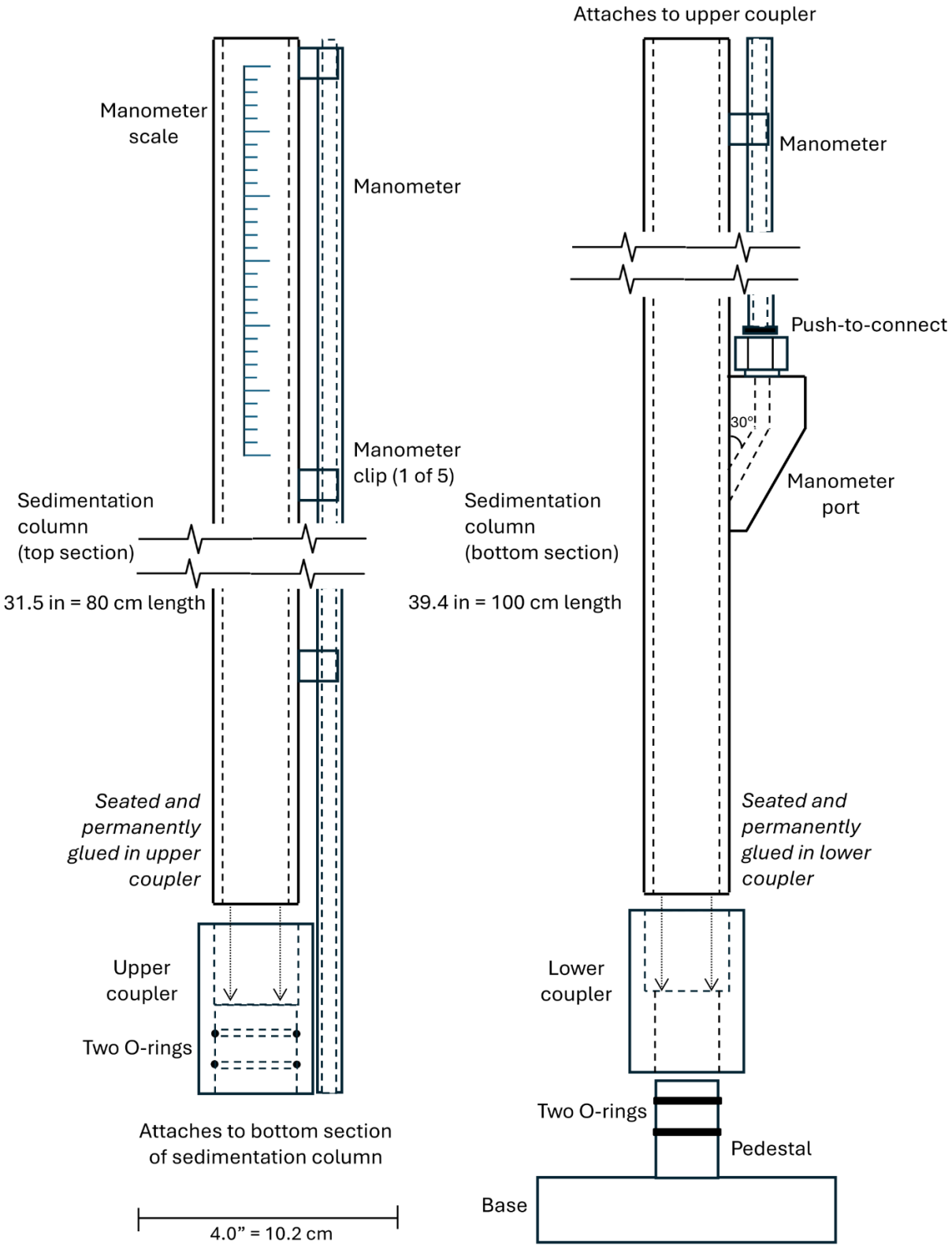


Figure 4.2: Schematic Diagram of the m-Sed System.

4.2 Pressure Stages during an m-Sed Test

Unlike the *u*-Sed system, in which the pressure transducer measures pressure at the port without appreciable fluid exchange with the sedimentation column and the governing equations follow directly from hydrostatic equilibrium, the m-Sed system measures pressure through changes in the manometer water level. Changes in pressure therefore induce water exchange between the manometer and the sedimentation column, causing the water levels and fluid volumes in both components to vary simultaneously. The governing equations of the m-Sed test are consequently derived in detail in this chapter because they provide the basis for understanding how the system operates and how its measurements are interpreted. The following derivation accounts explicitly for pressure equilibrium and fluid-volume conservation throughout the four testing stages.

Figure 4.3 illustrates four stages (A through D) of the m-Sed test. In Stage A, a fluid, typically tap water at room temperature, is in the manometer and in the sedimentation column awaiting the soil specimen. At the elevation of the manometer port the pressure can be thought of as being due to the fluid in the column, p_c or due to the fluid in the manometer, p_m. Naturally,

$$p_c = p_m \tag{4.1}$$

or, in terms of the height of fluid:

$$\gamma_f h_c^A = \gamma_f h_m^A \tag{4.2}$$

where γ_f is the unit weight of the fluid while h_C^A and h_M^A are the heights of liquid above the connection. The superscript indicates that these height readings are during Stage A. Since the fluid is the same in both the column and manometer, we have:

$$h_c^A = h_m^A \tag{4.3}$$

which is a trivial observation but useful to introduce the notation used hereafter in development of the m-Sed equations.

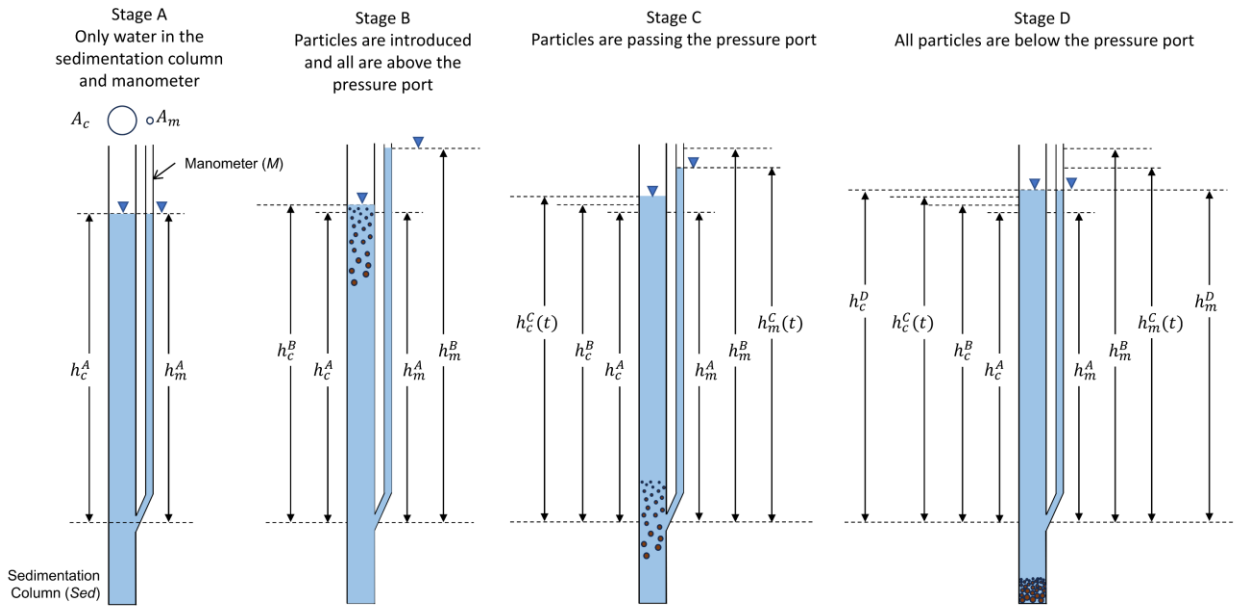


Figure 4.3: Four stages during an m-Sed test.

In Stage B, the soil specimen has been introduced into the sedimentation column and the particles are settling and sorting by size, but none have yet arrived at the manometer port. The height of water in both the column and manometer has risen but $h_c^B < h_m^B$. The increase in water height in the manometer results from water flowing from the column into the manometer, whereas the rise in water level within the column is caused by the introduced soil particles displacing water. These two heights remain constant until the first (i.e., largest) particles arrive at the connector.

During Stage B, the pressure at the connector in terms of the weights of the contents of the sedimentation column is:

$$p_c = \frac{W_f + W_S}{A_c} \tag{4.4}$$

where W_f and W_s are the weights of fluid and solids in the column above the port and A_c is the inside cross-sectional area of the column. Equation (4.4) may be written:

$$p_c = \frac{V_f \gamma_f + G_s V_s \gamma_w}{A_c} \tag{4.5}$$

where V_f and V_s are the volumes of fluid and solids in the column above the port, G_s is the specific gravity of solids and γ_w is the unit weight of pure water at 4 degrees C. Generally, γ_f will be different from γ_w.

Meanwhile, from the manometer's perspective,

$$p_m = h_m^B \gamma_f \tag{4.6}$$

Invoking Eq. (4.1):

$$\frac{V_f \gamma_f + G_s V_s \gamma_w}{A_c} = h_m^B \gamma_f \tag{4.7}$$

Since the volume of fluid in the sedimentation column is the total volume less the volume of solids:

$$\frac{(h_c^B A_c - V_s)\gamma_f + G_s V_s \gamma_w}{A_c} = h_m^B \gamma_f \tag{4.8}$$

which can be solved for the water level in the column during Stage B:

$$h_c^B = \frac{h_m^B \gamma_f A_c - (G_s \gamma_w - \gamma_f) V_s}{A_c \gamma_f} \tag{4.9}$$

The volume of solids must equal the volume of displaced fluid:

$$V_s = (h_c^B A_c + h_m^B A_m) - h_m^A (A_c + A_m) \tag{4.10}$$

where A_m is the inside cross-sectional area of the manometer.

Inserting Eq. (4.9) into Eq. (4.10):

$$V_S = (\frac{h_m^B \gamma_f A_c - (G_s \gamma_w - \gamma_f) V_s}{A_c \gamma_f}) A_c + h_m^B A_m - h_m^A (A_c + A_m) \tag{4.11}$$

which reduces to:

$$V_s = \frac{(h_m^B - h_m^A)(A_c + A_m)\gamma_f}{G_s \gamma_w} \tag{4.12}$$

The corresponding total weight of solids is:

$$W_S = (h_m^B - h_m^A)(A_c + A_m)\gamma_f \tag{4.13}$$

During Stage C, the particles are passing the connector thereby decreasing the water pressure at that elevation. Water is now flowing from the manometer back into the column. As such, the fluid level in the manometer progressively drops, and simultaneously rises in the column. The total volume decrease in the manometer at any time *t* must equal the volume increase in the column:

$$(h_m^B - h_m^C(t))A_m = (h_c^C(t) - h_c^B)A_c \tag{4.14}$$

By analogy to Eq. (4.8) during Stage B, in Stage C we have:

$$\frac{(h_c^C(t)A_c - V_s^C(t))\gamma_f + G_s \gamma_w V_s^C(t)}{A_c} = h_m^C(t)\gamma_f \tag{4.15}$$

in which $V_s^C(t)$ is the volume of solids still above the connector at any time *t*. Equation (4.15) is solved for the water level in the column during Stage C:

$$h_c^C(t) = \frac{h_m^C(t)\gamma_f A_c - (G_s\gamma_w - \gamma_f)V_s^C(t)}{A_c\gamma_f} \tag{4.16}$$

Next, we bring the expression for h_c^B by Eq. (4.9) and the expression for $h_c^C(t)$ by Eq. (4.16) into the volume balance by Eq. (4.14):

$$(h_m^B - h_m^C(t))A_m = (\frac{h_m^C(t)\gamma_f A_c - (G_s\gamma_w - \gamma_f)V_s^C(t)}{A_c\gamma_f} - \frac{h_m^B\gamma_f A_c - (G_s\gamma_w - \gamma_f)V_s}{A_c\gamma_f})A_c \tag{4.17}$$

which simplifies to the volume of solids that have passed the connector at time t during Stage C:

$$(V_s - V_s^C(t)) = \frac{(h_m^B - h_m^C(t))(A_m + A_c)\gamma_f}{(G_s\gamma_w - \gamma_f)} \tag{4.18}$$

The corresponding weight of solids that have passed the connector at time t is:

$$(W_s - W_s^C(t)) = \frac{G_s\gamma_w(A_c + A_m)\gamma_f}{(G_s\gamma_w - \gamma_f)}(h_m^B - h_m^C(t)) \tag{4.19}$$

Once all of the particles have passed the connector, we enter Stage D. With reference to Eq. (4.19), $h_m^C(t)$ now becomes a constant h_m^D and $W_s^C(t)$ becomes W_s^D which, by definition of Stage D, is zero. Thus,

$$W_s = \frac{G_s\gamma_w(A_c + A_m)\gamma_f}{(G_s\gamma_w - \gamma_f)}(h_m^B - h_m^D) \tag{4.20}$$

According to Eqs. (4.19) and (4.20), the percentage of the particles by weight still above the connection at any given time (*t*) during Stage C is:

$$\frac{W_s^C(t)}{W_S} = \frac{h_m^C(t) - h_m^D}{h_m^B - h_m^D} \tag{4.21}$$

During Stage D, the water levels in both the column and manometer become the same and constant at new levels:

$$h_c^D = h_m^D \tag{4.22}$$

These are higher than the heights during Stage A because of the presence of the accumulated soil solids at the base of the column. The volume of solids is therefore:

$$V_s = (h_m^D - h_m^A)(A_c + A_m) \tag{4.23}$$

We can equate this expression for V_s to the one given by Eq. (4.12):

$$\frac{(h_m^B - h_m^A)(A_c + A_m)\gamma_f}{G_s\gamma_w} = (h_m^D - h_m^A)(A_c + A_m) \tag{4.24}$$

which may be solved for the specific gravity of solids:

$$G_s = \frac{(h_m^B - h_m^A)\gamma_f}{(h_m^D - h_m^A)\gamma_w} \tag{4.25}$$

As the particles settle, they naturally sort by size. Therefore, at any given time during Stage C, the proportion of finer particles relative to those passing the manometer port elevation can be determined using Eq. (4.21). Furthermore, Eqs. (4.13) and (4.21) reveal that G_s is not needed to determine either the weight of the soil particles or the percentage of particles finer than those passing the port. However, G_s as computed by Eq. (4.25) will be needed for the particle settling velocity model, which will be used to determine the size of the particles traveling past the manometer port at any time t.

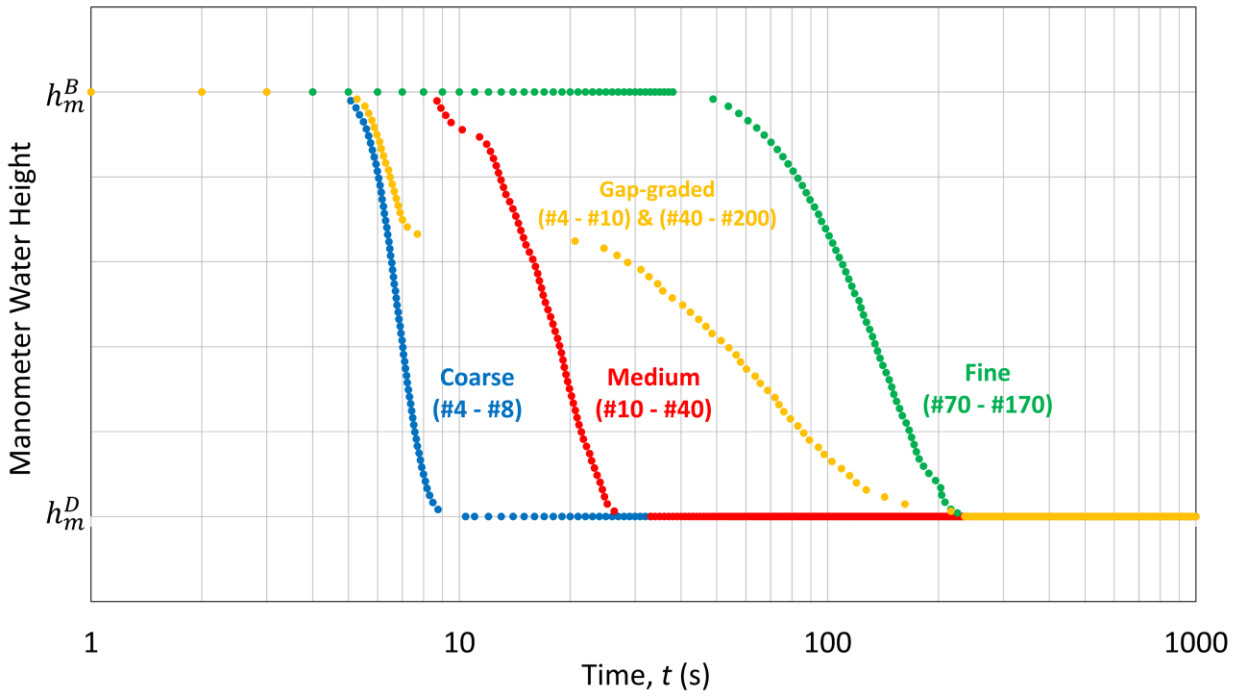


Figure 4.4: Typical manometer water height time histories for fine, medium, coarse and gap-graded sands.

4.3 Manometer Material and Diameter Selection

The inner diameter of the manometer tube is a critical parameter influencing the accuracy and responsiveness of the m-Sed system. A diameter that is too small amplifies capillary rise, inhibiting the prompt stabilization of the water level at a height reflecting the actual pressure. Conversely, an excessively large diameter introduces pronounced inertial effects, resulting from the larger volume of water that must move between the sedimentation column and the manometer

tube during the test. These inertial effects can potentially cause problems during Stages B and C of an m-Sed test:

1. Failure to achieve an initial stable manometer water level in Stage B:

Following the initial introduction of soil into the sedimentation column, the water pressure at the manometer port rises sharply, driving water from the column into the manometer tube. If the manometer tube diameter is too big, a large volume of water must flow rapidly, creating significant inertia. Consequently, the water level takes longer to stabilize, potentially failing to reach equilibrium before the largest particles arrive at the manometer port. The absence of a stable manometer water height during Stage B (h_m^B) compromises the analysis, as this initial equilibrium height serves as an essential baseline reference for subsequent calculation of PSD. Without it, accurate PSDs cannot be developed.

2. Delayed manometer response during Stage C:

As sedimentation proceeds and particles pass the measurement port, the water pressure gradually decreases, prompting reverse flow from the manometer tube back into the sedimentation column. A large tube diameter again results in substantial inertial effects, slowing the water's return flow and delaying the reestablishment of equilibrium. This sluggish response reduces the precision of water-level measurements during the sedimentation, ultimately affecting the precision of the PSD.

Through experimentation with different manometer diameters, a tube with an inner diameter of 3.2 mm (1/8 in.) was found to be optimal. This diameter effectively balances the competing effects of capillary force and inertial response, ensuring rapid stabilization and accurate PSD measurement.

The selection of the manometer tube material also significantly affects the responsiveness of the m-Sed system. A polyurethane rubber tube was specifically chosen for its high surface wettability which minimizes capillary rise, thereby reducing meniscus curvature. The smoothness of polyurethane rubber also promotes rapid water flow within the tube, providing swift and accurate responses to dynamic pressure changes. Finally, as mentioned earlier, the entire length of a polyurethane rubber tube manometer is easily coiled for packing and transportation, so it can be one continuous tube.

4.4 The m-Sed Test Procedure

The m-Sed test begins with measuring the temperature of the test water and determining the fluid's kinematic viscosity and density from the water-property table provided in Appendix B. The fluid for the column and manometer is typically room-temperature tap water. The water is introduced into the sedimentation column from the top until its level reaches about the h_C^A mark. For the current m-Sed system, h_C^A is set at 1.40 m, as shown in Figs. 4.1 and 4.3. The top end of the manometer is then bent downward to allow water to flow out through the tube, effectively expelling any air bubbles from the tube. The manometer is then secured adjacent to the scale on the sedimentation column by pressing it into the clips. Additional test water is then carefully introduced into the sedimentation column until the water level reaches the h_C^A mark.

To develop continuous PSD curves, readings of time should be recorded at fixed increments of water-level drop in the manometer. Practice has shown that this is preferred to taking water level readings at specified times. Taking time readings at equal increments of water level drop results in PSD data points equally spaced along the vertical (percent passing) axis of a PSD plot. An interval of 1 mm was adopted in this study, as this spacing provides a sufficient number of data points to construct smooth PSD curves. For the current m-Sed system, when the soil's specific gravity is 2.65, a 1 mm drop in manometer water level corresponds to approximately 0.82 g of soil passing the manometer port. For a 50 g soil specimen with G_s=2.65, this yields about 60 data points, equally spaced along the vertical (percent passing) axis of a PSD plot.

A cell-phone camera may be used to record a video of the water level drop with time. Using a camera also provides immediate data storage and eliminates possible errors in PSDs due to initially missed, imprecise or incorrect readings. For the current m-Sed system, a 50 g sand specimen causes the water level in the manometer tube to rise by approximately 10 cm from Stage A to Stage B (i.e., $h_m^B - h_m^A \approx 10$ cm). Therefore, to ensure full visibility, a video recording should capture the region from the top of the water in the manometer during Stage A to 15 cm above it. In this study, videos of all tests were recorded by a cellphone at a frequency of 60 Hz.

The 50 g soil specimen must be quickly introduced into the top of the sedimentation column using a wide-mouth funnel to ensure that all the particles have almost the same settlement starting time. For the determination of settling velocity of the particles at the port elevation, the relationship $v = L/t$ was employed, where L is defined as $(h_C^A + h_C^D)/2$, as shown in Fig. 4.3, and t represents the duration of particle settling. The time required for settlement depends on the smallest particle

size in the specimen. This is typically under 15 s for coarse sand, less than 30 s for medium sand, and less than 5 min for fine sand. Once the water height history in the manometer is recorded, the size of the particles passing through the manometer port elevation at any given time can be determined using Eq. (2.12). After that, Eq. (4.21) is used to determine the percent finer by weight than these particles. Development of the PSD easily follows.

4.5 Tested Materials and Test Results

Eight specimens were engineered from six soils that had been pre-sieved in accordance with ASTM C136/C136M-19 (ASTM 2019), *Standard Test Method for Sieve Analysis of Fine and Coarse Aggregates*, to evaluate the agreement in results between the m-Sed test and traditional sieving methods. To ensure a comprehensive and systematic evaluation, the specimens included various combinations of coarse, medium, and fine fractions, along with pure coarse, pure medium, and pure fine sands, as defined by ASTM D2487-17 (ASTM 2017), *Standard Practice for Classification of Soils for Engineering Purposes (Unified Soil Classification System)*. The specimens covered a particle size range from 0.075 mm to 4.75 mm, representing the entire ASTM-defined sand particle size range.

Griffin, IN and Michigan 2NS, both natural glacial soils, were each processed into two different gradations, resulting in specimens 1 through 4, as detailed in Table 4.1. To create a pure coarse sand specimen, Peanut Sand, a construction material from Ann Arbor, MI was selected due to its uniform coarse particle size distribution. Indiana Beach sand, a naturally occurring shoreline deposit, was chosen to produce a mixed specimen containing both medium and fine sand fractions. Muskegon sand, a coastal and dune sediment from Lake Michigan, was chosen to represent a well-sorted pure medium sand specimen. Lastly, a pure fine sand specimen was formed using Houston TX sand, which originates from fluvial and coastal plain deposits of southeastern Texas.

Figure 4.5 shows images of the eight soil specimens captured using a camera at a magnification of 4.075 μm/pixel (i.e., 245.4 pixels per mm). Each image shows a 1 cm × 1 cm area of the specimen. The percentages of coarse, medium, and fine sand of each specimen are included in parentheses in Fig. 4.5. The sieve-based particle size compositions of each specimen, along with their maximum and minimum particle sizes are provided in Table 4.1. Notably, since the sizes reported in Table 4.1 are based on sieve opening sizes, they may not precisely represent the actual maximum or minimum particle sizes present in the specimens.

Table 4.1: Tested Soil Specimens and Size Composition

No.	Name	Grain Size			Particle Size	
		Coarse (%)	Medium (%)	Fine (%)	Maximum (mm)	Minimum (mm)
1	Griffin, IN	34	33	33	4.75	0.106
2	Griffin, IN	50	50	0	4.75	0.425
3	Michigan 2NS	65	0	35	4.75	0.106
4	Michigan 2NS	35	0	65	4.75	0.075
5	Peanut Sand	100	0	0	4.75	2.36
6	IN Beach	0	50	50	2.00	0.150
7	Muskegon	0	100	0	2.00	0.425
8	Houston, TX	0	0	100	0.212	0.090

In the tests, a CSF value of 0.7, as widely recommended for natural sands, was used for all specimens except Specimen No. 5 — Peanut sand. As shown in Fig. 4.5, Peanut sand exhibits a plate-like shape. To account for this, 25 randomly selected particles from the specimen were measured using a caliper to determine their three orthogonal dimensions (a, b, and c). The average CSF of these particles was found to be approximately 0.45. Therefore, a CSF value of 0.45 was used in the Jiménez and Madsen model for Test No. 5.

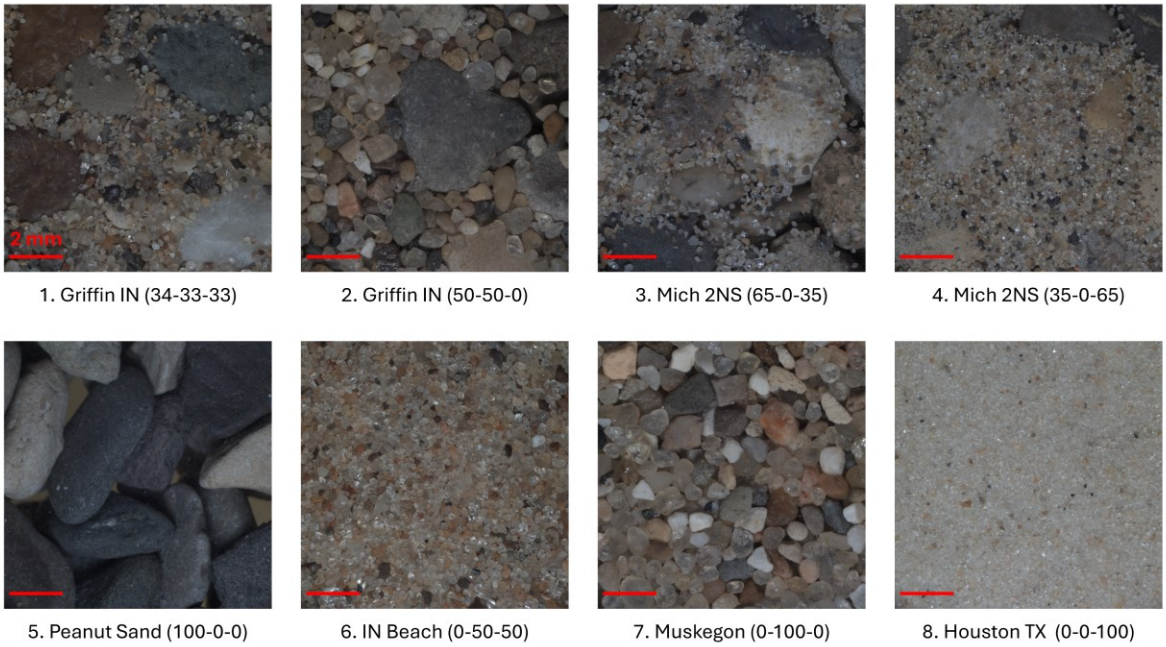


Figure 4.5: The eight tested soil specimens with their percentages of coarse, medium and fine sand.

Figure 4.6 presents the PSD curves obtained from the m-Sed test and by sieving. The PSD curves generated by the m-Sed test exhibit almost perfect agreement with the data points from sieving (with slight differences, typically less than 0.1 mm). Given the strong agreement between the m-Sed results and sieving, the fitting curves to the sieve data were omitted in Fig. 4.6. For the gap-graded soils (Specimens 3 and 4), an absence of m-Sed data points is observed in the intermediate particle size range. The reason for this is obvious: within this range, no soil particles exist to pass the manometer port, causing the manometer water level to remain constant.

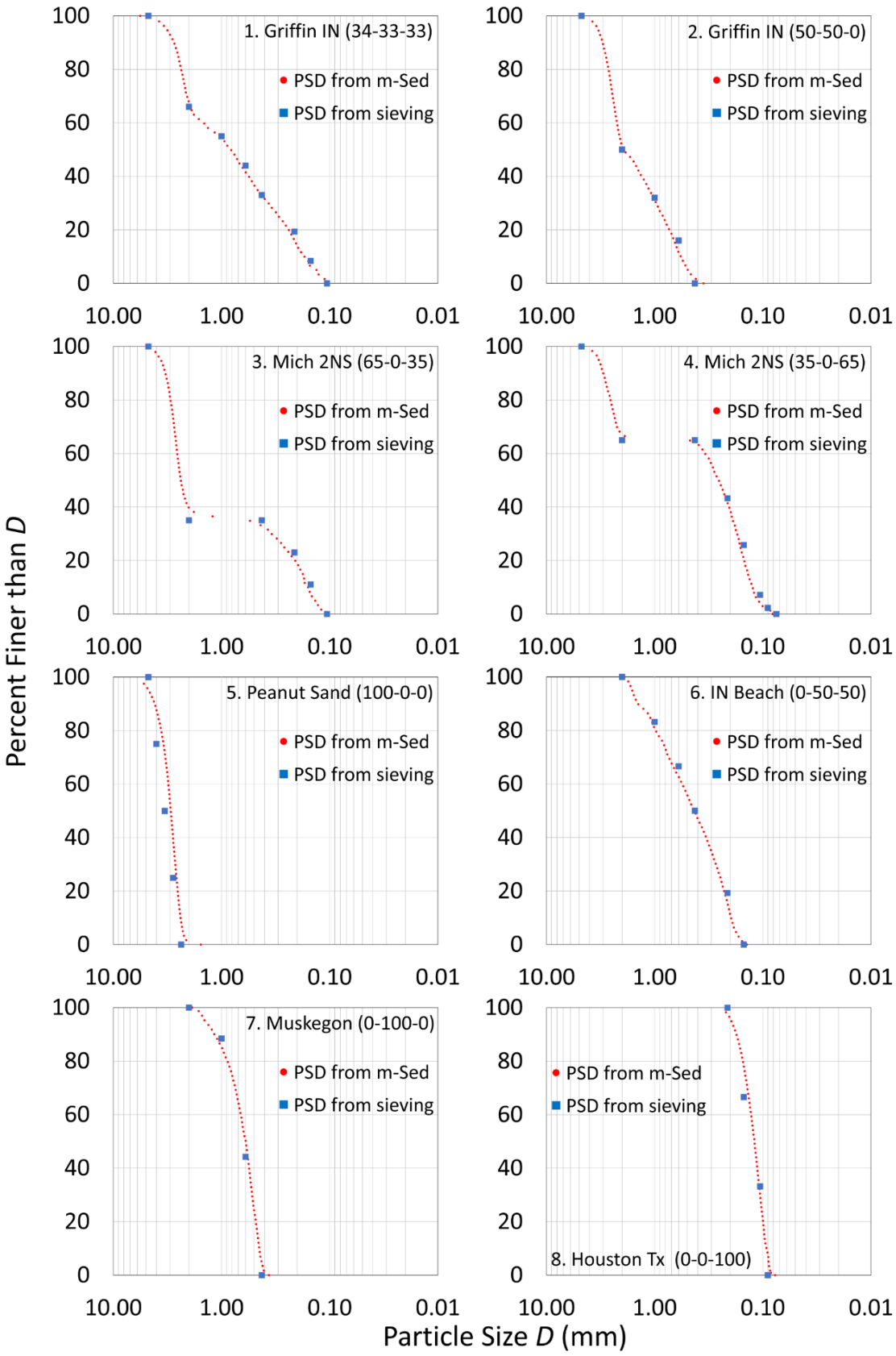


Figure 4.6: Comparison of PSDs from the m-Sed and sieve tests.

Table 4.2: Comparison of Particle Size Distribution Metrics between Sieve and m-Sed.

No.	Name	Sieve						m-Sed					
		D_{60} (mm)	D_{50} (mm)	D_{30} (mm)	D_{10} (mm)	C_u	C_c	D_{60} (mm)	D_{50} (mm)	D_{30} (mm)	D_{10} (mm)	C_u	C_c
1	Griffin, IN	1.45	0.82	0.37	0.16	9.06	0.59	1.45	0.82	0.37	0.17	8.53	0.56
2	Griffin, IN	2.23	2.00	0.98	0.57	3.91	0.76	2.23	2.00	0.98	0.57	3.91	0.76
3	Michigan 2NS	2.57	2.39	0.33	0.15	17.13	0.28	2.57	2.39	0.34	0.16	16.06	0.28
4	Michigan 2NS	0.34	0.25	0.16	0.11	3.09	0.68	0.34	0.25	0.17	0.12	2.83	0.71
5	Peanut Sand	3.40	3.35	2.75	2.50	1.36	0.89	3.11	2.96	2.68	2.40	1.30	0.96
6	IN Beach	0.54	0.43	0.27	0.20	2.70	0.68	0.55	0.43	0.27	0.20	2.75	0.66
7	Muskegon	0.67	0.60	0.52	0.45	1.49	0.90	0.67	0.60	0.52	0.45	1.49	0.90
8	Houston, TX	0.14	0.12	0.11	0.09	1.56	0.96	0.13	0.12	0.11	0.09	1.44	1.03

Table 4.2 quantitatively compares the PSD results from the sieve test and the m-Sed test via the particle size distribution metrics (D_{60}, D_{50}, D_{30}, and D_{10}) obtained by both methods. Comparisons of the coefficients of uniformity (C_u) and curvature (C_c) are also included in the table. Overall, the results of the m-Sed test show close agreement with the sieve test results. In practical terms, the remaining differences between the two methods are negligible relative to the natural spatial variability of soil PSDs within a deposit and the variability arising from sampling, specimen preparation, and routine laboratory testing.

Beyond PSD determination, the m-Sed test also enables the measurement of specific gravity (Eq. 4.25) and soil specimen mass (Eq. 4.13). Table 4.3 compares the specific gravity values derived from the m-Sed test and those from the specific gravity test according to ASTM D854-23 (ASTM 2023), *Standard Test Methods for Specific Gravity of Soil Solids by the Water Displacement Method*. Notably, for the same soil type (e.g., Specimen No. 1 and Specimen No. 2), specimens with different gradations or from different samples may show slight differences in specific gravity. In the ASTM specific gravity test, a single 150 g bulk specimen of well-graded

soil was tested, and that value is used to represent the specific gravity of the soil type. By contrast, the m-Sed test determines specific gravity individually on each 50 g specimen, which reveals minor differences between specimens. Such minor differences in specific gravity have been shown by Zhang and Hryciw (2025) to have virtually no effect on the PSD results. The comparison between the soil specimen mass determined by the m-Sed test and that measured using a laboratory weight scale is also presented in Table 4.3. As the results show, the m-Sed test provides highly reliable values of specific gravity and soil specimen mass.

Table 4.3: Comparison of Specific Gravity and Specimen Mass

No.	Name	Specific Gravity			Specimen Mass		
		m-Sed	ASTM	Difference	m-Sed (g)	Weight Scale (g)	Difference (%)
1	Griffin, IN	2.69	2.68	0.01	49.76	49.89	0.3
2	Griffin, IN	2.67	2.68	0.01	50.02	49.90	0.2
3	Michigan 2NS	2.66	2.66	0	50.28	49.93	0.7
4	Michigan 2NS	2.68	2.66	0.02	49.63	49.79	0.3
5	Peanut Sand	2.70	2.71	0.01	50.05	49.95	0.2
6	IN Beach	2.68	2.67	0.01	49.63	49.88	0.5
7	Muskegon	2.65	2.65	0	49.76	49.93	0.3
8	Houston, TX	2.65	2.66	0.01	49.63	49.95	0.6

4.6 Repeatability and Comparison with the *u*-Sed Test

Specimen #1, with a composition of 34% coarse sand, 33% medium sand, and 33% fine sand, was tested three times to confirm the repeatability of the m-Sed test. As shown in Fig. 4.7, the three m-Sed tests on the same specimen not only exhibit a strong agreement with the comparatively sparse data points from the sieve test, but also demonstrate consistency among themselves in the regions between the sieve data points, thus confirming the repeatability of the m-Sed test.

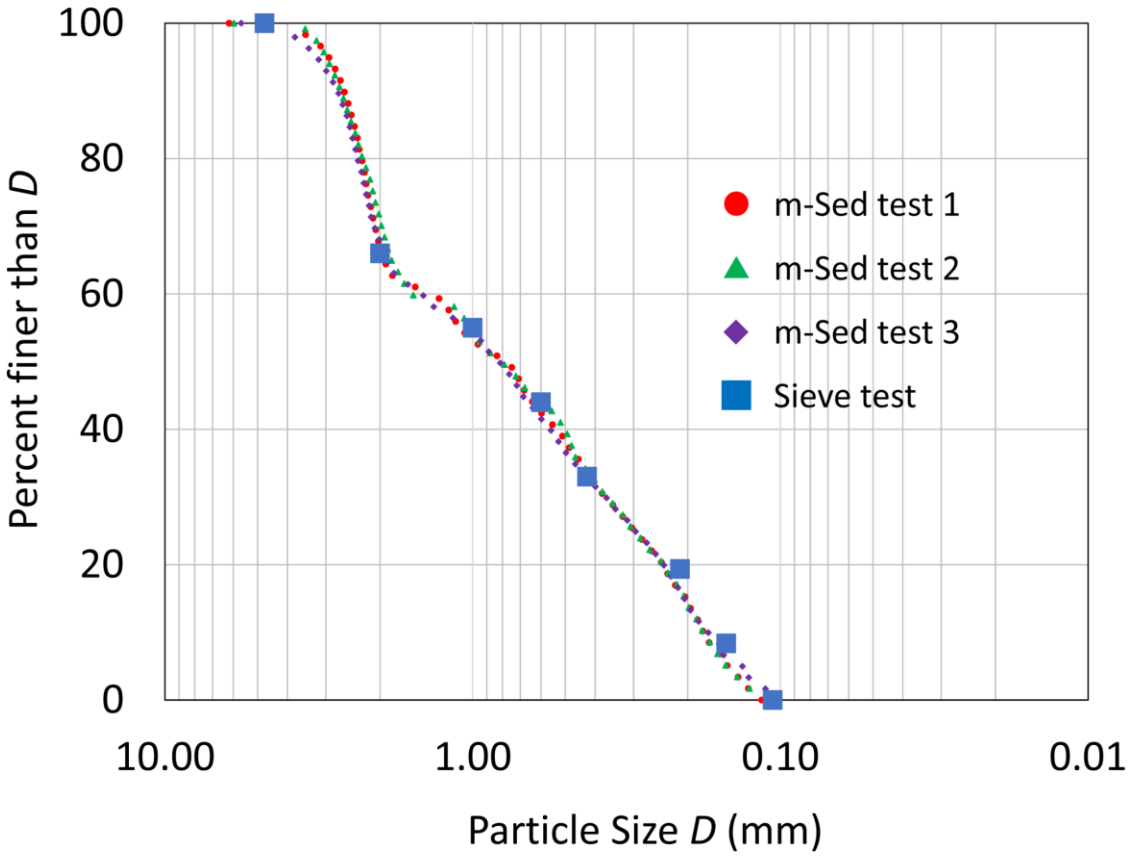


Figure 4.7: Repeatability Assessment of the m-Sed test.

The PSD of Specimen #1 was also determined using the original *u*-Sed test (Zhang and Hryciw 2025) with a pressure transducer. A comparison of the PSD results obtained from the m-Sed, *u*-Sed, and sieve tests is presented in Fig. 4.8. As shown in the figure, both the *u*-Sed and m-Sed tests not only exhibit excellent agreement with the sieve test, but also show agreement with each other.

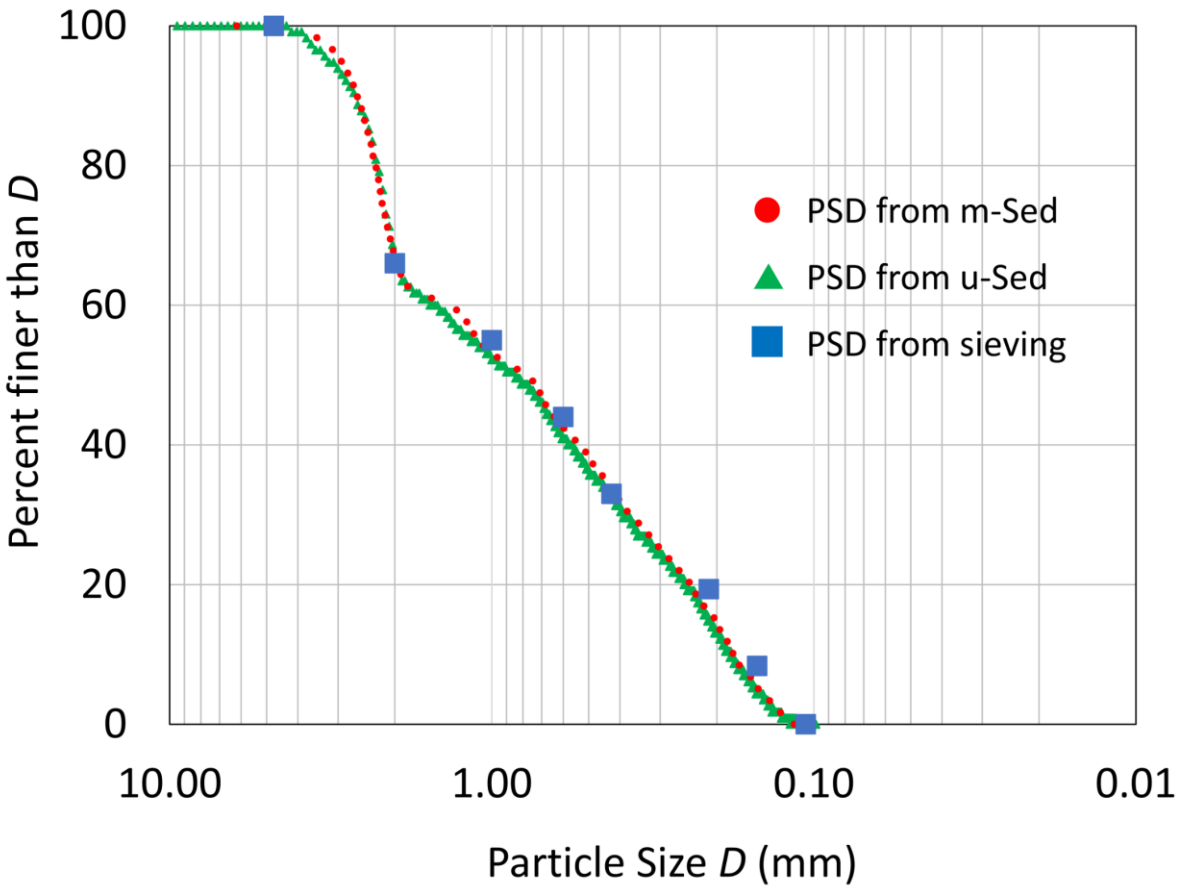


Figure 4.8: Comparison of PSD results from the m-Sed, *u*-Sed, and sieve tests.

4.7 Factors Affecting PSD Determination in the *u*-Sed and m-Sed Tests

Following the repeatability assessment and direct comparison presented in Section 4.6, the factors affecting PSD determination can now be considered jointly for the two systems. The *u*-Sed and m-Sed tests use the same sedimentation column, particle-introduction procedure, and settling-velocity framework, differing primarily in how the pressure response is measured. Factors associated with particle settling and specimen introduction are therefore generally common to both systems. System-specific measurement factors—such as transducer resolution and sampling rate for the *u*-Sed test and manometer material and tube diameter for the m-Sed test—were addressed in Sections 3.5 and 4.3, respectively. This section first considers the effects of particle specific gravity, fluid viscosity, and specimen mass evaluated in Section 3.5, followed by additional material and environmental factors relevant to both systems.

The sensitivity analyses presented in Section 3.5 showed that small variations in the assumed particle specific gravity G_s, and minor temperature-induced variations in the kinematic viscosity of water have negligible effects on the PSDs obtained from the u-Sed test. Particle size in both the u-Sed and m-Sed tests is determined from the same settling-velocity relationships using the measured settling time, particle specific gravity, and fluid viscosity. Therefore, similarly small variations in G_s and kinematic viscosity also have negligible effects on the PSDs obtained from the m-Sed test.

Specimen-mass considerations are also common to both systems. If the specimen mass is too small, the resulting pressure or manometer-head response is reduced, thereby decreasing measurement sensitivity and PSD resolution. Conversely, if a substantially larger specimen is used, more time is required for all particles to pass through the funnel and enter the sedimentation column. The particles may then begin settling at appreciably different times, violating the assumption that sedimentation begins nearly simultaneously for the complete specimen. As demonstrated for the u-Sed test in Section 3.5, specimen masses between 40 and 60 g produced consistent PSD results. Because the present m-Sed system uses the same 1-in.-diameter column geometry and the same particle-introduction procedure, this range is also adopted as the recommended specimen-mass range for the current m-Sed configuration.

In addition to the factors evaluated in Chapter 3, particle shape can influence the PSDs obtained from both systems because particle morphology affects settling velocity. As illustrated in Figure 2.2 by Jiménez and Madsen (2003), the *Corey Shape Factor* (CSF) of sand particles directly affects the coefficients A_{JM} and B_{JM} in Eq. (2.12), which in turn affects the particle size inferred from a measured settling velocity and therefore influences the resulting PSD. Figure 4.9 presents the relationship between settling velocity and particle size by Eq. (2.12) for natural sand with different CSF values. To produce these curves, typical values of $G_s = 2.65$ and $\vartheta = 0.8926\ mm^2/s$ were assumed. The plot illustrates that larger particles exhibit greater sensitivity to variations in CSF, with higher CSF values corresponding to higher settling velocities. As particle size decreases, the effect of CSF on settling velocity becomes progressively less significant.

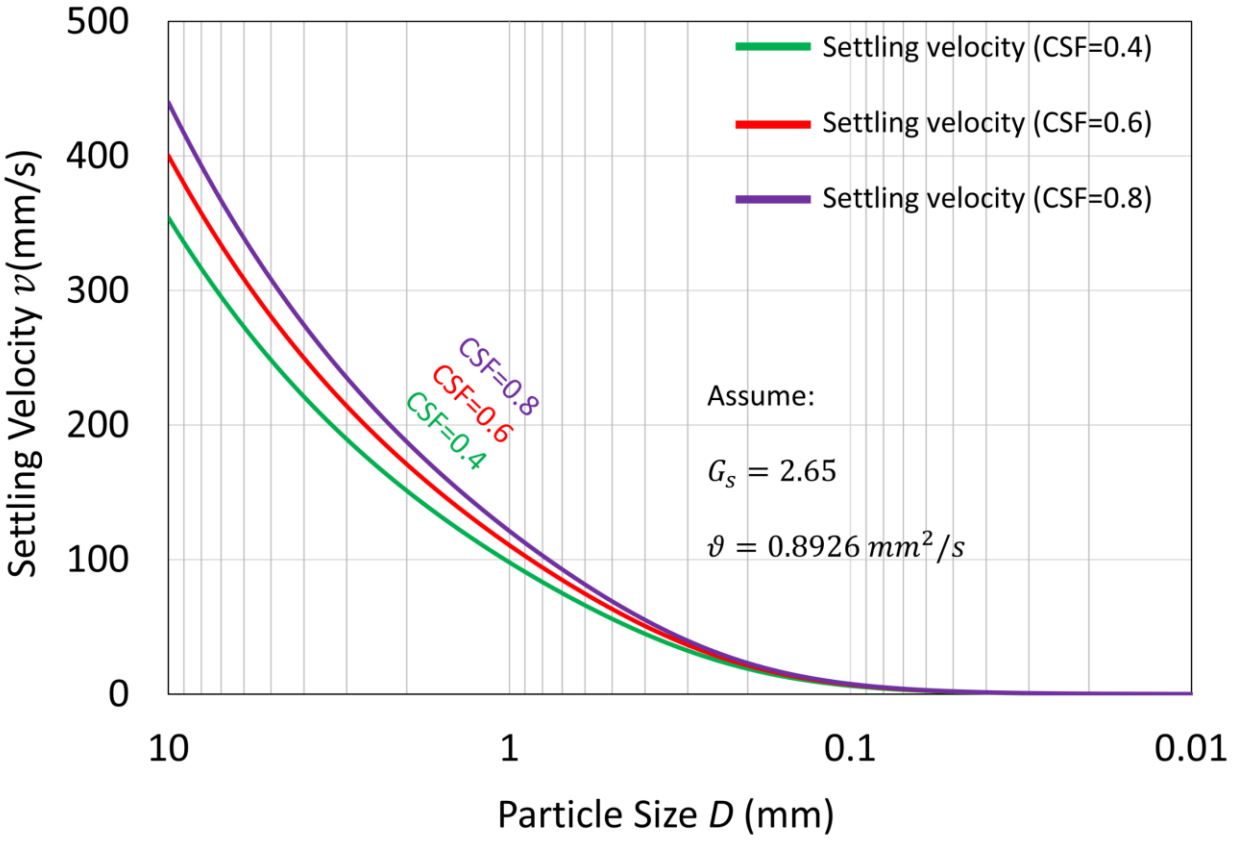


Figure 4.9: Effect of CSF values on particle settling velocity.

To further evaluate the influence of particle shape on the resulting PSDs, the water-height–time histories obtained from the m-Sed tests on Specimen #1 (Griffin IN) and Specimen #8 (Houston TX) were analyzed using different assumed CSF values. As shown in Fig. 4.10, the influence of CSF on the calculated particle size diminishes with decreasing particle size and becomes relatively small for the finer fractions. In contrast, variations in CSF produce appreciable differences in the particle sizes calculated for coarse sand. Although this parametric analysis was performed using m-Sed measurements, the same conclusion applies to the *u*-Sed test when the Jiménez and Madsen model is used because both systems convert measured settling velocity to particle size using the same relationship. Particle shape should therefore be characterized appropriately when either system is applied to sands containing coarse, platy, elongated, or otherwise atypically shaped particles.

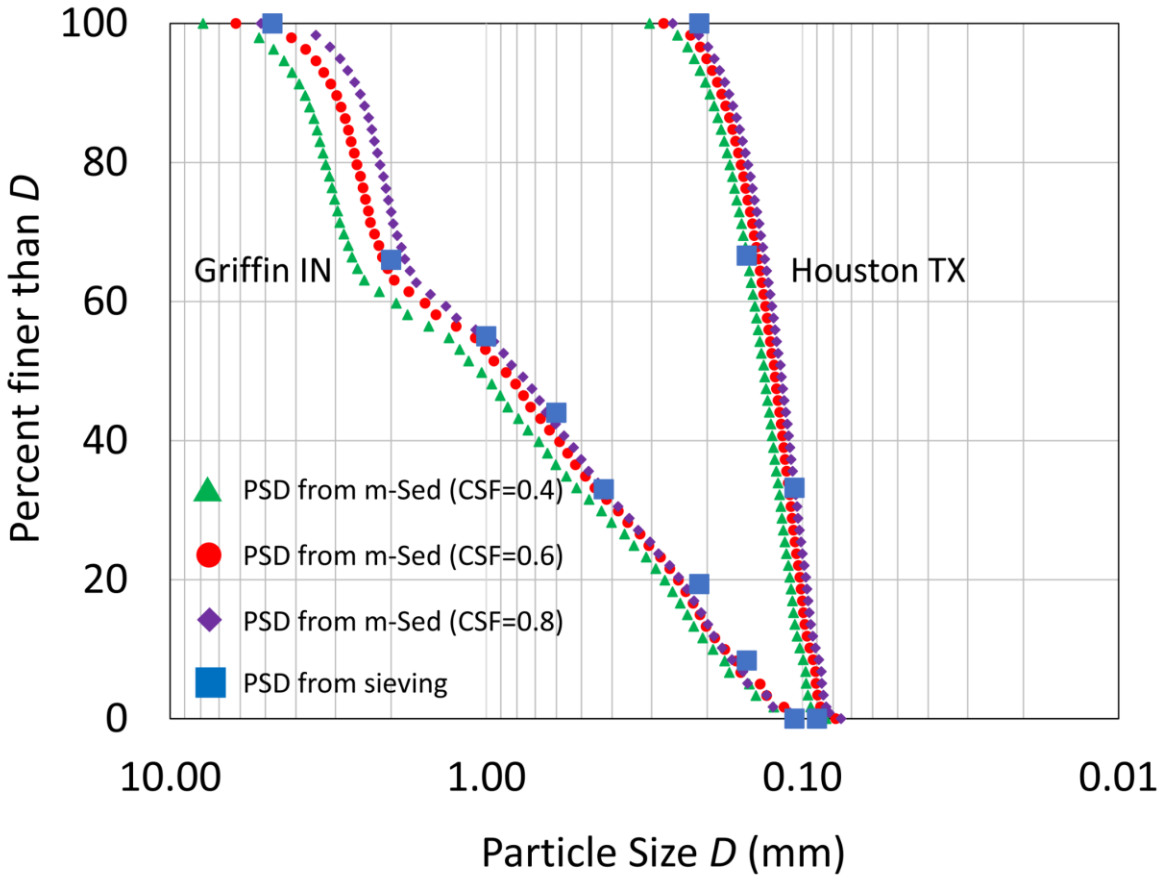


Figure 4.10: The effect of CSF values on PSDs from the m-Sed test.

The possible influences of dissolved air and atmospheric-pressure variations were also considered. Previous studies, including Caw and Wylie (1961), Jones and Harris (1992), and Blahut et al. (2019), have shown that, within the ranges typical of laboratory testing, neither factor produces appreciable changes in water density or viscosity. These factors are therefore not expected to measurably affect the PSDs obtained from either the *u*-Sed or m-Sed test.

Finally, two uncommon but noteworthy limitations also apply to both systems. First, if particles are porous (e.g., calcareous sands with skeletal or open intragranular voids), entrapped air may reduce their effective density and thereby alter their settling velocities, which can introduce errors in the PSDs. Second, if the specific gravities of particles exhibit pronounced variations from one size range to another, the resulting PSD would be affected.

4.8 Chapter Summary

This chapter introduced the m-Sed test, a sedimentation-based method for determining the particle size distributions of sands in which the pressure response during particle settling is measured by a simple manometer rather than an electronic pressure transducer. The method extends the pressure-based sedimentation concept developed in the *u*-Sed test, but replaces the electronic pressure transducer with a simple manometer tube. This modification eliminates the need for electrical power, electronic pressure sensing, and sensor calibration, making the system more suitable for field use, remote locations, wet environments, and resource-limited conditions.

The m-Sed system consists of a two-part acrylic sedimentation column, a fixed manometer port, a flexible polyurethane rubber manometer tube, and a scale. During testing, the introduction and settlement of soil particles cause water to move between the sedimentation column and the manometer. As particles pass the manometer port, the water level in the manometer decreases with time. This water-height history provides the percentage of specimen solids remaining above the port, while the Jiménez and Madsen settling-velocity model is used to convert elapsed time into particle size.

The governing equations for the m-Sed test were derived from four pressure stages. Unlike the *u*-Sed system, in which the pressure transducer records pressure without appreciable fluid exchange, the m-Sed system requires bidirectional flow between the column and the manometer. This makes the formulation more complex, but it allows PSD, specimen mass, and soil specific gravity to be determined without electronic instrumentation. The chapter also showed that manometer tube selection is critical. A 3.2-mm (1/8 in.) inner-diameter polyurethane tube was found to provide an effective balance between capillary effects and inertial response, enabling rapid stabilization and reliable tracking of pressure changes during sedimentation.

The m-Sed test was validated using eight engineered sand specimens spanning the full ASTM sand-size range. These specimens included mixtures of coarse, medium, and fine sand, gap-graded sands, and uniform coarse, medium, and fine sands. The PSDs obtained from the m-Sed test showed excellent agreement with sieve-based PSDs. Quantitative comparisons of D_{60}, D_{50}, D_{30}, D_{10}, C_u, and C_c confirmed the accuracy of the method. Repeated tests on the same specimen produced nearly identical PSDs, demonstrating strong repeatability. A direct comparison among m-Sed, *u*-Sed, and sieve results also showed that the manometer-based system can reproduce the accuracy of the pressure-transducer-based *u*-Sed system.

The chapter further examined the influence of particle shape on m-Sed PSDs. Because the Jiménez and Madsen model accounts for particle shape and roundness through the Corey Shape Factor, shape effects are most important for coarse particles and become progressively less significant for finer sands. This indicates that shape information is most critical when the tested material contains a substantial coarse sand fraction, especially if the particles are plate-like or highly angular.

Compared with sieve analysis, the m-Sed test provides a rapid, quiet, dust-free, compact, low-energy, and nearly continuous alternative for sand PSD determination. Compared with the *u*-Sed test, its principal advantage is operational simplicity: it requires no pressure transducer, no data acquisition system, no electrical power, and essentially no electronic maintenance. If desired, a cellphone camera can be used only as an optional recording device rather than as a required component of the measurement system. The main limitations of the method are similar to those of the *u*-Sed test: porous particles with entrapped air may alter effective settling density, and specimens with strong specific-gravity differences among size fractions may bias the computed PSD. Overall, the m-Sed test provides a simple, accurate, and field-portable sedimentation system for determining nearly continuous PSDs of sand-sized soils.

Chapter 5 The Δ-Sed Test

Chapters 3 and 4 demonstrated that sedimentation-based pressure measurements can be used to determine nearly continuous particle size distributions (PSDs) of sands. In the *u*-Sed and m-Sed tests, a dry sand specimen is introduced at the top of a water column, after which the particles settle, sort by size, and pass a fixed measurement port. The resulting pressure response is interpreted through a mass balance on the particles above the port. These two tests showed strong agreement with sieve analysis across the ASTM sand-size range, with the m-Sed test further eliminating the need for electrical power by replacing the pressure transducer with a manometer. However, this testing concept cannot be directly extended to fine-grained soils (silts and clays).

The difficulty is not the use of sedimentation, but the specimen preparation and pressure-measurement framework required for reliable fines analysis. Dry silts and clays cannot simply be poured into the top of a water column because they tend to remain at or near the water surface. Introducing fines as a wet slurry is also unsuitable because the denser slurry descends through the water as unstable viscous plumes, preventing the particles from settling independently. Therefore, sedimentation analysis of fines must begin with a fully dispersed, spatially uniform suspension, as in conventional hydrometer analysis.

This chapter presents the Δ-Sed test, an automated differential-pressure sedimentation method developed for determining the PSD of fine-grained soils. Unlike the *u*-Sed and m-Sed tests, which monitor the passage of sand particles past a measurement port after dry introduction, the Δ-Sed test monitors the time-dependent concentration of an initially uniform fine-grained suspension. The system measures the differential pressure between two fixed sidewall ports separated vertically within the sedimentation cylinder. This differential pressure reflects the average bulk density of the suspension within the interval between the two ports. The average concentration over this fixed interval is then used to approximate the local concentration at the midpoint elevation, following a spatial-averaging principle conceptually analogous to that used in hydrometer analysis.

The chapter begins by developing the sedimentation theory for fines and the relationship among local concentration, settling time, particle size, and percent finer. It then compares concentration measurement in the pipette, hydrometer, integral suspension pressure, and Δ-Sed methods. The governing equations for the Δ-Sed test are derived from differential pressure measurements between two fixed ports. Numerical simulations are then used to evaluate the effects of port spacing, upper port depth, soil specific gravity, suspension temperature, and gradation on the accuracy of the method. The optimized Δ-Sed hardware is subsequently described. Finally, the method is validated using four fine-grained soils, and its repeatability, sensitivity to input parameters, resistance to evaporation-induced pressure offsets, and applicable particle-size range are evaluated.

5.1 Sedimentation Theory for Fines

The sedimentation-based method for determining the PSD of soils is based on differences in particle settling velocities in a fluid under gravity. For fine-grained soils (silts and clays), the procedure begins by mixing a soil specimen of known mass with a dispersing agent—typically sodium hexametaphosphate—within a dispersion cup. Mechanical stirring ensures complete dispersion and prevents the fine particles from coalescing or flocculating. After mixing and stirring, the dispersed suspension is transferred to a sedimentation cylinder and diluted with distilled or demineralized water to a prescribed total volume, typically 1000 mL. Prior to sedimentation, the suspension is thoroughly homogenized—using either a hand agitator or the inversion method to achieve a spatially uniform initial state.

Mathematically, let the discrete particle-size classes within the specimen be denoted as D_1, D_2 , D_3 ,…, D_i ,… D_n , where $D_1 > D_2 > D_3 > \cdots > D_i > \cdots D_n$. At the exact onset of sedimentation ($t = 0$), the suspension is assumed to be perfectly uniform. Furthermore, let $m_{s,i}$ denote the total mass of soil particles in size class D_i. The corresponding initial concentration of this size class, C_i, is therefore:

$$C_i = \frac{m_{s,i}}{V} \tag{5.1}$$

where V= the total volume of the mixture. Because the suspension is fully homogenized at $t = 0$, C_i is uniformly distributed with depth at the start. Summing Eq. (5.1) over all size classes yields the initial total soil concentration:

$$C_{\text{total}} = \sum_{i=1}^{n} C_i = \frac{m_s}{V} \tag{5.2}$$

For $m_s = 50$ g and $V = 1000$ mL, $C_{\text{total}} = 0.05$ g/mL.

Immediately after thorough mixing, the sedimentation cylinder is placed on a stable surface, and particles commence settling under gravity. Consider now a specific measurement depth, z, referenced from the suspension surface, and focus on particles belonging to size class D_i. Among all particles in this class, those initially located at the suspension surface will be the last to pass depth z.

During sedimentation, soil particles undergo progressive size-sorting due to their differences in settling velocity—coarser particles settle faster, followed by finer ones. Let t_i denote the time at which the last particles of size class D_i (originating from the suspension surface) pass depth z. At this exact instant t_i, the following conditions hold: for any coarser size class D_j where $D_j > D_i$ (i.e., $j < i$), their corresponding "last particles" have already fallen below depth z, resulting in a local concentration of zero ($C_j(t_i, z) = 0$). Conversely, for any finer size class D_j where $D_j < D_i$ (i.e., $j > i$), their "last particles" have not yet reached depth z, meaning their concentration remains at the initial value ($C_j(t_i, z) = C_j$). Consequently, at time t_i, the local concentration of a specific particle size class C_j at depth z can be expressed as:

$$C_j(t_i, z) = \begin{cases} 0, & j \le i \\ C_j, & j > i \end{cases} \tag{5.3}$$

Accordingly, the soil concentration at depth z and time t_i is:

$$C(t_i, z) = \sum_{j=i+1}^{n} C_j \tag{5.4}$$

To determine the PSD, the ‘‘percent finer’’ than size class D_i, denoted as $P(D_i)$, is defined as the percentage of the mass of particles finer than D_i to the total mass of particles in the specimen. Since $D_j < D_i$ corresponds to $j > i$, $P(D_i)$ can be expressed as:

$$P(D_i) = \frac{\sum_{j=i+1}^{n} m_{s,j}}{m_s} \times 100\% = \frac{\sum_{j=i+1}^{n} C_j}{C_{\text{total}}} \times 100\% \tag{5.5}$$

Combining Eqs. (5.4) and (5.5) yields:

$$P(D_i) = \frac{C(t_i, z)}{C_{\text{total}}} \times 100\% \tag{5.6}$$

Equation (5.6) indicates that once the transient soil concentration $C(t_i, z)$ is determined, the percent finer $P(D_i)$ follows directly. Thus, the continuous PSD can be constructed by evaluating the soil concentration at depth z across a sequence of times $\{t_i\}$. The remaining task is

to establish the mapping between time and particle size, i.e., to determine D_i associated with the elapsed time t_i. This can be obtained from a settling velocity model, such as Stokes' law:

$$v = \frac{g(\rho_s - \rho_f)D^2}{18\mu} \tag{5.7}$$

where v = the settling velocity, g = the acceleration due to gravity, ρ_s = the density of the soil particles, ρ_f = the density of the fluid, D = the particle diameter, μ= the dynamic viscosity of the fluid.

The diameter of the last particles of size class D_i passing depth z at time t_i can be obtained by rearranging Eq. (5.7) as:

$$D_i = \sqrt{\frac{18\mu}{g(\rho_s - \rho_f)} \times \frac{z}{t_i}} \tag{5.8}$$

By deploying Eqs. (5.6) and (5.8) at equivalent times, t_i, the soil PSD can be explicitly determined. It follows that the central experimental task in a sedimentation-based method is the determination of the soil concentration at a specified depth z and time t_i, $C(t_i, z)$.

5.2 Soil Concentration Determination during Sedimentation

In conventional geotechnical sedimentation analysis, the localized soil concentration is evaluated either directly, by extracting a suspension sample at a prescribed depth, or indirectly, via the buoyancy equilibrium of a floating hydrometer. As illustrated in Fig. 5.1, the pipette method involves inserting its tip to a specified depth, z, at predetermined time intervals to withdraw a known volume of the suspension. The mass of the extracted soil is then used to determine the concentration, which is used to represent the soil concentration at that precise localized depth.

The hydrometer analysis evaluates soil concentration without fluid extraction, relying instead on buoyant equilibrium. A standard hydrometer consists of a slender graduated stem and a larger-volume bulb. Because the submerged stem volume is negligible relative to the bulb, the center of buoyancy is approximated as the geometric centroid of the bulb volume. The vertical distance between this fixed centroid and any graduation mark on the stem is predetermined through calibration. During testing, the stem reading at the suspension surface indicates the average density of the fluid displaced by the submerged bulb. Through standard calibration, this measured bulk density is converted into a soil concentration. In practice, this average value is assumed to represent the localized concentration at the elevation of the bulb's centroid. Consequently, the hydrometer does not measure a true point concentration, but rather an average value integrated over a finite

sampling zone defined by the bulb's volume. As particles settle and the overall suspension density decreases, the hydrometer sinks progressively deeper to maintain buoyant equilibrium. This continuous downward translation means that the effective sampling zone does not remain at a fixed elevation but shifts continuously downward within the sedimentation cylinder throughout the test.

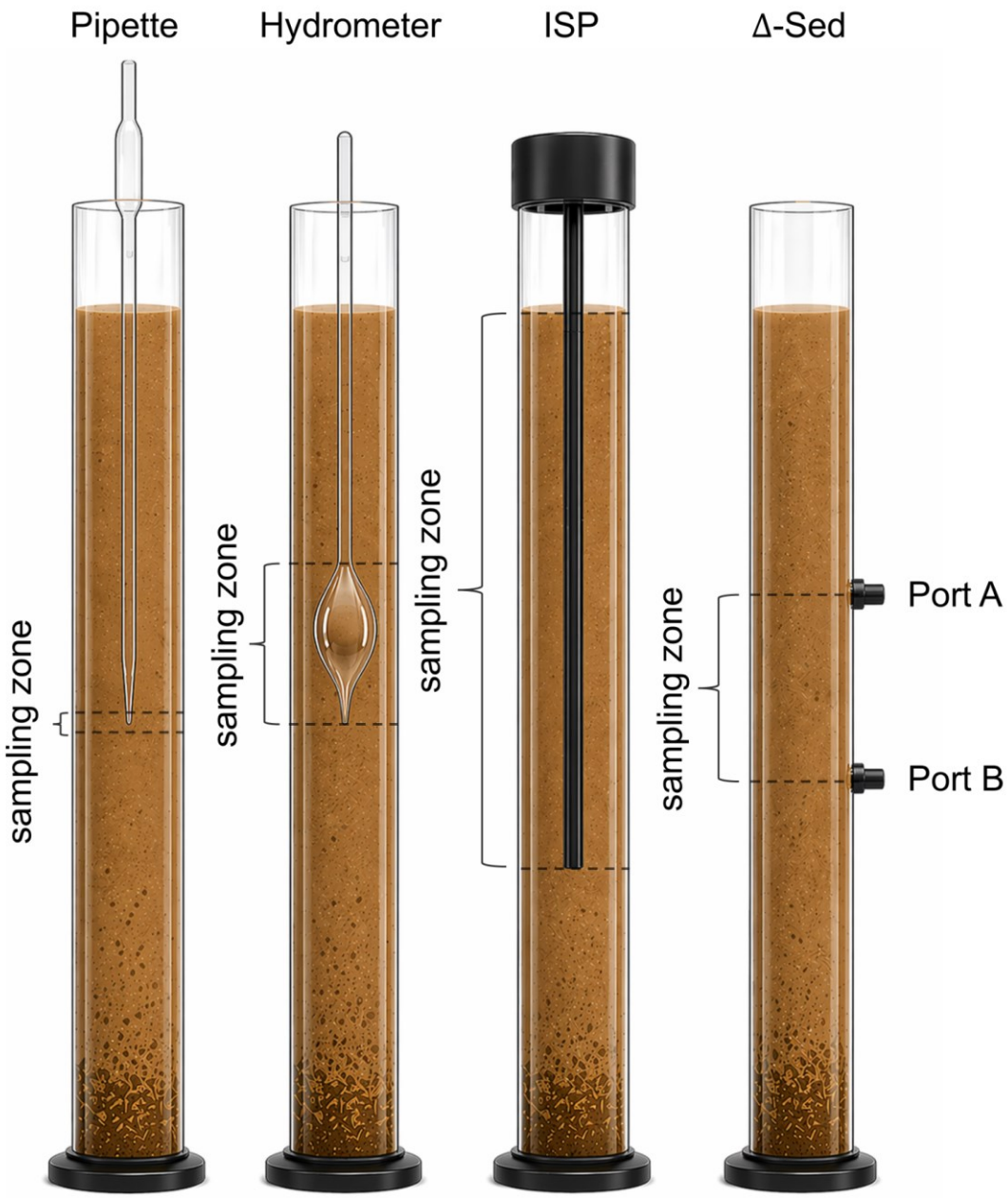


Figure 5.1: Schematic illustration of sampling zones for sedimentation-based particle size analysis methods: pipette, hydrometer, ISP, and Δ-Sed.

In the ISP method, a pressure sensor is positioned at a predetermined depth to continuously monitor the water pressure of the suspension throughout the test. This measured pressure is used to calculate the total mass of soil particles suspended in the fluid above the sensor. Consequently, the sampling zone in the ISP method differs fundamentally from those of the pipette and hydrometer methods: rather than estimating a localized concentration at a specific point or within a small moving volume, the ISP method measures the bulk suspension pressure to evaluate the spatial integral of the concentration from the suspension surface down to the sensor's elevation. To derive the PSD from this integrated measurement, the method forward-simulates the expected temporal evolution of pressure based on an assumed parameterized PSD and utilizes a global optimization algorithm to iteratively adjust the measurement depth and PSD parameters until the simulated pressure time-series best fits the observed measurements.

In the Δ-Sed method, soil concentration is determined using a spatial averaging principle which is conceptually analogous to that employed in hydrometer analysis. Rather than relying on physical fluid extraction or a shifting buoyant equilibrium, the Δ-Sed system measures the differential pressure between two fixed ports at prescribed elevations along the sedimentation column, as illustrated in Fig. 5.1. This differential pressure directly reflects the localized bulk density of the suspension within the vertical interval between the two ports, from which the average soil concentration can be inferred. In the Δ-Sed formulation, the soil concentration at the midpoint elevation between the two ports is approximated as the average concentration over the interval defined by the ports. This approximation is conceptually similar to that used in hydrometer analysis, wherein the density at the center of buoyancy is approximated as the average density over the bulb sampling zone. However, unlike the hydrometer method, the Δ-Sed sampling zone remains spatially fixed throughout the test.

At the upper pressure port, Port A, the pressure can be expressed as:

$$p_A = \frac{W_{saA}+W_{faA}}{A_c} \tag{5.9}$$

where W_{saA} = weight of soil above Port A; W_{faA} = weight of fluid above Port A; A_c = inside cross-sectional area of the sedimentation column.

The weights W_{saA} and W_{faA} in Eq. (5.9) can be expressed in terms of their respective volumes:

$$p_A = \frac{V_{saA}G_s\gamma_w+V_{faA}\gamma_f}{A_c} \tag{5.10}$$

where V_{saA} = the volume of soil above Port A; G_s = the specific gravity of soil solids; V_{faA} = the volume of fluid above Port A; γ_f = the unit weight of the fluid, γ_w = the unit weight of pure water at 4°C = 9.81 kN/m^3.

Since the total volume of soil and fluid above Port A is:

$$V_A = V_{saA} + V_{faA} \tag{5.11}$$

Eq. (5.10) may be written:

$$p_A = \frac{V_{saA}G_s\gamma_w + (V_A - V_{saA})\gamma_f}{A_c} \tag{5.12}$$

Since $V_A = h_A A_c$, where h_A is the vertical distance between the suspension surface and Port A, Eq. (5.12) is reorganized as:

$$p_A = \frac{V_{saA}(G_s\gamma_w - \gamma_f)}{A_c} + h_A\gamma_f \tag{5.13}$$

By analogy to Eq. (5.13), the pressure at Port B is:

$$p_B = \frac{V_{saB}(G_s\gamma_w - \gamma_f)}{A_c} + h_B\gamma_f \tag{5.14}$$

Subtracting Eq. (5.13) from Eq. (5.14), the difference in pressure between the two ports is:

$$\Delta p = p_B - p_A = \frac{(V_{saB} - V_{saA})(G_s\gamma_w - \gamma_f)}{A_c} + \Delta z\gamma_f \tag{5.15}$$

where Δz = the vertical distance between the two ports.

The volume of soil between Port A and Port B is:

$$V_{saB} - V_{saA} = \frac{(\Delta p - \Delta z\gamma_f)A_c}{(G_s\gamma_w - \gamma_f)} \tag{5.16}$$

The corresponding mass of soil between the two ports is:

$$m_{s,AB} = \frac{G_s(\Delta p - \Delta z\gamma_f)A_c}{(G_s\gamma_w - \gamma_f)} \tag{5.17}$$

Since the volume between the two ports is $A_c\Delta z$, the average soil concentration between them is:

$$C_{avg} = \frac{G_s(\Delta p - \Delta z\gamma_f)}{(G_s\gamma_w - \gamma_f)\Delta z} \tag{5.18}$$

Consistent with the approximation described above, in the Δ-Sed test the soil concentration at the midpoint elevation between the two ports is approximated as the average soil concentration within the interval bounded by the ports. Therefore, at time *t*, the soil concentration at the midpoint elevation is approximated as:

$$C(t,z) = \frac{G_s(\Delta p(t) - \Delta z\gamma_f)}{(G_s\gamma_w - \gamma_f)\Delta z} \tag{5.19}$$

5.3 Numerical Simulation

The performance and accuracy of the spatial averaging principle employed in the Δ-Sed test are intrinsically dependent on the geometric configuration of the two pressure ports—specifically, the depth of the upper port (h_A) and the vertical spacing between the two ports (Δz). These two parameters define the boundaries of the spatial sampling zone over which the suspension density is averaged. To systematically investigate the optimal port configuration and evaluate the theoretical performance of the spatial averaging principle, a series of numerical simulations were conducted.

For a suspension consisting of discrete particle diameter classes D_i, let t_{iA} (i.e., $t_{iA} = h_A/v_i$) and t_{iB}(i.e., $t_{iB} = (h_A + \Delta z)/v_i$), denote the time required for the last D_i-sized particles, initially at the fluid surface, to settle past Port A and Port B, respectively. At any elapsed time t_j, the total mass of soil particles that has passed Port A is:

$$m_{spA} = \sum_1^n A_c C_i v_i \times \min(t_j,\ t_{iA}) \tag{5.20}$$

Consequently, the total mass of soil particles remaining above Port A at time t_j is:

$$m_{saA} = h_A A_c C_{total} - \sum_1^n A_c C_i v_i \times \min(t_j,\ t_{iA}) \tag{5.21}$$

By analogy to Eq. (5.21), the total mass of soil particles still above Port B at time t_j is:

$$m_{saB} = h_B A_c C_{total} - \sum_1^n A_c C_i v_i \times \min(t_j,\ t_{iB}) \tag{5.22}$$

By subtracting Eq. (5.21) from Eq. (5.22), the mass of particles between Port A and Port B at time t_j is:

$$m_{s_interval} = \Delta z A_c C_{total} - [\sum_1^n A_c C_i v_i \times \min(t_j,\ t_{iB}) - \sum_1^n A_c C_i v_i \times \min(t_j,\ t_{iA})] \tag{5.23}$$

Dividing through by the volume of the inter-port zone ($\Delta z A_c$) yields the average soil concentration between the ports at time t_j:

$$C(t_j) = C_{total} - [\sum_1^n C_i v_i \times \min(t_j,\ t_{iB}) - \sum_1^n C_i v_i \times \min(t_j,\ t_{iA})]/\Delta z \tag{5.24}$$

In the Δ-Sed test, the localized soil concentration at the geometric midpoint between the ports (at depth $z = h_A + \Delta z/2$) is approximated by this interval-averaged concentration. By substituting Eq. (5.24) into Eq. (5.6), the percent finer, $P(D_j)$, corresponding to the characteristic diameter D_j can be expressed as:

$$P(D_j) = 100\% - \frac{[\sum_1^n C_i v_i \times \min(t_j, t_{iB}) - \sum_1^n C_i v_i \times \min(t_j, t_{iA})]}{\Delta z \times C_{\text{total}}} \times 100\% \tag{5.25}$$

where D_j represents the diameter of the particles that were initially at the suspension surface and are passing the midpoint depth at time t_j, which is governed by Stokes' Law (Eq. 5.8) and the corresponding settling velocity (z/t_j). Through these fundamental governing principles, the complete continuous PSD can be constructed.

To conduct a parametric study, an idealized soil gradation was assumed, featuring a uniform mass distribution across 75 discrete particle-size classes ranging from 0.075 mm down to 0.001 mm (in 0.001 mm increments). This virtual specimen was assumed to be thoroughly mixed into a 1000 mL suspension within a sedimentation cylinder having an internal diameter of 57.15 mm (2.25 in.), yielding an initial fluid height of approximately 39 cm. The suspension was assumed to be perfectly homogeneous at $t = 0$ and the settling behavior of particles followed Stokes' Law (Eq. 7). Material properties were assigned to reflect typical laboratory conditions: soil specific gravity of $G_s = 2.75$, the fluid density $\rho_f = 0.9982$ g/cm^3, and dynamic viscosity μ =1.0016 mPa·s (representing pure water property at 20 °C).

During the simulation tests, the pressures at Port A and Port B (Eqs. 5.13 and 5.14) were computed at 1-second intervals over an 86400 s (24-hour) sedimentation period. The resulting difference between these two pressures served as the temporal output of a virtual differential pressure transducer (at a virtual sampling frequency of 1 Hz). This simulated $\Delta p(t)$ data was then processed using Eq. (5.19) to compute the interval-averaged concentration, and subsequently Eq. (5.6) to back-calculate the percent finer, $P(D)$. As described earlier, D is determined from the settling velocity and Stokes' law (Eq. 5.8).

5.4 Influence of Port Configuration

5.4.1 Influence of Vertical Spacing between Ports

The numerical analysis was first utilized to evaluate the influence of the vertical spacing between the two ports, Δz, on the performance of the Δ-Sed test. In this analysis, the depth of the upper port was fixed at $h_A = 10$ cm. Four values of Δz were considered: 2, 6, 10, and 14 cm. The corresponding simulation results are presented in Fig. 5.2. The results indicate that the performance of the Δ-Sed test deteriorates as Δz increases. This error stems directly from the spatial averaging assumption inherent to the method. As Δz becomes larger, the deviation between the midpoint concentration and the interval-averaged concentration increases, leading to greater approximation error in the calculated PSD.

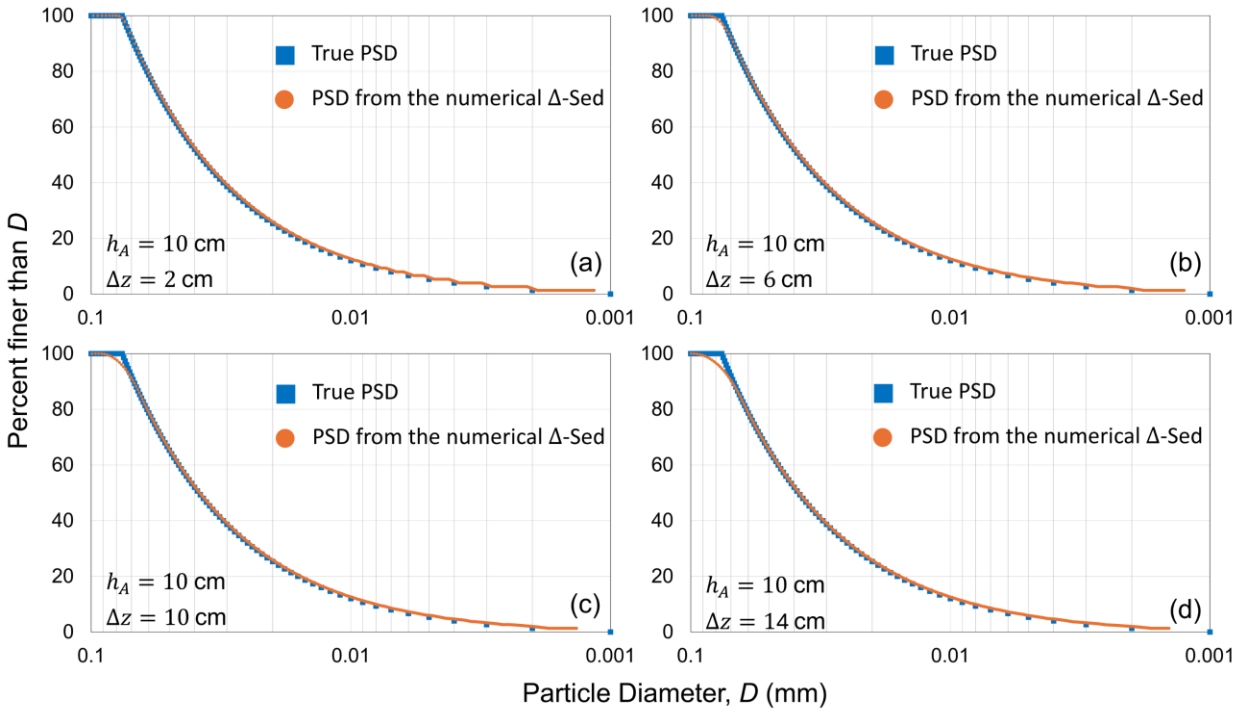


Figure 5.2: Effect of vertical spacing between pressure ports on numerical Δ-Sed test results: (a) Δz = 2 cm; (b) Δz = 6 cm; (c) Δz = 10 cm; (d) Δz = 14 cm.

It should be noted that the preceding numerical simulations generated theoretically exact pressure values, effectively assuming an ideal, zero-instrumental-error scenario. Under such idealized conditions, a smaller port spacing (Δz) strictly minimizes spatial averaging errors. In practice, however, any real differential pressure transducer is subject to inherent accuracy limitations. Reducing Δz decreases the volume of suspension between the ports, including both the fluid and suspended soil, thereby diminishing the magnitude of the measured differential pressure. This reduction in the signal magnitude amplifies the relative impact of the unavoidable transducer's instrumental error, making its influence on the calculated "percent finer" more significant. The present system employs a differential pressure transducer with a specified accuracy of ± 0.7 Pa. For a 50 g soil specimen with $G_s = 2.75$, adopting a port spacing of $\Delta z = 10$ cm yields an estimated uncertainty of approximately ± 2.2% in the calculated "percent finer''. This level of precision compares favorably against the conventional hydrometer test, which exhibits an uncertainty of approximately 3.14% (Zhang and Tumay 1995). Because this configuration strikes an optimal balance between mitigating theoretical spatial averaging errors and maintaining a robust signal-to-noise ratio, $\Delta z = 10$ cm was adopted for the actual Δ-Sed system.

5.4.2 Influence of Upper Port Depth

A second parametric study was conducted to evaluate the influence of the upper port depth, h_A. With Δz fixed at 10 cm, four values of h_A were considered: 0, 10, 20, and 25 cm. The simulation results, shown in Fig. 5.3, indicate that increasing h_A progressively enhances the fidelity of the predicted PSD. This improvement is physically rooted in the non-linear relationship between settling distance and particle size governed by Stokes' Law. As the upper port's depth increases, the settling distance for the particles also increases; consequently, at any elapsed time *t*, the difference between the characteristic diameters of the "last particles" reaching the upper and lower ports significantly diminishes. This reduction results in a more gradual vertical concentration gradient within the measurement interval, thereby minimizing the discrepancy between the interval-averaged concentration and the true localized concentration at the midpoint. However, beyond $h_A = 20$ cm, further increases in h_A lead to only marginal improvements in the predicted PSD while prolonging the required test duration. Consequently, an upper port depth of $h_A = 20$ cm was selected. This configuration positions the lower port at an elevation of $h_B = 30$ cm. Given the initial suspension height of approximately 39 cm, this geometry strategically preserves a 9-cm clearance zone at the base of the cylinder, ensuring that the accumulating sediment bed does not interfere with the lower port during the test.

Weighing the combined effects of spatial averaging errors, signal-to-noise ratio, and operational efficiency, a final hardware configuration of $h_A = 20$ cm and $\Delta z = 10$ cm was adopted for the Δ-Sed system. Under these optimized geometric parameters, for a standard 50 g soil specimen with $G_s = 2.75$, the intrinsic ± 0.7 Pa accuracy of the differential pressure transducer translates to an uncertainty of approximately ± 2.2% in the calculated ‘‘percent finer’’. The test duration required to resolve the PSD down to a particle diameter of $D = 2$ μm is approximately 16 h at a testing temperature of 25°C.

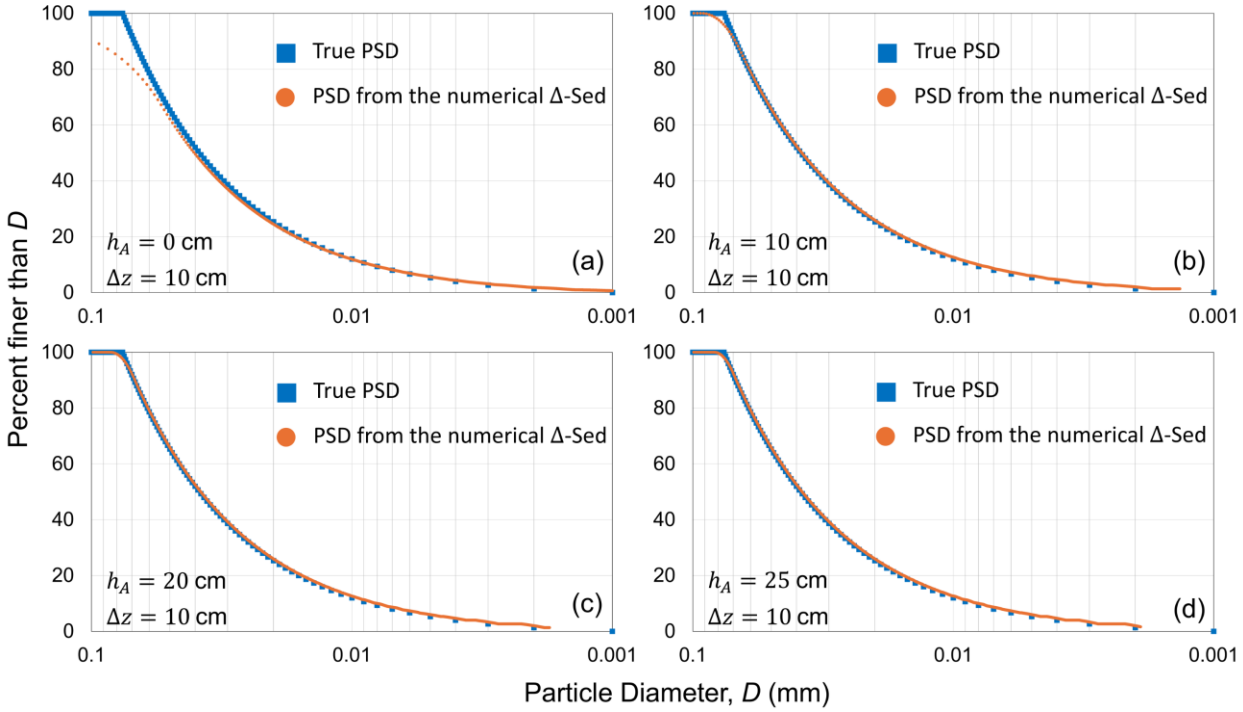


Figure 5.3: Effect of upper pressure port depth on numerical Δ-Sed test results: (a) h_A = 0 cm; (b) h_A = 10 cm; (c) h_A = 20 cm; (d) h_A = 25 cm.

5.5 Influence of Soil Specimen and Suspension Temperature

Because the settling behavior of soil particles depends on their specific gravity, variations in G_s will influence the sedimentation and therefore the vertical distribution of concentration within the suspension. To verify the analytical stability of the Δ-Sed formulation across diverse mineralogies, simulations were conducted using the finalized configuration ($h_A = 20$ cm and $\Delta z = 10$ cm) for four distinct specific gravities: 2.5, 2.7, 2.9, and 3.1. In this analysis, the fluid properties corresponding to pure water at 20 °C were used for the viscosity and density. As depicted in Fig. 5.4, the derived PSDs exhibit excellent conformance with the true PSDs across all tested values, demonstrating that the spatial averaging assumption remains robust regardless of particle density. Figure 5.4 also illustrates that for a fixed test duration of 24 h, the minimum resolved particle diameter logically decreases as G_s increases. This occurs because a higher specific gravity yields a greater settling velocity, thereby allowing finer particles to settle past the measurement zone within the same timeframe.

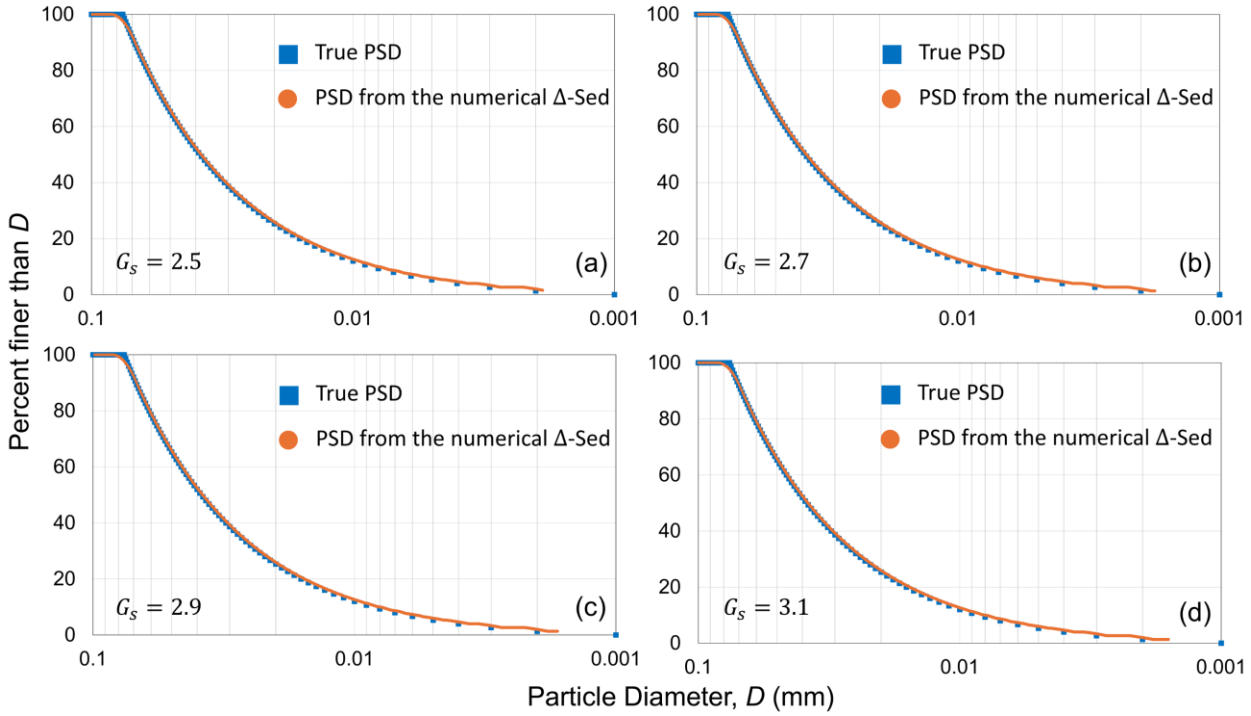


Figure 5.4: Performance of the numerical Δ-Sed test for different soil specific gravities: (a) $G_s = 2.5$; (b) $G_s = 2.7$; (c) $G_s = 2.9$; (d) $G_s = 3.1$.

Similarly, ambient temperature dictates the dynamic viscosity and density of the suspension fluid, which subsequently affect the settling behavior of soil particles. To assess the system's reliability under varying temperature conditions, numerical simulations were performed at four different fluid temperatures ranging from 5°C to 35°C (in 10°C increments), holding G_s constant at 2.75. The results, presented in Fig. 5.5, confirm that the Δ-Sed algorithm accurately captures the true PSD across the entire temperature range considered.

Finally, having validated the system against both material and environmental variables, its capacity to resolve complex gradation geometries was evaluated. Four distinct synthetic soil profiles were simulated: a well-graded soil, a gap-graded soil, and two random distributions. As illustrated in Fig. 5.6, the mathematically derived curves closely trace the true input PSDs in all scenarios. This exceptional agreement verifies the versatility of the underlying Δ-Sed formulation, proving its capability to accurately characterize fine-grained soils with diverse gradations.

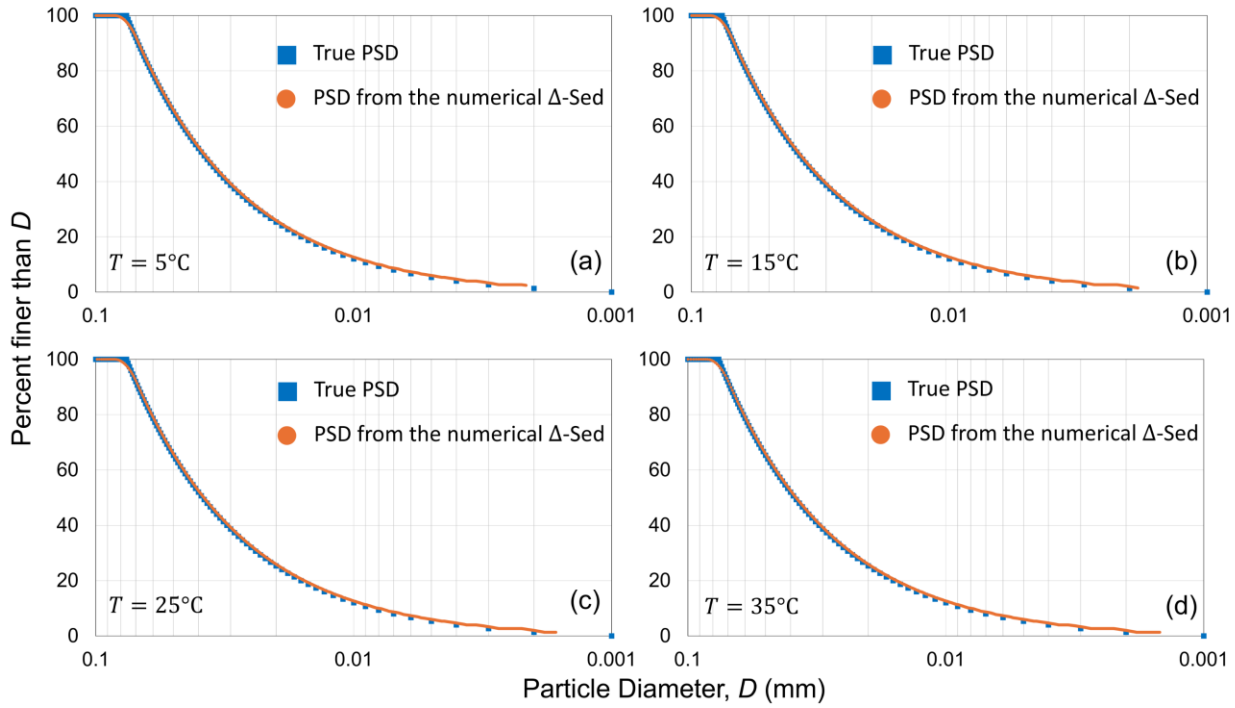


Figure 5.5: Performance of the numerical Δ-Sed test under different suspension temperatures: (a) T = 5 °C; (b) T = 15 °C; (c) T = 25 °C; (d) T = 35 °C

.

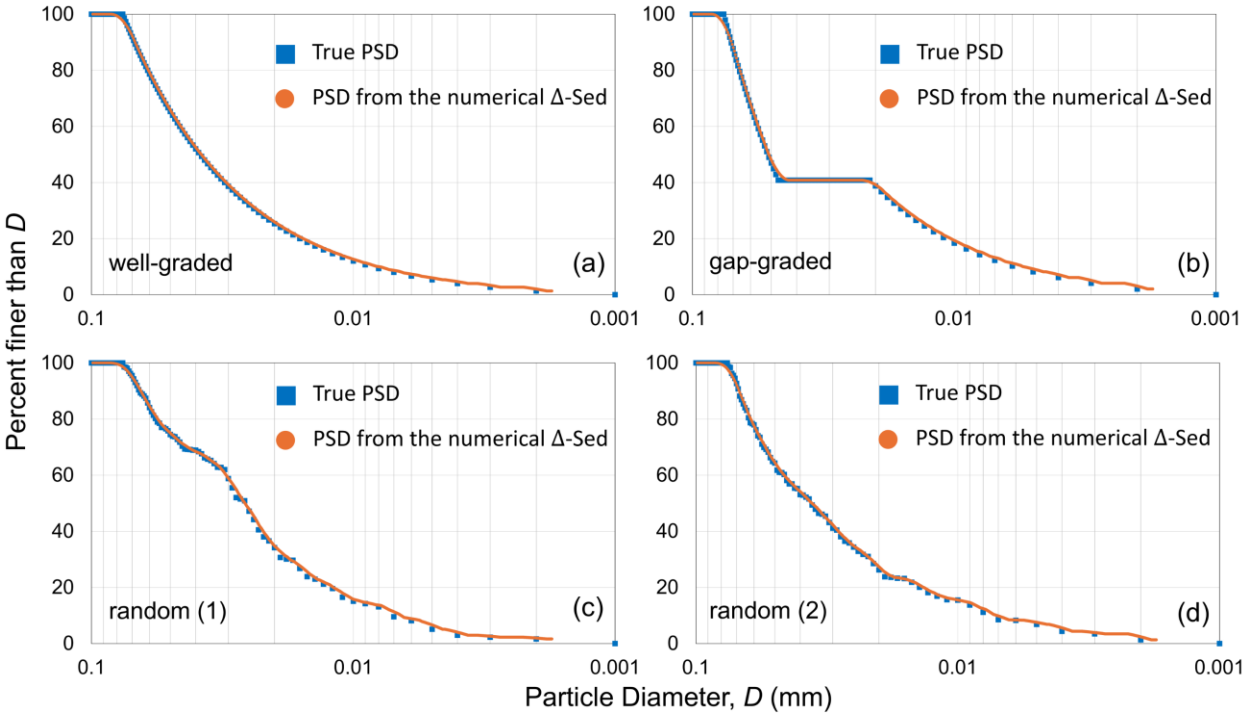


Figure 5.6: Performance of the numerical Δ-Sed test for different soil gradations: (a) well-graded distribution; (b) gap-graded distribution; (c) random distribution 1; (d) random distribution 2.

5.6 The Δ-Sed System Hardware

The Δ-Sed system consists of a sedimentation cylinder and a differential pressure transducer, as shown in Fig. 5.7. The clear acrylic cylinder measures 500 mm (19.69 in.) in height, with an inner diameter of 57.15 mm (2.25 in.) and a wall thickness of 6.35 mm (0.25 in.). The lower end of the cylinder is permanently bonded to a rigid acrylic base to provide structural support and to ensure a watertight seal during testing.

For a 500-mm-tall sedimentation cylinder with an inner diameter of 57.15 mm, a standard suspension volume of 1,000 mL results in a water level 110 mm below the top of the cylinder. Based on the optimal configuration identified from the numerical simulations described previously, the upper and lower pressure ports in the present system are installed at depths of 310 mm and 410 mm from the top of the column, respectively. The two pressure ports are positioned with a horizontal angular separation of 90°. This offset was adopted because the vertical spacing between the two ports is insufficient to accommodate both along the same vertical axis on the column wall. The inlet of each pressure port is inclined 30° from the vertical to prevent soil particles from entering the tubing during mixing of the suspension within the cylinder.

The differential pressure between the two ports was measured using a Validyne P55F differential pressure transducer (model P55F-1-N-1-22-G-4-A; Validyne Engineering). The transducer has a 0–1.4 kPa full-scale measurement range and a specified accuracy of ±0.05% of full scale, equivalent to ±0.7 Pa. The lower and upper pressure ports were connected to the high- and low-pressure sides of the transducer, respectively, through plastic tubing with an outer diameter of 6.35 mm (0.25 in.) and push-to-connect fittings.

In the Δ-Sed test, the soil suspension is homogenized within the sedimentation cylinder using a hand agitator, shown in Fig. 5.7(c), in accordance with ASTM D7928 (ASTM 2021). Compared to the tipping (inversion) method, the hand agitator method is the preferred/referee mixing procedure specified by the standard. This approach minimizes entrained air bubbles and thoroughly homogenizes the suspension without generating large transient pressure fluctuations within the column. Avoiding such fluctuations is critical for the Δ-Sed system because excessive pressure fluctuations could exceed the overpressure limit of the differential pressure transducer and potentially damage it.

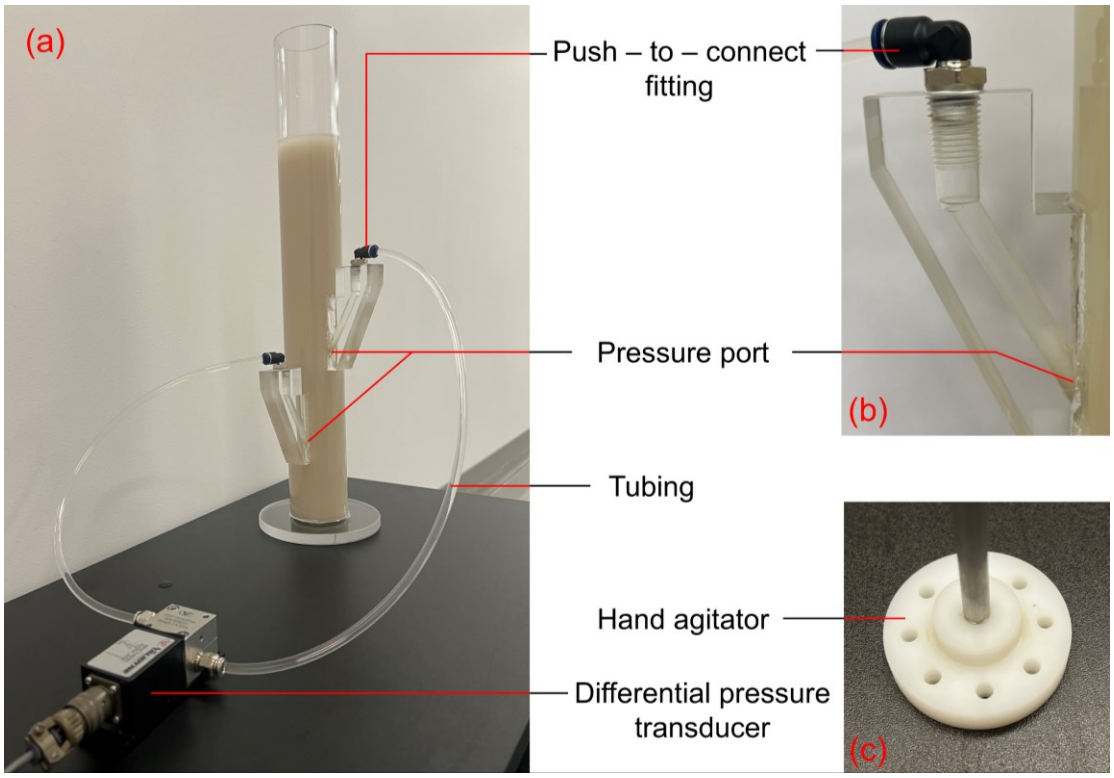


Figure 5.7: The Δ-Sed system: (a) sedimentation cylinder and differential pressure transducer; (b) close-up view of the pressure port and push-to-connect fitting; and (c) hand agitator.

5.7 Tested Materials and Results

To evaluate the performance of the Δ-Sed across a spectrum of real fine-grained materials, four soils with distinct mineralogical and plasticity characteristics were selected for laboratory validation, and their resulting PSDs were compared with those obtained from the traditional hydrometer analysis, which is widely used as the reference method for fines PSD determination. As detailed in Table 5.1, the test matrix comprised two processed commercial materials—a silica powder (MIN-U-SIL 40, U.S. Silica Holdings Inc.) and a Goldart clay (fireclay, Cedar Heights Clay Company)—and two natural specimens recovered from infrastructure investigation projects in Michigan, namely Mills Creek silt and Black River clay.

Each material was selected to represent a distinct fine-grained soil type with different characteristics. The silica powder consists of high-purity, ground crystalline quartz ($G_s = 2.65$), serving as a non-plastic reference typical of quartz-based silts. The Goldart clay is a commercially refined fireclay sourced from southern Ohio and was selected as a high-plasticity clay material to evaluate the performance of the Δ-Sed system for highly plastic fine-grained soils. The remaining

two samples are natural soils retrieved from geotechnical drill cuttings in Sanilac, Michigan: the Mills Creek silt is a non-plastic silt sampled from a depth interval of 3.66–8.53 m (12-28 ft), whereas the Black River clay is a lean clay exhibiting moderate plasticity, recovered from a deeper stratum between 15.24 m and 27.89 m (50-91.5 ft).

Table 5.1: Tested Soil Specimens

Specimen	Source	Soil Type	G_s
Silica powder	U.S. Silica Holdings Inc.	Silica	2.65
Goldart clay	Cedar Heights Clay Company	Stoneware clay	2.76
Mills Creek silt	Sanilac, Michigan	Natural silt	2.74
Black River clay	Sanilac, Michigan	Natural clay	2.76

All tests were conducted in a constant-temperature controlled laboratory environment using 50.00 g of soil per specimen. The preparation of the soil suspension—including specimen preparation, addition of test water (deionized water), soil dispersion, and mixing procedures—strictly followed ASTM D7928 specifications, resulting in a uniform suspension with a total volume of 1,000 mL. Regarding the dispersing agent, 5.0 g of sodium hexametaphosphate was added to prepare the solution following the recommendations of ASTM D7928 to prevent the coalescence or flocculation of fine particles.

The density and dynamic viscosity of the deionized water were determined based on the ambient laboratory temperature using the table provided in Appendix B. Following the homogenization of the suspension using a hand agitator, the differential pressure signal required a short period to stabilize. Observations indicated that the pressure readings typically stabilized approximately 5 s after mixing. To be conservative, only data recorded 10 s after mixing were utilized for subsequent analysis. All four tests were conducted at a sampling frequency of 1 Hz, with a total recording duration of approximately 16 hours per test.

To eliminate redundant data points in the plotted PSD curves, the recorded high-frequency data were systematically down sampled prior to visualization. This simplification was performed on a logarithmic time scale by restricting the resolution to 0.01 decades of time. Specifically, only

one data point was retained for each 0.01 increment in log (t), yielding a maximum of approximately 100 points per time decade. This filtering procedure effectively preserves the features of the PSD curve while significantly reducing dataset clutter. As illustrated in Fig. 5.8, the continuous PSD curves generated by the Δ-Sed tests demonstrate strong agreement with the discrete data points obtained from conventional hydrometer tests.

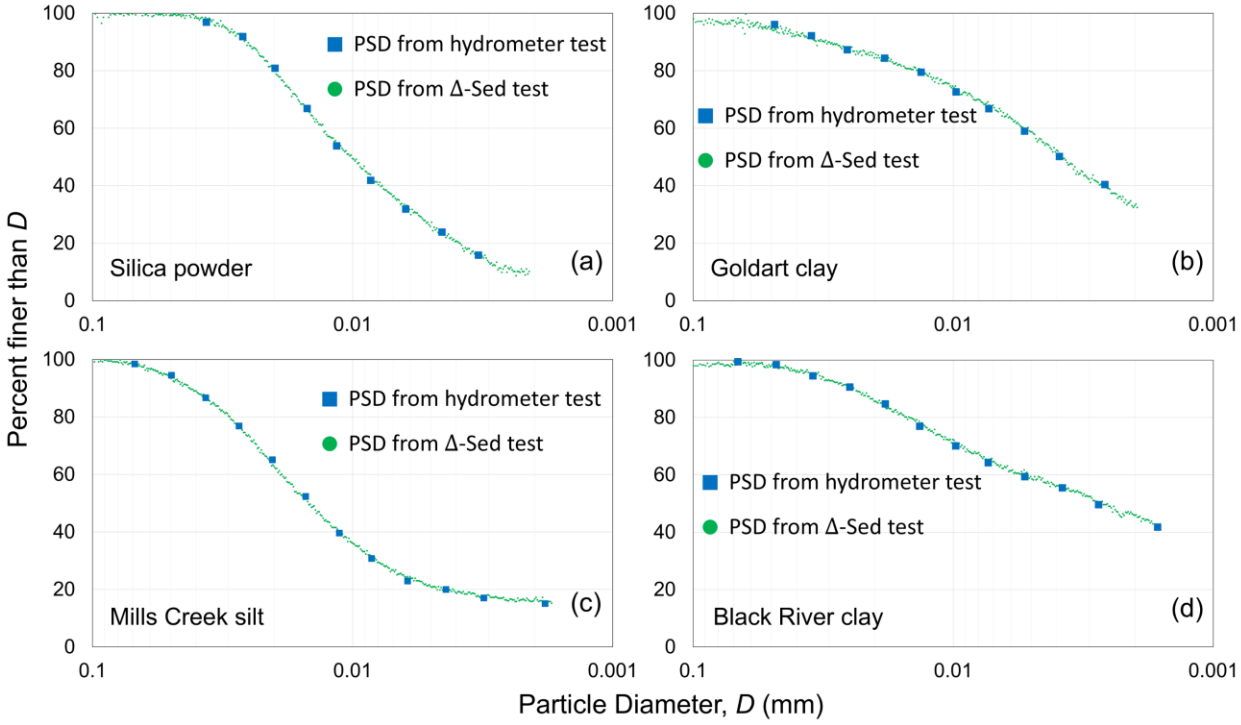


Figure 5.8: Comparison of PSDs from Δ-Sed and hydrometer tests for four fine-grained soils: (a) Silica powder; (b) Goldart clay; (c) Mills Creek silt; (d) Black River clay.

5.8 Repeatability and Sensitivity Analysis

To evaluate the repeatability of the Δ-Sed test, the Goldart clay specimen in Table 5.1 was tested three times. As shown in Fig. 5.9, the resulting PSD curves obtained from the three tests are nearly identical, demonstrating the high repeatability of the Δ-Sed test.

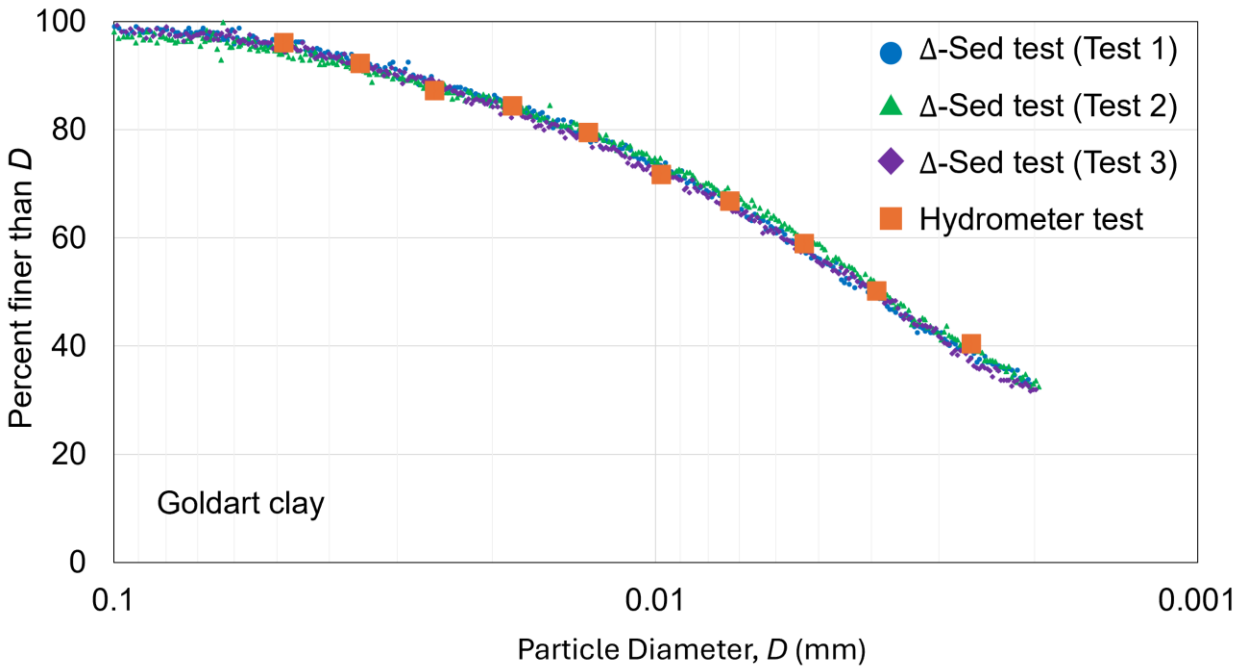


Figure 5.9: Repeatability analysis of the Δ-Sed test.

A sensitivity analysis was subsequently conducted to evaluate the effect of deviations in key input parameters on the computed PSDs. The examined parameters included the specific gravity of the soil (G_s), as well as the dynamic viscosity (μ) and density (ρ_f) of the suspension fluid. This parametric study utilized the differential pressure–time history acquired from the Min-U-SIL 40 silica powder test. Specifically, assumed G_s values of 2.62, 2.65 (the actual G_s), and 2.68 were evaluated. Similarly, the influence of fluid properties was assessed by using the dynamic viscosity and density of water corresponding to temperatures of 23, 25 (the actual test temperature), and 27 °C.

As illustrated in Fig. 5.10, small variations in G_s have a negligible effect on the PSD curves. In contrast, Fig. 5.11 demonstrates that temperature variations exceeding approximately 4 °C begin to induce some deviations in the PSDs. Consequently, temperature control is somewhat important during Δ-Sed testing. It is recommended to adhere to the ASTM D7928 specification, which mandates that the suspension temperature must not vary by more than ± 2 °C throughout the duration of a test.

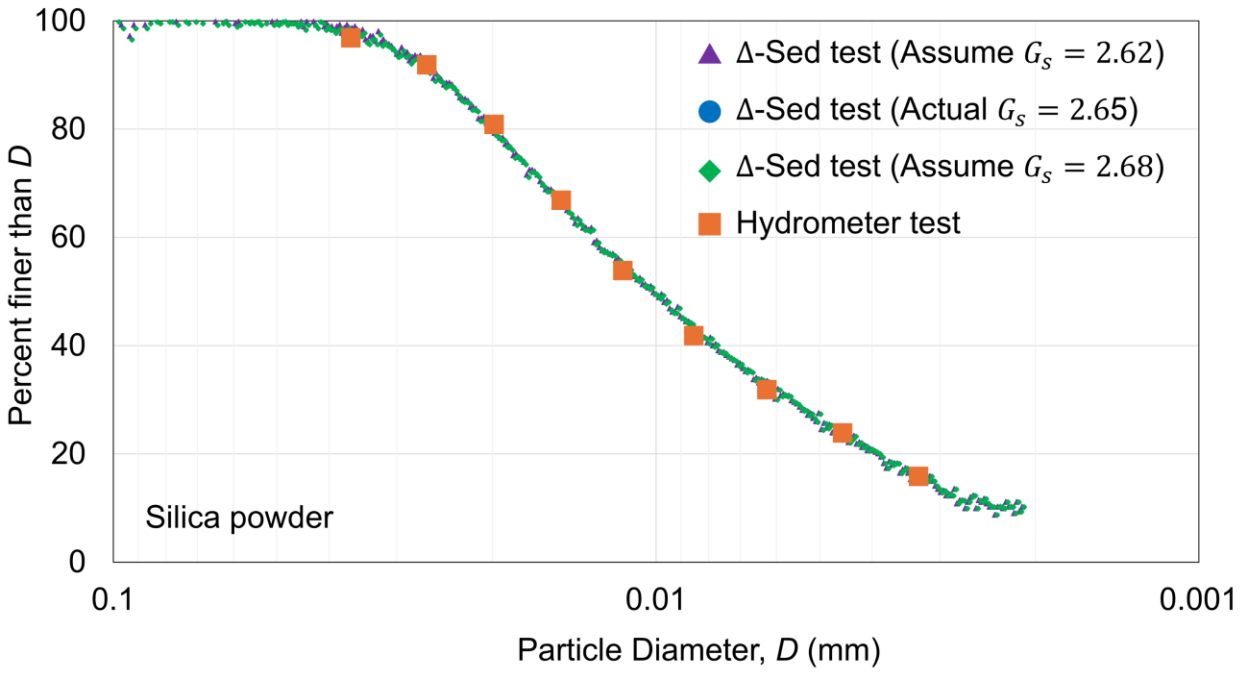


Figure 5.10: Effect of assumed soil specific gravity deviations on the Δ-Sed test results.

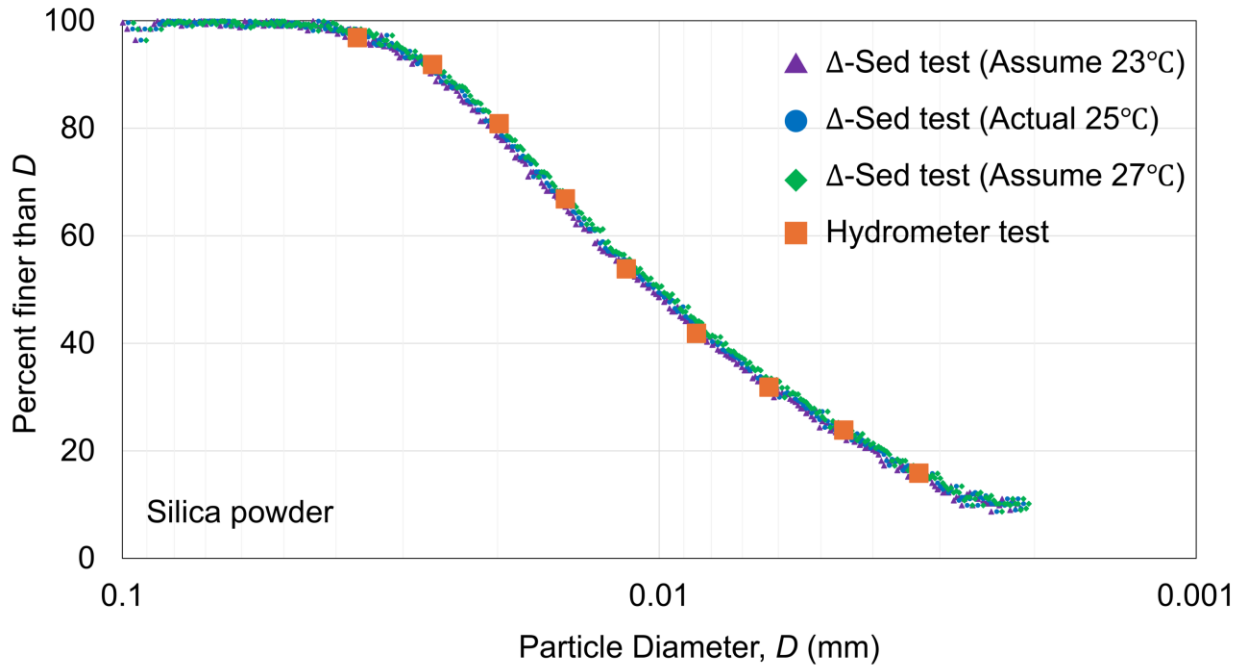


Figure 5.11: Effect of assumed suspension temperature deviations on the Δ-Sed test results.

Unlike the integral suspension pressure (ISP) method, which measures single-point pressure within the suspension, the Δ-Sed test captures the differential pressure between two fixed ports. Because the Δ-Sed measures pressure difference rather than absolute pressures, fluid evaporation should have no effect on PSDs. To confirm this, two parallel tests were conducted using the Goldart clay. In the first test, the sedimentation cylinder was tightly covered with a rubber stopper to minimize evaporation, whereas in the second test, the cylinder was left uncovered. By the end of the uncovered test, the suspension surface had dropped by approximately 5 mm due to evaporation. As shown in Fig. 5.12, the PSDs obtained from these two tests confirm that evaporation had a negligible influence on the Δ-Sed results. This resilience is attributed to the fact that evaporation occurs at a relatively slow rate compared to the sedimentation process; thus, most particles initially near the suspension surface settle past the uppermost layer subject to evaporation well before the liquid level decreases appreciably. Even in the extreme case where exceptionally fine particles remain within the evaporative zone, the evaporation-induced reduction in their settling distance is minuscule compared to their total settling depth. Consequently, realistic evaporation exerts a negligible influence on the Δ-Sed test results.

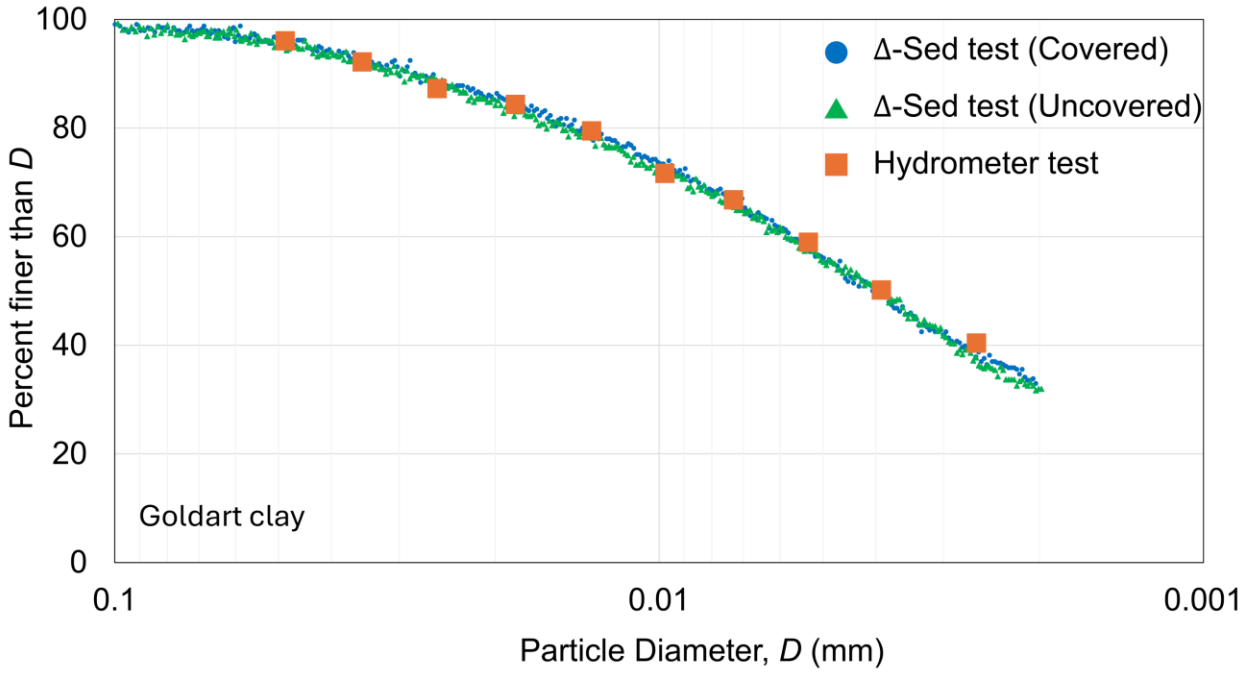


Figure 5.12: Effect of evaporation on the Δ-Sed test results.

5.9 Δ-Sed Particle Size Testing Range

The lower particle size limit for the Δ-Sed test is 0.002 mm. Below this size, Brownian motion and interparticle attractions become significant compared to Stokesian settlement. The same issue holds for hydrometer and ISP testing. Also, assuming a typical soil specific gravity of 2.75 and a testing temperature of 25°C, resolving particles down to 0.002 mm requires a test duration of approximately 16 hours for the current Δ-Sed system configuration. Extending the size range down to 0.001 mm would drastically increase the required testing time to roughly 65 hours.

Because sand particles are relatively heavy and settle rapidly during and immediately after mixing, they cannot be reliably lifted and uniformly distributed throughout the sedimentation column. Except for very fine sand grains, sand particles will settle before the first pressure readings can be taken. Moreover, Stokes' Law applicability does not extend very far into the sand size range so other particle settling-velocity models such as by Ahrens (2000) or Jiménez and Madsen (2003) (which are invoked in the *u*-Sed test), would have to be used. As such, it is recommended that the upper particle size limit for the Δ-Sed test be conservatively set at 0.075 mm.

In light of the inability to prepare a uniform sand mixture in a sedimentation column, and the previously described requirement to create such a uniform mixture for fines, it is challenging to develop a single combined sedimentation test system that would develop PSDs spanning the full sand-to-clay particle size range. Thus, currently, a specimen containing both coarse grains and fines still requires two separate tests. Nevertheless, if the previously described *u*-Sed (or m-Sed) test is employed for the coarse fraction alongside the Δ-Sed for fines, the two sedimentation systems become a powerful tandem for the development of essentially continuous PSDs while overcoming most of the limitations of sieving and hydrometer testing.

5.10 Chapter Summary

This chapter introduced the Δ-Sed test, an automated differential-pressure sedimentation method for determining the particle size distributions of fine-grained soils. The method extends the pressure-based sedimentation framework developed in Chapters 3 and 4, but it is based on a measurement strategy specifically suited to fines. The *u*-Sed and m-Sed tests determine sand PSDs by introducing dry sand at the top of a water column and interpreting the pressure response as particles settle past a fixed measurement port. In contrast, the Δ-Sed test begins with a fully dispersed and spatially uniform suspension of silts or clays and determines the time-dependent soil concentration within a fixed measurement interval. This distinction is essential because fine-

grained soils cannot be reliably introduced into a sedimentation column as dry particles or as a top-introduced slurry.

The theoretical basis of the Δ-Sed test was developed from the sedimentation behavior of an initially uniform fine-grained suspension. As particles settle under gravity, the local soil concentration at a given depth decreases with time, and this concentration can be related directly to the percent finer corresponding to the particle size reaching that depth at that time. The Δ-Sed system determines this concentration from the differential pressure between two fixed sidewall ports. The measured pressure difference reflects the average bulk density of the suspension between the ports, and this interval-averaged concentration is used to approximate the concentration at the midpoint elevation. Each differential pressure reading can therefore be converted directly into a PSD data point without requiring manual hydrometer readings or global inverse fitting.

Numerical simulations were used to evaluate the spatial-averaging approximation and optimize the Δ-Sed geometry. The vertical spacing between ports controls the balance between spatial-averaging error and pressure signal magnitude, while the upper port depth affects both accuracy and test duration. Based on these considerations, an upper port depth of 20 cm and a port spacing of 10 cm were selected as the final configuration. This arrangement provides an appropriate balance between theoretical accuracy, signal-to-noise ratio, and operational efficiency.

The accuracy of the Δ-Sed test was evaluated using four fine-grained materials: silica powder, Goldart clay, Mills Creek silt, and Black River clay. The resulting PSDs showed very good agreement with conventional hydrometer results. Repeatability testing produced nearly identical PSD curves, confirming the consistency of the method. Sensitivity analyses showed that small deviations in assumed soil specific gravity have negligible influence on the computed PSDs, while temperature control is more important because fluid viscosity and density directly affect settling velocity. The differential-pressure configuration also made the method resistant to fluid-level-induced zero-offset errors, including those caused by evaporation or delayed return of water droplets from the cylinder wall.

The recommended testing range of the Δ-Sed method is 0.002 to 0.075 mm. The lower limit reflects the increasing influence of Brownian motion, interparticle attractions, and excessive test duration below 0.002 mm. The upper limit is set at 0.075 mm because sand-sized particles

settle too rapidly to remain uniformly suspended after mixing, and Stokes' law is not generally appropriate for most sand-sized particles.

Overall, the Δ-Sed test provides a direct, automated, and high-resolution alternative to hydrometer analysis for fine-grained soils. Together with the u-Sed and m-Sed tests for sands, it forms a coherent sedimentation-based framework for determining nearly continuous PSDs across the major soil particle-size domains while overcoming many limitations of conventional sieve and hydrometer testing.

Chapter 6 Summary and Future Recommendations

Building on the particle-size determination framework established in Chapter 2, Chapters 3 through 5 developed and validated three complementary sedimentation-based systems for determining soil particle size distributions (PSDs) from water-pressure responses during particle settling. The *u*-Sed and m-Sed tests were developed for sands, whereas the Δ-Sed test was developed for fine-grained soils. Although the three systems employ measurement strategies appropriate to the different initial conditions and settling behaviors of sands and fines, they share a common analytical framework: particle size is inferred from settling velocity, while the corresponding percent finer is determined from the measured hydraulic response. Together, these systems provide high-resolution sedimentation-based alternatives to conventional sieve and hydrometer analyses across the sand and fine-grained particle-size ranges.

This final chapter synthesizes the principal findings and contributions of the dissertation and identifies directions for further development. Section 6.1 summarizes the theoretical development, experimental validation, principal advantages, and practical limitations of the *u*-Sed, m-Sed, and Δ-Sed tests, both individually and as a complementary family of methods. Section 6.2 presents recommendations for future research aimed at extending their applicability and improving their operational efficiency, including scaling of the *u*-Sed and m-Sed systems for larger specimens, reduction of the Δ-Sed test duration, integration of image analysis for particle-shape characterization, and development of a unified sedimentation test for sands and fines.

6.1 Summary

The principal findings, contributions, and practical limitations of the three sedimentation-based systems developed in this dissertation are summarized below.

6.1.1 The u-Sed test

The *u*-Sed test was developed as an electronic pressure-monitored sedimentation method for determining nearly continuous PSDs of sands. A dry sand specimen is rapidly introduced near the top of a water-filled sedimentation column, where the particles sort by size as they settle. A

pressure transducer connected to a fixed sidewall port continuously records the water pressure change as particles pass the port elevation. The normalized pressure response determines the percentage of specimen solids remaining above the port, while the elapsed settling time and travel distance provide the corresponding particle settling velocity. Inversion of the Ahrens or Jiménez and Madsen settling-velocity model then yields the sieve-equivalent particle size associated with each pressure measurement.

The governing relationships developed for the *u*-Sed test demonstrate that the PSD can be determined from pressure differences between well-defined testing stages without reliance on absolute pressure measurements. The same pressure record also provides independent estimates of the specimen mass and soil specific gravity, which serve as useful internal checks on test quality. Because pressure is recorded continuously throughout sedimentation, a single test generates tens to hundreds of PSD data points without mechanically separating the specimen into discrete size fractions.

The *u*-Sed test was evaluated using 16 sand specimens spanning the ASTM sand-size range and representing different gradations, particle shapes, angularities, specific gravities, and geologic origins. The resulting PSDs showed strong agreement with conventional sieve analyses. For most natural sands, the Ahrens and Jiménez and Madsen models produced similar results. For coarse sands containing highly angular or plate-like particles, the Jiménez and Madsen model generally provided better agreement because this model explicitly accounts for particle shape and roundness. Repeated tests produced nearly identical PSD curves, and sensitivity analyses showed that small deviations in assumed soil specific gravity and water viscosity had little influence on the calculated PSDs. Consistent results were also obtained for specimen masses between 40 and 60 g in the current sedimentation column, which is 1.8 m tall and has an inside diameter of 25.4 mm.

Compared with conventional sieve analysis, the *u*-Sed test is fast, quiet, dust-free, compact, and requires less energy, cleaning, and maintenance. Its continuous pressure record also provides substantially higher PSD resolution than the limited number of particle sizes defined by a conventional sieve stack. The principal limitations arise for materials containing porous particles with entrapped air, specimens in which particle specific gravity varies substantially among size fractions, and coarse sands whose unusual particle shapes require supplemental shape characterization. Overall, the *u*-Sed test provides an accurate and practical alternative to conventional sieve analysis for sand PSD determination.

6.1.2 The m-Sed test

The m-Sed test extends the pressure-based sedimentation framework of the *u*-Sed test by replacing the electronic pressure transducer and data acquisition system with a simple manometer. As sand particles settle past the fixed pressure port, water moves from the manometer into the sedimentation column, causing the manometer water level to decrease. The resulting water-height history determines the fraction of specimen solids remaining above the port, while the Jiménez and Madsen settling-velocity model converts elapsed settling time into the corresponding sieve-equivalent particle size.

Because water is exchanged between the sedimentation column and the manometer, the governing formulation is more complex than that of the *u*-Sed test. The equations developed from the four principal pressure stages account for this bidirectional fluid movement and permit the PSD, specimen mass, and soil specific gravity to be determined without electronic pressure-sensing equipment. Manometer tube properties were found to be important because the tube must minimize capillary resistance while responding sufficiently rapidly to pressure changes. A polyurethane tube with an inside diameter of approximately 3.2 mm provided an effective balance between capillary and inertial effects.

The m-Sed test was validated using eight engineered specimens that included uniform, broadly graded, and gap-graded sands spanning the ASTM sand-size range. The resulting PSDs showed excellent agreement with conventional sieve analysis, and the characteristic particle sizes and gradation coefficients obtained by the two methods were consistent. Repeated tests produced nearly identical PSD curves. Direct comparisons among the m-Sed, *u*-Sed, and sieve results further demonstrated that the manometer-based system can reproduce the accuracy and high resolution achieved by the electronic *u*-Sed system.

The principal contribution of the m-Sed test is its operational simplicity. It requires no electronic pressure transducer, data acquisition system, electrical power, or electronic sensor calibration. The system is therefore particularly suitable for field testing, remote locations, wet environments, and resource-limited settings. Its principal limitations are similar to those of the *u*-Sed test, including the potential effects of entrapped air, particle-density variations among size fractions, and unusual particle shapes. Overall, the m-Sed test provides an accurate, field-portable, and electricity-free method for determining nearly continuous PSDs of sands.

6.1.3 The Δ-Sed test

The Δ-Sed test was developed as an automated differential-pressure sedimentation method for determining the PSDs of fine-grained soils. Unlike sands, dry silts and clays cannot be reliably introduced at the top of a water column, while a concentrated fine-grained slurry may descend as unstable plumes rather than as independently settling particles. The Δ-Sed test therefore begins with a fully dispersed and spatially uniform suspension, as is done in conventional hydrometer analysis.

The system measures the differential pressure between two vertically separated fixed sidewall ports. This pressure difference represents the average bulk density, and therefore the average soil concentration, within the interval between the ports. The interval-averaged concentration is used to approximate the local concentration at the midpoint elevation. At each elapsed time, the ratio of the measured concentration to the initial concentration provides the percent finer, while the settling distance and elapsed time are used with Stokes' law to determine the corresponding equivalent spherical diameter. Each differential-pressure measurement can therefore be converted directly into an independent PSD data point without manual hydrometer readings or global inverse fitting of the complete pressure record.

Numerical simulations were used to evaluate the spatial-averaging approximation and optimize the measurement geometry. The vertical spacing between the ports was found to control the balance between approximation accuracy and pressure-signal magnitude, while the depth of the upper port influenced both accuracy and test duration. An upper-port depth of 20 cm below the suspension surface and a vertical port spacing of 10 cm provided an appropriate balance among theoretical accuracy, signal magnitude, and operational efficiency.

The Δ-Sed test was experimentally validated using four fine-grained materials with contrasting mineralogical and plasticity characteristics: silica powder, Goldart clay, Mills Creek silt, and Black River clay. The resulting PSDs showed very good agreement with conventional hydrometer analyses, and repeated tests produced nearly identical curves. Sensitivity analyses indicated that small deviations in assumed soil specific gravity had negligible effects on the computed PSDs, whereas accurate suspension temperature was more important because fluid density and viscosity directly influence the inferred particle size.

An important advantage of the Δ-Sed test is its differential-pressure configuration. Minor changes in the suspension surface elevation act on both pressure ports and are therefore cancelled.

Consequently, the method is resistant to fluid-level-induced zero-offset errors caused by evaporation or the delayed return of water retained on the cylinder wall after mixing. The fixed sidewall ports also eliminate repeated hydrometer insertion and removal, thereby avoiding intrusion into and disturbance of the settling suspension while enabling automated, high-resolution data acquisition.

The recommended particle-size range of the Δ-Sed test is 0.002–0.075 mm. The lower limit reflects the increasingly long settling duration and the growing influence of Brownian motion and interparticle interactions at smaller particle sizes. The upper limit is governed primarily by the difficulty of establishing and maintaining a spatially uniform initial suspension when sand-sized particles settle rapidly during and immediately after mixing. Within this range, the Δ-Sed test provides a direct, automated, and high-resolution alternative to conventional hydrometer analysis.

Taken together, the *u*-Sed, m-Sed, and Δ-Sed tests demonstrate that water-pressure responses during sedimentation can be used to determine high-resolution PSDs across both the sand and fine-grained particle-size ranges. The systems retain particle-size interpretations consistent with their respective conventional reference methods while addressing many of the operational and measurement limitations of sieve and hydrometer analyses. Collectively, they establish a coherent foundation for further development of pressure-based sedimentation testing for routine soil characterization.

6.2 Future Recommendations

The research presented in this dissertation established the theoretical feasibility and experimental accuracy of the *u*-Sed, m-Sed, and Δ-Sed tests for determining high-resolution PSDs of sands and fine-grained soils. Nevertheless, these systems remain at different stages of development, and further research is needed to expand their applicability, improve their operational efficiency, and support their eventual adoption in routine geotechnical practice. The following recommendations are presented in approximate order of increasing technical scope and complexity. They begin with modifications that build directly on the existing system designs—scaling the *u*-Sed and m-Sed systems for larger specimens and reducing the duration of the Δ-Sed test. They then progress to the integration of image analysis for particle-shape characterization and conclude with the more challenging long-term objective of developing a unified sedimentation test for sands and fines.

6.2.1 Scaling of the u-Sed and m-Sed Systems for Larger Specimens

The current *u*-Sed and m-Sed systems use sedimentation columns with an inside diameter of 25.4 mm (1 in.) and are designed for sand specimens weighing approximately 40–60 g, with 50 g recommended as the nominal specimen mass. Tests conducted within this range produced accurate and repeatable PSDs. However, a specimen of this size may not adequately represent the bulk gradation of some natural sands, particularly heterogeneous or broadly graded materials containing a substantial coarse fraction. Because individual coarse particles represent a relatively large proportion of a small specimen mass, sampling variability may become significant even when the measurement system itself performs accurately.

Future research should investigate scaling the *u*-Sed and m-Sed systems to accommodate larger and more representative specimens. Increasing the column diameter would allow the specimen mass to be increased, but the system cannot necessarily be enlarged through simple geometric scaling. For a given specimen mass, an increase in column cross-sectional area reduces the pressure change produced by the particles above the measurement port. The specimen mass, column diameter, pressure-sensor range, and measurement resolution must therefore be considered together to preserve a sufficiently large and accurately measurable hydraulic response.

Scaling may also affect particle introduction, particle interactions, wall effects, and the extent to which all particles begin settling at approximately the same time. These effects should be investigated because the conversion from settling time to particle size assumes a known travel distance and a well-defined initial settling time. For the m-Sed system, increasing the column diameter would additionally alter the relationship between fluid displacement in the sedimentation column and water-level change in the manometer. The manometer diameter and port configuration may therefore require reoptimization to maintain adequate sensitivity while limiting capillary and inertial effects.

A systematic experimental program should evaluate several column diameters and corresponding specimen masses. The scaled systems should be compared with the existing 1-in.-diameter systems and with conventional sieve analysis using both engineered and natural sands. Performance should be assessed in terms of PSD accuracy, repeatability, pressure or water-height resolution, specimen-mass calculation, specific-gravity determination, and particle-introduction consistency. Such research would establish practical scaling relationships and determine whether

larger specimens can improve sample representativeness without compromising the accuracy and resolution of the *u*-Sed and m-Sed methods.

6.2.2 Reduction of the Δ-Sed Test Duration

The second recommendation concerns improving the operational efficiency of the Δ-Sed test by reducing its duration. Under the current Δ-Sed configuration, approximately 16 h is required at a suspension temperature of 25°C to resolve particle sizes down to 0.002 mm. Although data acquisition is automated and does not require continuous operator involvement, the relatively long duration limits laboratory throughput and may hinder routine application. Reducing the test duration while retaining the accuracy, repeatability, and direct interpretation of the method is therefore an important direction for future research.

The most direct means of shortening the test is to reduce the effective settling distance associated with the finest particles. This can be achieved by placing a pressure-measurement interval closer to the suspension surface. However, the numerical results presented in Chapter 5 showed that a shallower upper-port depth can increase the difference between the interval-averaged concentration and the local concentration at the midpoint. Therefore, simply moving the existing port pair upward may reduce test duration at the expense of PSD accuracy.

A promising alternative is to add a second differential pressure transducer connected to an additional pair of ports located closer to the suspension surface. The shallower measurement interval could be used to determine the finer portion of the PSD within a shorter settling time, while the existing deeper interval could continue to provide reliable measurements for coarser particles and an overlapping range for comparison. Preliminary calculations indicate that an appropriately designed two-transducer configuration may reduce the time required to reach 0.002 mm from approximately 16 h to about 5 h at 25°C. The overlapping particle-size ranges obtained from the two measurement intervals could also provide an internal consistency check and a basis for combining the two records into a single continuous PSD.

Future work should optimize the depths and vertical spacings of both measurement intervals through numerical simulation. The optimization should consider spatial-averaging error, differential-pressure magnitude, sensor resolution, test duration, and the overlap between the particle-size ranges obtained from the two transducers. Experimental validation should then be conducted using fine-grained soils with different gradations, specific gravities, mineralogies, and plasticity characteristics. Particular attention should be given to acquiring synchronized

measurements from both transducers and ensuring that the PSD segments obtained from the two intervals agree within their overlapping range.

Alternative approaches—including more sensitive differential-pressure transducers, reduced port spacing, improved correction of the spatial-averaging approximation, accelerated sedimentation, or prediction of the remaining fine fraction from a partial pressure record—may also be investigated. However, methods based on accelerated settling or extrapolation would require especially rigorous validation because they may alter particle interactions or weaken the direct physical interpretation of each PSD data point. Among the available approaches, a multi-depth differential-pressure configuration appears particularly promising because it can shorten the effective settling distance while preserving the fundamental measurement principle of the Δ-Sed test.

6.2.3 Integration of Image Analysis for Particle-Shape Characterization

Whereas the preceding recommendations focus primarily on system dimensions and operational efficiency, further development should also address the influence of particle morphology on the interpretation of sedimentation measurements. The *u*-Sed and m-Sed results demonstrated that particle shape can influence settling velocity and therefore the particle sizes inferred from sedimentation measurements. This effect is especially important for coarse sands containing highly angular or plate-like particles. The Jiménez and Madsen model accounts for particle shape and roundness through the Corey Shape Factor (CSF) and associated model coefficients. In the present study, the three orthogonal dimensions of 25 randomly selected particles were measured manually using a caliper to estimate an average CSF for each unusually shaped sand. Although this approach provided useful shape information, it is labor-intensive, evaluates only a small portion of the specimen, and assigns a single average shape parameter to particles that may exhibit size-dependent morphology.

Water-pressure measurements alone cannot independently determine particle shape. Future research should therefore investigate the integration of image analysis with the *u*-Sed and m-Sed tests. Images could be acquired either before sedimentation testing or from the sediment bed formed at the base of the column upon completion of the test. Automated particle detection and measurement could then be used to characterize a substantially larger number of particles than is practical through manual caliper measurements. Relevant parameters may include projected axis

ratios, circularity, angularity, roundness, sphericity, and other descriptors related to settling behavior.

Because CSF depends on three orthogonal particle dimensions, conventional two-dimensional images may not be sufficient for reliable determination of this parameter. Multi-view imaging, particle rotation, stereoscopic imaging, or three-dimensional reconstruction should therefore be investigated. The resulting methods should be validated using particles whose three dimensions have also been measured independently.

Image-derived shape parameters could then be incorporated directly into the Jiménez and Madsen settling-velocity model when converting measured settling velocities into sieve-equivalent particle sizes. Ideally, particle shape would be characterized separately for different size fractions rather than represented by a single specimen-wide average. Such integration would reduce manual measurement effort, improve the interpretation of unusual particle geometries, and extend the reliability of the *u*-Sed and m-Sed tests for highly angular, elongated, or plate-like sands.

6.2.4 Development of a Unified Sedimentation Test for Sands and Fines

The most technically challenging and integrative direction for future research is the development of a unified sedimentation test for sands and fines. The systems developed in this dissertation demonstrate that sands and fine-grained soils require fundamentally different initial conditions for reliable sedimentation analysis. In the *u*-Sed and m-Sed tests, a dry sand specimen is introduced near the top of a water-filled column and begins settling immediately. The pressure response is then related to the redistribution of particle mass above a fixed measurement elevation. In contrast, the Δ-Sed test requires the fine-grained particles to be fully dispersed and uniformly distributed throughout the suspension before sedimentation begins. The differential-pressure response is interpreted in terms of the time-dependent soil concentration within a fixed vertical interval. These differences currently require the sand and fine fractions of a mixed soil to be tested separately.

Future research should investigate whether a unified specimen-preparation and measurement procedure can be developed to determine both fractions from a single specimen. Potential approaches include staged particle introduction, controlled release of the sand fraction into a previously prepared fine-grained suspension, or sequential establishment of the initial conditions required by the two measurement frameworks. The system would need to accommodate the rapid pressure response generated by sand sedimentation as well as the substantially slower

concentration changes associated with fine particles. This may require multiple pressure ports, sensors with different measurement ranges, or a hybrid configuration combining absolute, differential, and manometric pressure measurements.

A unified data-processing framework would also be required. Settling velocities of sand-sized particles should be interpreted using an appropriate non-Stokes model, whereas fine-particle sizes should remain based on Stokes' law to preserve consistency with conventional hydrometer analysis. Particular attention should be given to the transition near the sand–fines boundary, where differences in particle dispersion, settling regime, and measurement interpretation may introduce discontinuities in the resulting PSD. Validation should include soils with systematically varied fines contents, broadly graded and gap-graded distributions, and different mineralogical and plasticity characteristics. The ultimate objective would be to determine a continuous PSD across the sand and fine-grained particle-size ranges from a single specimen without preliminary physical separation or two independent tests.

Appendices

Appendix A: Derivation of *u*-Sed Test Equations

This appendix provides derivations of Eq. (3.2) for specific gravity, G_s and Eq. (3.3) for total weight of solids, W_s. Equation (3.1) for the unit weight of the column fluid, γ_f is straightforward and requires no derivation. Reference here is made to the *u*-Sed test Stages and notation in Fig. 3.2.

During Stage D, the pressure at the elevation of the pressure port is:

$$u^D = \gamma_f h_2 \tag{A-1}$$

During Stage F, the pressure is due to both the fluid and the solids above the pressure port:

$$u^F = \frac{W_s + W_f^F}{A_c} \tag{A-2}$$

where W_f^F = weight of fluid above the pressure port elevation during Stage F.

A_c = inside cross-sectional area of the sedimentation column.

The weights W_s and W_f^F in Eq. (A-2) can be expressed in terms of their respective volumes:

$$u^F = \frac{V_s G_s \gamma_w + V_f^F \gamma_f}{A_c} \tag{A-3}$$

where V_s= total volume of solids.

V_f^F= volume of fluid above the pressure port elevation during Stage F.

γ_w= unit weight of pure water at 4°C = 9.807 kN/m^3.

Since the total volume of soil and fluid above the pressure port elevation during Stage F is:

$$V = V_s + V_f^F \tag{A-4}$$

Eq. (A-3) may be written:

$$u^F = \frac{V_s G_s \gamma_w + (V - V_s)\gamma_f}{A_c} \tag{A-5}$$

and since $V = h_3 A_c$ as shown in Fig. 3.2, Eq. (A-5) is reorganized as:

$$u^F = \frac{V_s (G_s \gamma_w - \gamma_f)}{A_c} + h_3 \gamma_f \tag{A-6}$$

In Stage G, solids are passing the pressure port. Since the weight of solids above the port is decreasing, there is a corresponding reduction in pressure. By analogy to Eq. (A-6), during Stage G, the pressure becomes:

$$u^G = \frac{V_s^G(G_s\gamma_w - \gamma_f)}{A_c} + h_3\gamma_f \tag{A-7}$$

where V_s^G= volume of solids above the pressure port during Stage G.

The reduction in pressure from Stage F to any time during Stage G is:

$$u^F - u^G = (V_s - V_s^G)\frac{(G_s\gamma_w - \gamma_f)}{A_c} \tag{A-8}$$

which may be rearranged to obtain the volume of the solids that have passed the pressure port at any time during Stage G:

$$(V_s - V_s^G) = \frac{(u^F - u^G)A_c}{(G_s\gamma_w - \gamma_f)} \tag{A-9}$$

The corresponding weight of solids that have passed the pressure port is then:

$$(W_s - W_s^G) = \frac{(u^F - u^G)A_cG_s\gamma_w}{(G_s\gamma_w - \gamma_f)} \tag{A-10}$$

where W_s^G= weight of solids above the pressure port during Stage G.

In Stage H, all the soil particles have passed the pressure port, V_S^G becomes zero and Eq. (A-9) becomes the expression for the total volume of solids:

$$V_s = \frac{(u^F - u^H)A_c}{(G_s\gamma_w - \gamma_f)} \tag{A-11}$$

Accordingly, the total weight of specimen solids is:

$$W_s = \frac{(u^F - u^H)A_cG_s\gamma_w}{(G_s\gamma_w - \gamma_f)} \tag{A-12}$$

During Stage H, the pressure becomes constant once again and is due solely to the fluid above:

$$u^H = \gamma_f h_3 \tag{A-13}$$

The pressure difference between Stage H and Stage D (Eq. (A-1)) was caused by the introduction of the solids into the column which raised the fluid level from h_2 to h_3 as shown in Fig. 3.2. Thus,

$$u^H - u^D = \gamma_f(h_3 - h_2) \tag{A-14}$$

The volume of displaced fluid is the same as the volume of solids, so:

$$(h_3 - h_2) = \frac{V_s}{A_c} \tag{A-15}$$

Substituting Eq. (A-15) into Eq. (A-14), we solve for the total volume of solids:

$$V_s = \frac{(u^H - u^D)A_c}{\gamma_f} \tag{A-16}$$

Since Eq. (A-11) and Eq. (A-16) are both expressions for V_s we equate them:

$$\frac{(u^F - u^H)A_c}{(G_s\gamma_w - \gamma_f)} = \frac{(u^H - u^D)A_c}{\gamma_f} \tag{A-17}$$

Eq. (A-17) can then be solved for the specific gravity of solids:

$$G_s = \left(\frac{u^F - u^H}{u^H - u^D} + 1\right)\frac{\gamma_f}{\gamma_w} \tag{A-18}$$

Appendix B: Temperature-Dependent Density and Viscosity of Water

Table B.1 lists the dynamic viscosity, kinematic viscosity, and density of water over the temperature range reported by Anton Paar. These properties are used as applicable in the *u*-Sed, m-Sed, and Δ-Sed analyses.

Table B.1: Density and Viscosity of Water as a Function of Temperature

Temperature (°C)	Dynamic Viscosity (mPa·s)	Kinematic Viscosity (mm²/s)	Density (g/cm³)
2	1.6735	1.6736	0.9999
3	1.619	1.6191	1
4	1.5673	1.5674	1
5	1.5182	1.5182	1
6	1.4715	1.4716	0.9999
7	1.4271	1.4272	0.9999
8	1.3847	1.3849	0.9999
9	1.3444	1.3447	0.9998
10	1.3059	1.3063	0.9997
11	1.2692	1.2696	0.9996
12	1.234	1.2347	0.9995
13	1.2005	1.2012	0.9994
14	1.1683	1.1692	0.9992
15	1.1375	1.1386	0.9991
16	1.1081	1.1092	0.9989
17	1.0798	1.0811	0.9988
18	1.0526	1.0541	0.9986

Temperature (°C)	Dynamic Viscosity (mPa·s)	Kinematic Viscosity (mm²/s)	Density (g/cm³)
19	1.0266	1.0282	0.9984
20	1.0016	1.0034	0.9982
21	0.9775	0.9795	0.998
22	0.9544	0.9565	0.9978
23	0.9321	0.9344	0.9975
24	0.9107	0.9131	0.9973
25	0.89	0.8926	0.997
26	0.8701	0.8729	0.9968
27	0.8509	0.8539	0.9965
28	0.8324	0.8355	0.9962
29	0.8145	0.8178	0.9959
30	0.7972	0.8007	0.9956
31	0.7805	0.7842	0.9953
32	0.7644	0.7682	0.995
33	0.7488	0.7528	0.9947
34	0.7337	0.7379	0.9944
35	0.7191	0.7234	0.994
36	0.705	0.7095	0.9937
37	0.6913	0.6959	0.9933
38	0.678	0.6828	0.993
39	0.6652	0.6702	0.9926
40	0.6527	0.6579	0.9922
45	0.5958	0.6017	0.9902
50	0.5465	0.5531	0.988
55	0.5036	0.5109	0.9857
60	0.466	0.474	0.9832
65	0.4329	0.4415	0.9806

Temperature (°C)	Dynamic Viscosity (mPa·s)	Kinematic Viscosity (mm²/s)	Density (g/cm³)
70	0.4035	0.4127	0.9778
75	0.3774	0.3872	0.9748
80	0.354	0.3643	0.9718

Source: Anton Paar (2026).

Bibliography

Ahrens, J. P. 2000. "A fall-velocity equation." *J. Waterway, Port, Coastal, Ocean Eng.* 126 (2): 99–102. https://doi.org/10.1061/(ASCE)0733-950X(2000)126:2(99).

Anton Paar. 2026. "Viscosity of water: Viscosity table and viscosity chart." *Anton Paar Wiki*. Accessed July 12, 2026. https://wiki.anton-paar.com/us-en/water/.

ASTM. 2017. *Standard practice for classification of soils for engineering purposes (Unified Soil Classification System)*. ASTM D2487-17. West Conshohocken, PA: ASTM.

ASTM. 2019. *Standard test method for sieve analysis of fine and coarse aggregates*. ASTM C136/C136M-19. West Conshohocken, PA: ASTM.

ASTM. 2021. *Standard test method for particle-size distribution (gradation) of fine-grained soils using the sedimentation (hydrometer) analysis*. ASTM D7928-21e1. West Conshohocken, PA: ASTM.

ASTM. 2023. *Standard test methods for specific gravity of soil solids by the water displacement method*. ASTM D854-23. West Conshohocken, PA: ASTM.

ASTM. 2024. *Standard specification for woven wire test sieve cloth and test sieves*. ASTM E11-24. West Conshohocken, PA: ASTM.

Bagheri, G., and C. Bonadonna. 2016. "On the drag of freely falling nonspherical particles." *Powder Technol.* 301: 526–544. https://doi.org/10.1016/j.powtec.2016.06.015.

Blahut, A., J. Hykl, P. Peukert, V. Vinš, and J. Hrubý. 2019. "Relative density and isobaric expansivity of cold and supercooled heavy water from 254 to 298 K and up to 100 MPa." *J. Chem. Phys.* 151 (3): 034505. https://doi.org/10.1063/1.5100604.

Camenen, B. 2007. "Simple and general formula for the settling velocity of particles." *J. Hydraul. Eng.* 133 (2): 229–233. https://doi.org/10.1061/(ASCE)0733-9429(2007)133:2(229).

Caw, W. A., and R. G. Wylie. 1961. "Effect of dissolved air on the viscosity of water." *Nature* 189 (4769): 995–996. https://doi.org/10.1038/189995b0.

Cheng, N.-S. 1997. “Simplified settling velocity formula for sediment particle.” *J. Hydraul. Eng.* 123 (2): 149–152. https://doi.org/10.1061/(ASCE)0733-9429(1997)123:2(149).

Dietrich, W. E. 1982. “Settling velocity of natural particles.” *Water Resour. Res.* 18 (6): 1615–1626. https://doi.org/10.1029/WR018i006p01615.

Durner, W., and S. C. Iden. 2021. “The improved integral suspension pressure method (ISP+) for precise particle size analysis of soil and sedimentary materials.” *Soil Tillage Res.* 213: 105086. https://doi.org/10.1016/j.still.2021.105086.

Durner, W., S. C. Iden, and G. von Unold. 2017. “The integral suspension pressure method (ISP) for precise particle-size analysis by gravitational sedimentation.” *Water Resour. Res.* 53 (1): 33–48. https://doi.org/10.1002/2016WR019830.

Gibbs, R. J., M. D. Matthews, and D. A. Link. 1971. “The relationship between sphere size and settling velocity.” *J. Sediment. Petrol.* 41 (1): 7–18. https://doi.org/10.1306/74D721D0-2B21-11D7-8648000102C1865D.

Guo, J. 2002. “Logarithmic matching and its applications in computational hydraulics and sediment transport.” *J. Hydraul. Res.* 40 (5): 555–565. https://doi.org/10.1080/00221680209499900.

Hallermeier, R. J. 1981. “Terminal settling velocity of commonly occurring sand grains.” *Sedimentology* 28 (6): 859–865. https://doi.org/10.1111/j.1365-3091.1981.tb01948.x.

ISO. 2024. *Determination of particle size distribution by gravitational liquid sedimentation methods—Part 1: General principles, requirements and guidance*. ISO 13317-1:2024. Geneva: ISO.

Jiménez, J. A., and O. S. Madsen. 2003. “A simple formula to estimate settling velocity of natural sediments.” *J. Waterway, Port, Coastal, Ocean Eng.* 129 (2): 70–78. https://doi.org/10.1061/(ASCE)0733-950X(2003)129:2(70).

Jones, F. E., and G. L. Harris. 1992. “ITS-90 density of water formulation for volumetric standards calibration.” *J. Res. Natl. Inst. Stand. Technol.* 97 (3): 335–340. https://doi.org/10.6028/jres.097.013.

Kaszubkiewicz, J., and K. Papuga. 2023. “Equation for determining cumulative particle size distribution using the pressure of a sedimenting suspension.” *Measurement* 209: 112493. https://doi.org/10.1016/j.measurement.2023.112493.

Kovács, B., I. Czinkota, L. Tolner, and Gy. Czinkota. 2004. "The determination of particle size distribution (PSD) of clayey and silty formations using the hydrostatic method." *Acta Mineral. Petrogr.* 45: 29–34.

METER Group. 2026. *PARIO user manual*. Version 3.2026. Accessed June 10, 2026. https://library.metergroup.com/Manuals/20780_PARIO_Manual_Web.pdf.

Nemes, A., I. Czinkota, Gy. Czinkota, L. Tolner, and B. Kovács. 2002. "Outline of an automated system for the quasi-continuous measurement of particle-size distribution." *Agrokémia és Talajtan* 51 (1–2): 37–46. https://doi.org/10.1556/agrokem.51.2002.1-2.5.

Ohm, H.-S., and R. D. Hryciw. 2013. "Translucent segregation table test for sand and gravel particle size distribution." *Geotech. Test. J.* 36 (4): 592–605. https://doi.org/10.1520/GTJ20120221.

Ohm, H.-S., and R. D. Hryciw. 2014. "Size distribution of coarse-grained soil by SedImaging." *J. Geotech. Geoenviron. Eng.* 140 (4): 04013053. https://doi.org/10.1061/(ASCE)GT.1943-5606.0001075.

Raudkivi, A. J. 1990. *Loose boundary hydraulics*. 3rd ed. Oxford, UK: Pergamon Press.

Song, X., Z. Xu, G. Li, Z. Pang, and Z. Zhu. 2017. "A new model for predicting drag coefficient and settling velocity of spherical and non-spherical particle in Newtonian fluid." *Powder Technol.* 321: 242–250. https://doi.org/10.1016/j.powtec.2017.08.01.

Stokes, G. G. 1851. "On the effect of the internal friction of fluids on the motion of pendulums." *Trans. Cambridge Philos. Soc.* 9 (2): 8–106.

van Rijn, L. C. 1984. "Sediment transport, Part II: Suspended load transport." *J. Hydraul. Eng.* 110 (11): 1613–1641. https://doi.org/10.1061/(ASCE)0733-9429(1984)110:11(1613).

Ventola, A., R. Dolling, and R. D. Hryciw. 2020a. "Image analysis and hardware developments for the vision cone penetrometer (VisCPT)." In *Geo-Congress 2020: Modeling, Geomaterials, and Site Characterization*, Geotechnical Special Publication 317, edited by J. P. Hambleton, R. Makhnenko, and A. S. Budge, 640–648. Reston, VA: ASCE. https://doi.org/10.1061/9780784482803.068.

Ventola, A., G. Horstmeier, R. D. Hryciw, C. Kempf, and J. Eykholt. 2020b. "Particle size distribution of Kalamazoo River sediments by FieldSed." *J. Geotech. Geoenviron. Eng.* 146 (12): 05020012. https://doi.org/10.1061/(ASCE)GT.1943-5606.0002421.

Ventola, A., and R. D. Hryciw. 2019. “On-site particle size distribution by FieldSed.” In *Geo-Congress 2019: Engineering Geology, Site Characterization, and Geophysics*, edited by C. L. Meehan, S. Kumar, M. A. Pando, and J. T. Coe, 143–151. Reston, VA: ASCE. https://doi.org/10.1061/9780784482131.015.

Ventola, A., and R. D. Hryciw. 2023a. “The Sed360 test for rapid sand particle size distribution determination.” *Geotech. Test. J.* 46 (2): 422–429. https://doi.org/10.1520/GTJ20220032.

Ventola, A., and R. D. Hryciw. 2023b. “An autoadaptive Haar wavelet transform method for particle size analysis of sands.” *Acta Geotech.* 18 (10): 5341–5358. https://doi.org/10.1007/s11440-023-01856-x.

Waldschläger, K., and H. Schüttrumpf. 2019. “Effects of particle properties on the settling and rise velocities of microplastics in freshwater under laboratory conditions.” *Environ. Sci. Technol.* 53 (4): 1958–1966. https://doi.org/10.1021/acs.est.8b06794.

Zhang, L., and R. D. Hryciw. 2025. “Particle size distribution of sand by water pressure during sedimentation: The u-Sed test.” *J. Geotech. Geoenviron. Eng.* 151 (11): 04025121. https://doi.org/10.1061/JGGEFK.GTENG-13378.

Zhang, L., and R. D. Hryciw. 2026. “The manometer sedimentation (m-Sed) system for particle size distribution of sand.” *Geotech. Test. J.* 49 (2): 339–355. https://doi.org/10.1520/GTJ20250053.

Zhang, L., R. D. Hryciw, and A. Ventola. 2024. “The uSed system for soil particle size distribution determination.” In *Geo-Congress 2024: Geotechnical Site and Soil Characterization*, Geotechnical Special Publication 348, edited by T. M. Evans, N. Stark, and S. Chang, 136–145. Reston, VA: ASCE. https://doi.org/10.1061/9780784485309.015.

Zhang, Z., and M. T. Tumay. 1995. “Granulometric evaluation of particle size using suspension pressure during sedimentation.” *Geotech. Test. J.* 18 (1): 121–129. https://doi.org/10.1520/GTJ10129J.

Zheng, J., and R. D. Hryciw. 2017. “Particulate material fabric characterization by rotational Haar wavelet transform.” *Comput. Geotech.* 88: 46–60. https://doi.org/10.1016/j.compgeo.2017.02.021.

Zheng, J., and R. D. Hryciw. 2018. “Identification and characterization of particle shapes from images of sand assemblies using pattern recognition.” *J. Comput. Civ. Eng.* 32 (3): 04018016. https://doi.org/10.1061/(ASCE)CP.1943-5487.0000765.